Science and Technology Journal, Vol. 7 Issue: I ISSN: 2321-3388

Prioritization of Receivers for Minimum Possible Error Boundary in Time Difference of Arrival Algorithm

Sourav Kaity[1]*, Biswapati Jana[2], P.K. Das Gupta[3] and Lalatendu Das[4]
[1,4]Integrated Test Range, DRDO, Chandipur-756025
[2]Vidyasagar University, Midnapore-721102
[3]Proof and Experimental Establishment, DRDO, Chandipur-756025
E-mail: *souravkaity@gmail.com

Abstract—A lot of passive target tracking techniques are available to find out the unknown target location**.** In this literature, Time difference of arrival (TDOA), a widely used passive target tracking technique, is used to derive the position of the target. By applying cross-correlation techniques on signals received by two different receivers one hyperbolic equation can be formed. With the help of a minimum four receiving stations, a unique intersecting point can be derived from hyperbolic equations which give the position of a target precisely. The accuracy of the target position depends upon the geometric location of the receivers with respect to the target location. A simulation study was carried out with seven numbers of receivers**.** We considered all thirty**-**five combinations taking four receivers at a time out of seven**.** From this simulation study, a unique relation between target position measurement errors with the average range difference error is established. With the help of the above relation, receivers can be prioritized and four receivers could be placed in best geographical locations. By considering four high prioritized receivers minimum target position measurement error could be achieved. An attempt was focused to draw the error boundary, error factor of target position measurement with the range of the target. And it is clear that the error factor is varying linearly with the range of the target.

Keywords: TDOA, Hyperbolic Equation, Range Difference, Error Boundary

INTRODUCTION

A never**-**ending demand for finding the location and improving the measurement accuracy of target location either static or dynamic has been a most discussed topic among scientists as well as some technology-oriented organization. This helps largely in military prospects where the opponent's incoming target is estimated within milliseconds. Apart from this, it helps in emergency evacuation situations, navigation purposes, tracking a person, various search operations, etc. The aviation sector has also significantly modernized with the help of positional location technology.

For measurement of target location, there exists several passive target localization techniques likes Time on arrival (TOA), Angle of Arrival (AOA), Time Difference of Arrival (TDOA), Received Signal Strength (RSS), etc. and also some hybrid techniques which are a combination of two different localization algorithm mentioned above (Deligiannis *et al.,* 2010). AOA measures the angle of the source with respect to sensors. The power present in a received signal varies from a shorter distance to longer. RSS technique computes the position parameters by this energy level of the received signal. In TOA techniques the travel time of signal converted in distance to get positional parameters. Each method has its own advantages and disadvantages according to the application.

For an exact positional value, the TOA method requires strict clock synchronization between source and receiver station (Shin and Sung 2002). To avoid such a synchronization problem and to improve the accuracy of a target, TDOA techniques used. It is a cross-correlation technique and also known as hyperbolic position location techniques.

http://doi.org/10.22232/stj.2019.07.01.01

A fundamental approach presented by Krizman *et al.* (1997) with respect to TDOA considering basic radio frequency position location strategies**.** To find source location from noisy instances through range differences have proposed by Friedlander (1987). A weighted matrix was derived for the least square estimator and a simulation formed to analyze the results. The observation was only valid if the range difference measurement is unbiased.

An approach presented by Kossonou *et al.* (2014) is a non-iterative method and has less complex computing based on Chan's method for TDOA. Position estimation is done in two**-**steps, in first related position parameters of TDOA are computed then applied with position algorithm in the second step. The positioning algorithm should be obtained in a perfect channel.

Asynchronous time difference of arrival positioning system is proposed by He *et al.* (2017) where the position was calculated without time synchronization with all the receiver anchor and target nodes.

A positional algorithm is developed for a two-dimensional context, considering there are one transmitter and multiple receivers (Chan and Ho 1994). A set of equations formed from TDOA measurements is solved by the least square method. Here only TDOA estimation error was considered.

Due to the non-linearity of the hyperbolic equation, the TDOA measurement is uncertain. A comparing study between Monte Carlo based method and the gradient search algorithm was presented using a non-linear least square framework (Gustafsson 2003).

A detailed derived method was presented to find a position with four fixed stations (Potluri 2001)**.** A derived model was formed from the hyperbolic equation and the simulation result shows the accuracy level of the experiment.

For greater accuracy, we extend this approach for our experiment to calculate TDOA and also analysis the error. In section 2 we described our approach. Simulation results and error analysis was done in section 3 and finally, in section 4, we concluded the paper with our end result.

TDOA ALGORITHM FOR POSITION MEASUREMENT

In this section, we solved the localization problem using time difference of arrival (TDOA) methods. There are four receivers present which give us a hyperbolic equation. By solving these hyperbolic equations lead us to get the positional value. But it is very complex to solve those equations and hence the error analysis becomes a difficult task. This is due to the nonlinearity of the hyperbolic equation.

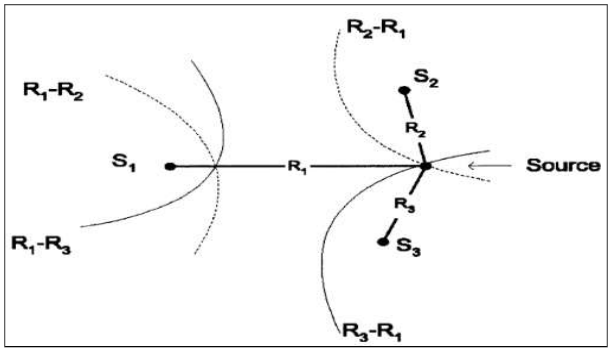

Fig. 1: A Sample Hyperbolic Position Location Solution (Three Receivers)

At first range difference between two receivers is calculated by the difference in time of arrival of the signal. The time of arrival (TOA) of two geo-spatial receivers was taken into consideration. The range can be calculated from the product of TDOA and the propagation speed. The propagation speed is equivalent to the speed of the light. This range difference yields to the hyperbolic equation between two receiver stations. In range difference measurement if the unknown quantity to be determined is equal to the number of the equation then there exists a unique solution. If there exist multiple intersections between two hyperbolae, then ambiguity exists in estimated position value.

Basically solving these hyperbolic equations is a challenge. The Taylor series expansion is used to linearize the equation. It is an iterative method. It can give an exact solution unless the initial guess is not correct. A method proposed by Frag (1990) gave a correct derivation to the linearization problem where the number of an unknown variable is equal to the number of the hyperbolic equation. But this method suffers because of inborn squaring operation. In terms of complexity computation, it is less intensive than the Taylor series expansion. Chan and Ho (1994) proposed execution method by solving repetitive estimation. This method is superior than the Taylor series and the Fang's method.

If (x, y, z) is source transmitter location and (x_i, y_i, z_i) is the location of the ith receiver, is a range of source transmitter from the ith receiver given by

$$R_i = \sqrt{(x_i - x)^2 + (y_i - y)^2 + (z_i - z)^2} \quad (1)$$

Then the range differences of four different combinations of the source to the receiver are calculated and the equation for the same represented below

$$R_{ij} = R_i - R_j = \sqrt{(x_i - x)^2 + (y_i - y)^2 + (z_i - z)^2} - \sqrt{(x_j - x)^2 + (y_j - y)^2 + (z_j - z)^2} \quad (2)$$

$$R_{ik} = R_i - R_k = \sqrt{(x_i - x)^2 + (y_i - y)^2 + (z_i - z)^2} - \sqrt{(x_k - x)^2 + (y_k - y)^2 + (z_k - z)^2} \quad (3)$$

$$R_{kj} = R_k - R_j = \sqrt{(x_k - x)^2 + (y_k - y)^2 + (z_k - z)^2} - \sqrt{(x_j - x)^2 + (y_j - y)^2 + (z_j - z)^2} \quad (4)$$

$$R_{kl} = R_k - R_l = \sqrt{(x_k - x)^2 + (y_k - y)^2 + (z_k - z)^2} - \sqrt{(x_l - x)^2 + (y_l - y)^2 + (z_l - z)^2} \quad (5)$$

Now The time difference of arrival between receiver i and receiver j can be expressed as

$$t_{ij} = \frac{R_i - R_j}{c} \quad (6)$$

Where i is greater than j and c is the velocity of light.

Let $x_i(t)$ and $x_j(t)$ be signals received at ith and jth receiver respectively. One way to calculate the time difference t_{ij} of the signal received at ith and jth receiver is given by means of the standard cross-correlation function.

Using nonlinear regression, this equation can be converted to the form a hyperbola. Once enough hyperbolas have been calculated, the position of the transmitter can be calculated by finding the intersection.

Let, (x_0, y_0, z_0) is the source location. Then range from ith receiver to source is r_i.

$$r_i = \sqrt{(x_0 - x_i)^2 + (y_0 - y_i)^2 + (z_0 - z_i)^2} \quad (7)$$

We would require four equations to obtain a solution here, which can be obtained by expressions of r_i, r_j, r_k, r_l

$$r_i - r_j = r_{ij} \quad (8)$$

$$r_i - r_k = r_{ik} \quad (9)$$

$$r_k - r_j = r_{kj} \quad (10)$$

$$r_k - r_l = r_{kl} \quad (11)$$

Where,

$$r_{ij} = \sqrt{(x_0 - x_i)^2 + (y_0 - y_i)^2 + (z_0 - z_i)^2} - \sqrt{(x_0 - x_j)^2 + (y_0 - y_j)^2 + (z_0 - z_j)^2} \quad (12)$$

$$r_{ik} = \sqrt{(x_0 - x_i)^2 + (y_0 - y_i)^2 + (z_0 - z_i)^2} - \sqrt{(x_0 - x_k)^2 + (y_0 - y_k)^2 + (z_0 - z_k)^2} \quad (13)$$

$$r_{kj} = \sqrt{(x_0 - x_k)^2 + (y_0 - y_k)^2 + (z_0 - z_k)^2} - \sqrt{(x_0 - x_j)^2 + (y_0 - y_j)^2 + (z_0 - z_j)^2} \quad (14)$$

$$r_{kl} = \sqrt{(x_0 - x_k)^2 + (y_0 - y_k)^2 + (z_0 - z_k)^2} - \sqrt{(x_0 - x_l)^2 + (y_0 - y_l)^2 + (z_0 - z_l)^2} \quad (15)$$

The four equations given above can be solved and rearranged to obtain two plane equations as follows

$$y = Ax_0 + Bz_0 + C \quad (16)$$

$$y = Dx_0 + Ez_0 + F \quad (17)$$

Where,

$$A = \frac{R_{ij}x_{ji} - R_{ij}x_{ki}}{R_{ij}y_{ki} - R_{ik}y_{ji}} \quad (18)$$

$$B = \frac{R_{ik}z_{ji} - R_{ij}z_{ki}}{R_{ij}y_{ki} - R_{ik}y_{ji}} \quad (19)$$

$$C = \frac{R_{ik}\left[R_{ij}^2 + x_i^2 - x_j^2 + y_i^2 - y_j^2 + z_i^2 + z_j^2\right] - R_{ij}\left[R_{ik}^2 + x_i^2 - x_k^2 + y_i^2 - y_k^2 + z_i^2 + z_k^2\right]}{2\left[R_{ij}y_{ki} - R_{ik}y_{ji}\right]} \quad (20)$$

$$D = \frac{R_{kl}x_{jk} - R_{kj}x_{lk}}{R_{kj}y_{lk} - R_{kl}y_{jk}} \quad (21)$$

$$E = \frac{R_{kl}z_{jk} - R_{kj}z_{lk}}{R_{kj}y_{lk} - R_{kl}y_{jk}} \quad (22)$$

$$F = \frac{R_{kl}\left[R_{kj}^2 + x_k^2 - x_j^2 + y_k^2 - y_j^2 + z_k^2 + z_j^2\right] - R_{kj}\left[R_{kl}^2 + x_k^2 - x_l^2 + y_k^2 - y_l^2 + z_k^2 + z_l^2\right]}{2\left[R_{kj}y_{lk} - R_{kl}y_{jk}\right]} \quad (23)$$

Solving Equations (16) and (17), gives a linear equation for x_0 in terms of z_0.

$$Ax_0 + Bz_0 + C = Dx_0 + Ez_0 + F \quad (24)$$

$$x_0 = Gz_0 + H \quad (25)$$

Where,

$$G = \frac{E - B}{A - D} \quad (26)$$

$$H = \frac{F - C}{A - D} \quad (27)$$

Substituting Equation (25) back into simplefied representation Equation (16) gives a linear equation for y_0 in terms of z_0.

$$y_0 = Iz_0 + J \quad (28)$$

Where,

$$I = AG + B \quad (29)$$

$$J = AH + C \quad (30)$$

Equations (25) and (28), if substituted back into simplefied representation of Equation (13) give

$$K = R_{ik}^2 + x_i^2 - x_k^2 + y_i^2 - y_k^2 + z_i^2 - z_k^2 + 2x_{ki}H + 2y_{ki}J \quad (31)$$

And,

$$L = 2[x_{ki}G + y_{ki}I + 2z_{ki}] \quad (32)$$

$$M = 4R_{ik}^2[G^2 + I^2 + 1] - L^2 \quad (33)$$

$$N = 8R_{ik}^2[G(x_i - H) + I(y_i - J) + z_i] + 2LK \quad (34)$$

$$O = 4R_{ik}^2\left[(x_i - H)^2 + (y_i - J)^2 + z_i^2\right] - K^2 \quad (35)$$

Final solution is as follows

$$z_0 = \frac{N}{2M} + \sqrt{\left(\frac{N}{2M}\right)^2 - \frac{O}{M}} \quad (36)$$

$$y_0 = Iz_0 + J \quad (37)$$

$$x_0 = Gz_0 + H \quad (38)$$

Finally after solving, the position of the target is obtained.

RESULT AND ANALYSIS

A python script was written to test on sample data because it is a high-level language and analysis of data is smoother and easier as compared to other programming languages. Source position is considered as *x, y, z*. The ranges differences R_{ij}, R_{ik}, R_{kj} and R_{kl} were calculated from the derived method above. This time difference of arrival means range difference is taken as input and by solving those hyperbolic equation mentioned above we found the source position as . This method applied to the projectile path of 1800 samples. The maximum range of 100km and height varies from zero to 35km approximately. In this simulation total, seven different locations are considered for receiver deployment. The proposed algorithm for estimating position using the TDOA method takes input of four different receivers so simulation was run on a total of 35 different combinations. All combinations of receiver measurements in different planes were analyzed. The behavior of all kinds of measurement was analyzed throughout the total path followed by the target. For showing the results of simulation we have considered only the best case and worst case.

The below figure shows the relation between the Range and Height,

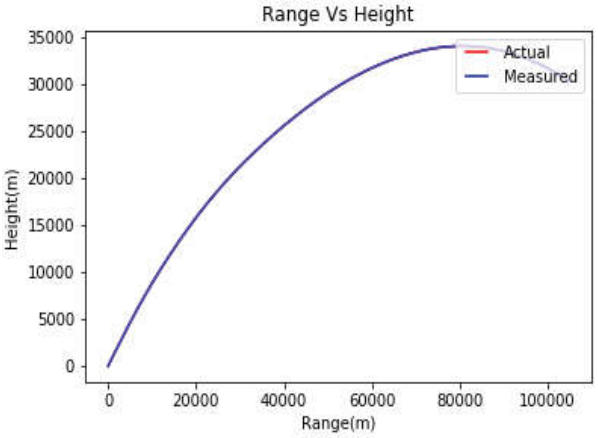

Fig. 2: Range vs Height (Best Case)

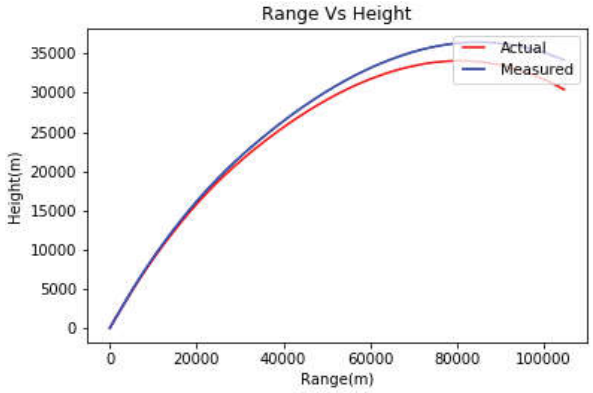

Fig. 3: Range vs Height (Worst Case)

Fig. 2 and Fig. 3 are showing the results of best and worst-case respectively in range vs height plane. In this case, it is clear that best-case results are overlapping but the differences of measurement are clearly visible in worst-case.

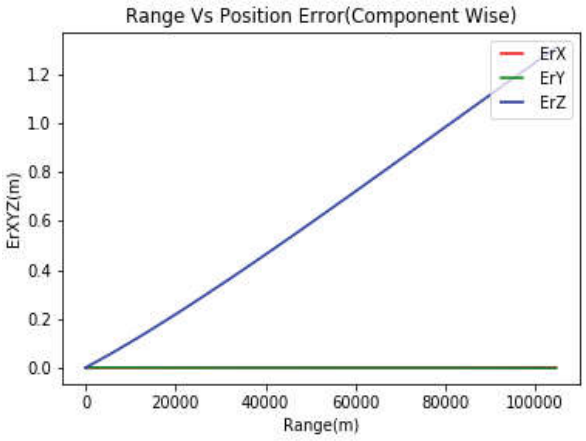

Fig. 4: Range vs Position Errors (Best Case)

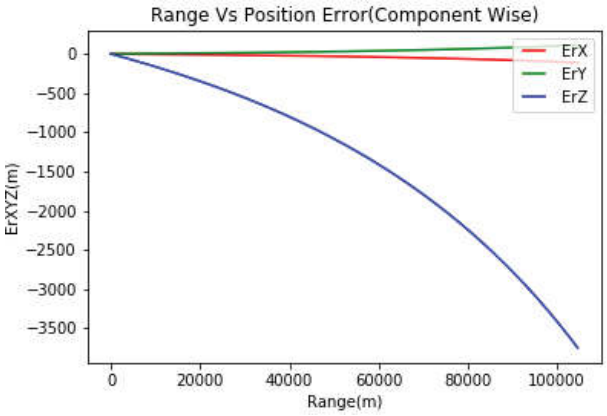

Fig. 5: Range vs Position Errors (Worst Case)

Fig. 4 and Fig. 5 are showing component-wise errors. An error was calculated by subtracting the actual and measured position in all three dimensions. Best case errors are in the order of 1 meter at 100km range. The worst-case maximum error reached up to 3.5km. All component errors are increasing as the range of the target increases. A similar pattern of component error was observed in all cases. Another important observation is that all the cases the major contribution of error comes in the z-axis. As all the receivers are along the same x-y plane so this hyperbolic equation solution produces more error in the z-axis.

Range difference error is calculated in the following manner.

$$R_{ij}Error = R_{ij} - r_{ij}$$

R_{ij} Calculated from the time difference of arrival and r_{ij} is calculated from the measured target position.

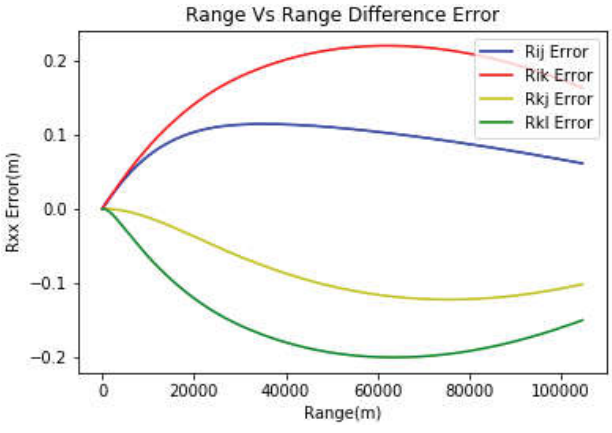

Fig. 6: Range vs Range Difference Errors (Best Case)

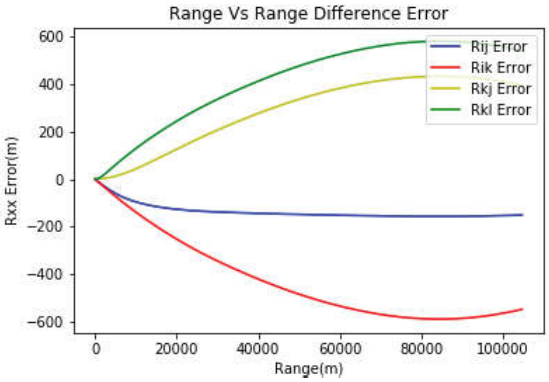

Fig. 7: Range vs Range Difference Errors (Worst Case)

Fig. 6 and Fig. 7 are showing the range difference error for all four combinations. Best case errors are in the order of .2 meter at 100km range. The worst-case maximum error reached up to 600meter. All combination errors are increasing as the range of the target increases. But at the end portion of the target location error is decreasing. As per the profile of the target, height is decreasing at the end portion. So the relation of range difference error depends upon range and height both. A similar pattern of error was observed in all cases.

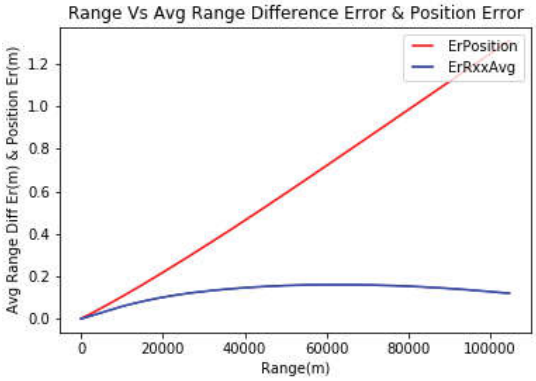

Fig. 8: Range vs Avg. Range Difference Errors and Position Error (Best Case)

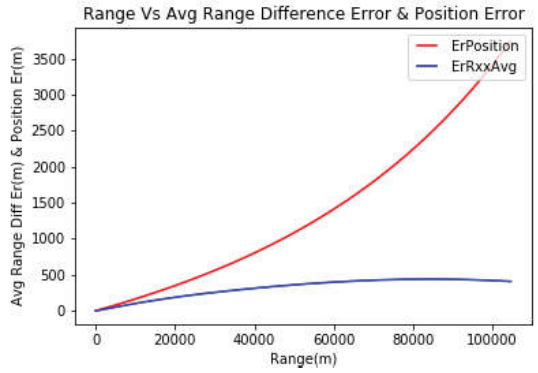

Fig. 9: Range vs Avg. Range Difference Errors and Position Error (Worst Case)

Fig. 8 and Fig. 9 are showing the position error and average range difference error. An error was calculated by subtracting the actual and measured position. Best case errors are in the order of 1 meter at 100km range. The worst-case maximum error reached up to 3.5km. Position error and average range difference error both are increasing as the range of the target increases. A similar pattern of error was observed in all cases.

To estimate the position measurement error average range difference error can be considered. In all cases, the relation between position errors varies with average range difference error linearly. And the same kind of results was observed in all cases from best case to worst case.

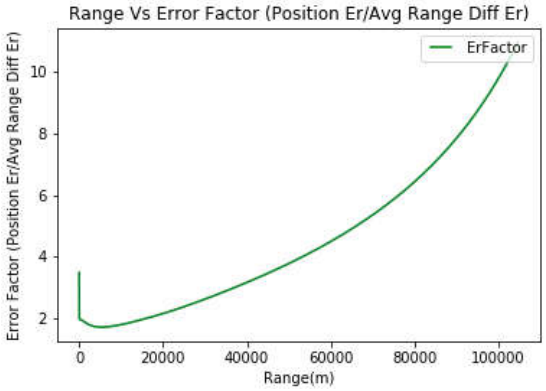

Fig. 10: Range vs Error Factor (Position Error/ Avg. Range Difference Errors) (Best Case)

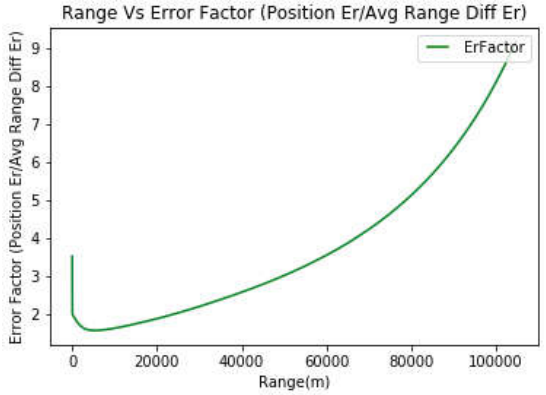

Fig. 11: Range vs Error Factor (Position Error/ Avg Range Difference Errors) (Worst Case)

An error factor is calculated just dividing position error by average range difference error.

Fig. 10 and Fig. 11 show the relation between error factors with range. The error factor is increasing as the range of target increases. A major observation is that error factor and range of target relationship is similar in all of the cases. In this best and worst case, it is clearly visible.

CONCLUSIONS AND FUTURE WORK

Target position finding algorithm using time difference of arrival considers four numbers of the receiver at a time to solve the hyperbolic equations. In our experiments, we considered four receivers at a time out of seven receivers, so we have a total of 35 numbers of combinations for the position finding of a target**.** As per the simulation results, it is clear that by calculating the average range difference error, we can prioritize the set of four-receiver location for minimum possible target position measurement error. The results were also able to establish the target position measurement error boundary. Error factor is calculated and the relation between target range and error factor is found linear irrespective of any combination of receivers. So our approach is able to find out the best possible combination of the receiver along with the target position measurement error boundary**.** The future study may be focused to find out more factors that can directly help in reducing the error boundary and prioritizing receivers. The probable target location zone could be formed using an error boundary. From this zone, one can simply assume the location of an incoming target. We are developing an automation tool, which will provide the position and measurement accuracy level of an incoming target with the help of the above result. It would be helpful for the aviation sector.

REFERENCES

Deligiannis N, Louvros S (2010) Hybrid TOA–AOA location positioning techniques in GSM networks. Wireless Personal Communications 54(2): 321-348.

Shin DH, Sung TK (2002) Comparisons of error characteristics between TOA and TDOA positioning. IEEE Transactions on Aerospace and Electronic Systems 38(1): 307-11.

Krizman KJ, Biedka TE, Rappaport TS. Wireless position location: fundamentals, implementation strategies, and sources of error. In 1997 IEEE 47th Vehicular Technology Conference. Technology in Motion; 1997 May 4; IEEE; 1997. pp. 919-923.

Friedlander B (1987) A passive localization algorithm and its accuracy analysis. IEEE Journal of Oceanic engineering 12(1): 234-245.

Kossonou KI, El Hillali Y, Bocquet M, Rivenq A, Assaad J (2014) Non-Iterative Three Dimensional Positioning Algorithm Based on Time Difference Of Arrival Technique. International Journal of Computer Science Issues; 2014 Mar 1; 11(2): 19.

He S, Dong X, Lu WS (2017) Localization algorithms for asynchronous time difference of arrival positioning systems. EURASIP Journal on Wireless Communications and Networking 1: 64.

Chan YT, Ho KC (1994) A simple and efficient estimator for hyperbolic location. IEEE Transactions on signal processing 42(8): 1905-1915.

Gustafsson F, Gunnarsson F. Positioning using time-difference of arrival measurements. In IEEE International Conference on Acoustics, Speech, and Signal Processing; 2003 Apr 6 2003; IEEE. Proceedings 2003, pp. VI-553.

Potluri S (2001) Hyperbolic position location estimator with tdoas from four stations. MS thesis, Van Houten library, NJIT University.

Fang BT (1990) Simple solutions for hyperbolic and related position fixes**.** IEEE transactions on aerospace and electronic systems 26(5): 748-753.

Science and Technology Journal, Vol. 7 Issue: I ISSN: 2321-3388

Some Results on Weakly Symmetric Kenmotsu Manifolds

J. P. Singh[1] and K. Lalnunsiami[2]*
Department of Mathematics & Computer Science, Mizoram University,
Aizawl-796004, Mizoram, India
E-mail: *siamiofficial@gmail.com

Abstract—In this paper, we investigate weakly symmetric, weakly Ricci symmetric, weakly concircular symmetric and weakly concircular Ricci symmetric properties of a Kenmotsu manifold admitting a semi-symmetric metric connection. Some results on weakly -projectively symmetric Kenmotsu manifold with respect to a semi-symmetric metric connection are obtained. An example of a weakly symmetric and weakly Ricci symmetric Kenmotsu manifold with respect to this connection is constructed.

Keywords: Weakly Ricci Symmetric Manifold, Weakly Concircular Symmetric Manifold, Weakly Concircular Ricci Symmetric Manifold, *m*-Projective Curvature Tensor, Weakly *m*-Projectively Symmetric Manifold.

2010 Mathematics Subject Classification: 53C15; 53C25; 53B05.

INTRODUCTION

Friedman and Schouten (1924) first studied semi-symmetric metric connection on a differentiable manifold. Hayden (1932) initiated the notion of a metric connection with torsion. Semi-symmetric metric connections were also investigated by Prvanovic (1975), Amur and Pujar (1978), Binh (1990), De and Biswas (1997) and many other geometers.

A semi-symmetric connection in a Riemmanian manifold is defined by Friedman and Schouten (1924) as a connection ∇ whose torsion tensor T satisfies

$$T(X_1, X_2) = \eta(X_2)X_1 - \eta(X_1)X_2, \tag{1.1}$$

where $g(X_1, \xi) = \eta(X_1)$ is a 1-form and ξ is a (1, 1) tensor field for all vector fields $X_1, X_2 \in \chi(M^n)$ where $\chi(M^n)$ is the set of all differentiable vector fields in M^n. In addition, if $\nabla g = 0$, then ∇ is known as a semi-symmetric metric connection.

The notion of a Kenmotsu manifold was first introduced by Kenmotsu (1972). A Kenmotsu manifold is not Sasakian. Weakly symmetric and weakly Ricci symmetric manifolds were first studied by Tamassy and Binh (1992). De and Ghosh (2005) defined the weakly concircular Ricci symmetric manifolds. Shaikh and Hui (2009) initiated the notion of weakly concircular symmetric manifolds.

A non-flat Riemannian manifold $M^n (n > 2)$ is called a weakly symmetric manifold (Tamassy and Binh 1992) if $\exists$ 1-forms B_1, B_2, B_3, B_4 not simultaneously zero such that the curvature tensor R satisfies

$$(\nabla_{X_1} R)(X_2, X_3)X_4 = B_1(X_1)R(X_2, X_3)X_4 + B_2(X_2)R(X_1, X_3)X_4 + B_3(X_3)R(X_2, X_1)X_4 + B_4(X_4)R(X_2, X_3)X_1 + g(R(X_2, X_3)X_4, X_1)P, \tag{1.2}$$

for all $X_1, X_2, X_3, X_4 \in \chi(M^n)$ and ∇ is the operator of covariant differentiation with respect to the Riemannian metric g.

A Riemannian manifold $M^n (n > 2)$ is known as a weakly Ricci symmetric manifold (Tamassy and Binh 1992) if $\exists$ 1-forms A_1, A_2, A_3, not simultaneously zero such that the Ricci tensor S is not identically zero and satisfies

$$(\nabla_{X_1} S)(X_2, X_3) = A_1(X_1)S(X_2, X_3) + A_2(X_2)S(X_1, X_3) + A_3(X_3)S(X_2, X_1), \tag{1.3}$$

for all $X_1, X_2, X_3 \in X(M^n)$.

A Riemannian manifold $M^n (n > 2)$ is said to be a weakly concircular symmetric manifold (Shaikh and Hui 2009) if $\exists$ $\exists$ 1-forms B_1, B_2, B_3, B_4, B_5 such that

$$(\nabla_{X_1} C)(X_2, X_3, X_4, X_5) = B_1(X_1)C(X_2, X_3, X_4, X_5) + B_2(X_2)C(X_1, X_3, X_4, X_5) + B_3(X_3)C(X_2, X_1, X_4, X_5) + B_4(X_4)C(X_2, X_3, X_1, X_5) + B_5(X_5)C(X_2, X_3, X_4, X_1), \tag{1.4}$$

http://doi.org/10.22232/stj.2019.07.01.02

where B_1, B_2, B_3, B_4, B_5 are not simultaneously zero and the concircular curvature tensor C is given by

$$C(X_2, X_3, X_4, X_5) = R(X_2, X_3, X_4, X_5) - \frac{r}{n(n-1)}[g(X_3, X_4)g(X_2, X_5) - g(X_2, X_4)g(X_3, X_5)] \quad (1.5)$$

is not identically zero, r being the scalar curvature of the manifold.

A Riemannian manifold $M^n(n > 2)$ is called a weakly concircular Ricci symmetric manifold (De and Ghosh 2005) if $\exists$ 1-forms A_1, A_2, A_3, not simultaneously zero such that the concircular Ricci tensor P given by

$$P(X_1, X_2) = \sum_{i=1}^{n} C(E_i, X_1, X_2, E_i) = S(X_1, X_2) - \frac{r}{n} g(X_1, X_2), \quad (1.6)$$

is not identically zero and satisfies

$$(\nabla_{X_1} P)(X_2, X_3) = A_1(X_1)P(X_2, X_3) + A_2(X_2)P(X_1, X_3) + A_3(X_3)P(X_2, X_1), \quad (1.7)$$

for all $X_1, X_2, X_3 \in \chi(M^n)$.

The m-projective curvature tensor is given by Pokhariyal and Mishra (1971) as

$$M(X_1, X_2)X_3 = R(X_1, X_2)X_3 - \frac{1}{2(n-1)}[S(X_2, X_3)X_1 - S(X_1, X_3)X_2 + g(X_2, X_3)QX_1 - g(X_1, X_3)QX_2], \quad (1.8)$$

where $S(X_1, X_2) = g(QX_1, X_2)$ is the Ricci tensor of type (0, 2) and Q is the Ricci operator.

Since the properties of the Riemannian curvature tensor are also the properties of the m-projective curvature tensor, we can define a weakly m-projectively symmetric manifold as a non m-projectively flat manifold $M^n(n > 2)$ where

$$(\nabla_{X_1} M)(X_2, X_3, X_4, X_5) = A_1(X_1)M(X_2, X_3, X_4, X_5) + A_2(X_2)M(X_1, X_3, X_4, X_5) + A_3(X_3)M(X_2, X_1, X_4, X_5) + A_4(X_4)M(X_2, X_3, X_1, X_5) + A_5(X_5)M(X_2, X_3, X_4, X_1), \quad (1.9)$$

where $M(X_2, X_3, X_4, X_5) = g(M(X_2, X_3)X_4, X_5)$ is the associative m-projective curvature tensor for all vector fields X_1, X_2, X_3, X_4, $X_5 \in X(M^n)$.

In 2015, Prakasha and Vikas studied weakly symmetric properties of Kenmotsu manifolds admitting a quarter-symmetric metric connection. This motivated us to study the properties of these manifolds with respect to a semi-symmetric metric connection.

This paper is divided into sections as follows: Section 2 is on a brief study of Kenmotsu manifolds. In section 3, we have some basic results on Kenmotsu manifolds admitting a semi-symmetric metric connection. Sections 4 and 5 are devoted to the study of weakly symmetric and weakly Ricci symmetric Kenmotsu manifolds admitting a semi-symmetric metric connection. In section 6, some results on weakly concircular and weakly concircular Ricci symmetric Kenmotsu manifolds with respect to a semi-symmetric metric connection are obtained. In section 7, we study some properties of a weakly m-projectively symmetric Kenmotsu manifold admitting a semi-symmetric metric connection. Finally, we construct an example of a weakly symmetric Kenmotsu manifolds with respect to a semi-symmetric metric connection which is also weakly Ricci symmetric.

PRELIMINARIES

An $n(= 2m + 1)$– dimensional differentiable manifold $M^n(n > 2)$ is called an almost contact manifold (Blair 1976) if $\exists$ an almost contact structure (φ, ξ, η, g) satisfying or equivalently,

$$\eta(\xi) = 1, \quad \varphi(\xi) = 0, \quad \eta(\varphi X_1) = 0, \quad (2.1)$$

$$g(\varphi X_1, \varphi X_2) = g(X_1, X_2) - \eta(X_1)\eta(X_2), \quad (2.2)$$

or equivalently,

$$g(X_1, \varphi X_2) = -g(\varphi X_1, X_2), \quad g(X_1, \xi) = \eta(X_1), \quad (2.3)$$

where φ is a (1, 1) tensor field, ξ is a vector field, η is a 1-form and g is the Riemmanian metric. In addition, if

$$\nabla_{X_1}\xi = X_1 - \eta(X_1)\xi, \quad (2.4)$$

$$(\nabla_{X_1}\varphi)(X_2) = g(\varphi X_1, X_2)\xi - \eta(X_2), \quad (2.5)$$

$$(\nabla_{X_1}\eta)(X_2) = g(X_1, X_2) - \eta(X_1)\eta(X_2), \quad (2.6)$$

where, X_1, X_2, $X_3 \in X(M^n)$ then M^n is called a Kenmotsu manifold. Here, ∇ is the operator of covariant differentiation with respect to the metric g.

In a Kenmotsu manifold, we have the following relations (Kenmotsu 1972):

$$R(X_1, X_2)\xi = \eta(X_1)X_2 - \eta(X_2)\xi, \quad (2.7)$$

$$R(X_1, \xi)X_2 = g(X_1, X_2)\xi - \eta(X_2)X_1, \quad (2.8)$$

$$R(\xi, X_1)\xi = X_1 - \eta(X_1)\xi, \quad (2.9)$$

$$S(X_1, \xi) = (n-1)\eta(X_1), \quad (2.10)$$

$$S(\xi, \xi) = (n-1), \quad (2.11)$$

where $X_1, X_2 \in X(M^n)$ and R and S are the Riemmanian curvature tensor and the Ricci tensor of M^n respectively.

SEMI-SYMMETRIC METRIC CONNECTION IN A KENMOTSU MANIFOLD

A semi-symmetric metric connection in a Kenmotsu manifold is given by Yano (1970) as

$$\tilde{\nabla}_{X_1} X_2 = \nabla_{X_1} X_2 + \eta(X_2)X_1 - g(X_1, X_2)\xi. \quad (3.1)$$

A relation between the Riemmanian curvature tensor R with respect to the Levi-Civita connection ∇ and the curvature tensor $\tilde{R}$ with respect to the semi-symmetric metric connection $\tilde{\nabla}$ is obtained as (Prakasha *et al.* 2013)

$$\tilde{R}(X_1, X_2)X_3 = R(X_1, X_2)X_3 - 3[g(X_2, X_3)X_1 - g(X_1, X_3)X_2] + 2[\eta(X_2)X_1 - \eta(X_1)X_2]\eta(X_3) - 2[g(X_1, X_3)\eta(X_2) - g(X_2, X_3)\eta(X_1)]\xi. \quad (3.2)$$

On contracting equation (3.2), we obtain

$$\tilde{S}(X_1, X_2) = S(X_1, X_2) - (3n-5)\, g(X_1, X_2) + 2(n-2)\eta(X_1)\eta(X_2), \quad (3.3)$$

where $\tilde{S}$ and S are the Ricci tensors with respect to the semi-symmetric metric connection $\tilde{\nabla}$ and the Levi-Civita connection ∇ respectively. Again by contraction, (3.3) reduces to

$$\tilde{r} = r - 2(n-1), \quad (3.4)$$

where $\tilde{r}$ and r are the scalar curvatures with respect to $\tilde{\nabla}$ and $\tilde{\nabla}$ respectively.

By making use of equations (2.2), (2.7), (2.8), (2.9), (2.10) and (2.11), we obtain

$$\tilde{R}(X_1, X_2)\xi = 2[\eta(X_1)X_2 - \eta(X_2)\xi], \quad (3.5)$$

$$\tilde{R}(X_1, \xi)X_2 = 2[g(X_1, X_2)\xi - \eta(X_2)X_1], \quad (3.6)$$

$$\tilde{R}(\xi, X_1)\xi = 2[X_1 - \eta(X_1)\xi], \quad (3.7)$$

$$\tilde{S}(X_1, \xi) = 2[(n-1)\eta(X_1)], \quad (3.8)$$

$$\tilde{S}(\xi, \xi) = 2(n-1). \quad (3.9)$$

WEAKLY SYMMETRIC KENMOTSU MANIFOLDS ADMITTING A SEMI-SYMMETRIC METRIC CONNECTION

Definition 4.1. A non-flat Kenmotsu manifold $M^n(n > 2)$ is called a weakly symmetric Kenmotsu manifold with respect to the semi-symmetric metric connection $\tilde{\nabla}$ if $\exists$ 1-forms B_1, B_2, B_3, B_4, not simultaneously zero and the curvature tensor $\tilde{R}$ with respect to the semi-symmetric metric connection $\tilde{\nabla}$ satisfies

$$(\tilde{\nabla}_{X_1}\tilde{R})(X_2, X_3)X_4 = B_1(X_1)\tilde{R}(X_2, X_3)X_4 + B_2(X_2)\tilde{R}(X_1, X_3)X_4 + B_3(X_3)\tilde{R}(X_2, X_1)X_4 + B_4(X_4)\tilde{R}(X_2, X_3)X_1 + g(\tilde{R}(X_2, X_3)X_4, X_1)P, \quad (4.1)$$

for all vector fields $X_1, X_2, X_3, X_4 \in X(M^n)$.

Theorem 4.1: In a weakly symmetric Kenmotsu manifold with respect to a semi-symmetric metric connection $\tilde{\nabla}$, the sum of the 1-forms $B_1 + B_3 + B_4$ vanishes.

Proof: Suppose equation (4.1) holds. Then, by contracting (4.1) with respect to, X_2 we obtain

$$(\tilde{\nabla}_{X_1}\tilde{S})(X_3, X_4) = B_1(X_1)\,\tilde{S}(X_3, X_4) + B_2(\tilde{R}(X_1, X_3)X_4) + B_3(X_3)\,\tilde{S}(X_1, X_4) + B_4(X_4)\tilde{S}(X_3, X_1) + B(\tilde{R}(X_1, X_4)X_3), \quad (4.2)$$

where $B(X_1) = g(X_1, P)$. Replacing X_4 by ξ in equation (4.2), we have

$$(\tilde{\nabla}_{X_1}\tilde{S})(X_3, \xi) = B_1(X_1)\,\tilde{S}(X_3, \xi) + B_2(\tilde{R}(X_1, X_3)\xi) + B_3(X_3)\,\tilde{S}(X_1, \xi) + B_4(\xi)\tilde{S}(X_3, X_1) + B(\tilde{R}(X_1, \xi)X_3). \quad (4.3)$$

Applying equations (3.5), (3.7), (3.8) in (4.3), we get

$$(\tilde{\nabla}_{X_1}\tilde{S})(X_3, \xi) = -2(n-1)[B_1(X_1)\eta(X_3) + B_3(X_3)\eta(X_1)] + 2\eta(X_1)B_2(X_3) - 2\eta(X_3)[B_2(X_1) + B(X_1)] + B_4(\xi)\tilde{S}(X_1, X_3) + 2B(\xi)g(X_1, X_3). \quad (4.4)$$

Also,

$$(\tilde{\nabla}_{X_1}\tilde{S})(X_3, \xi) = \tilde{\nabla}_{X_1}\tilde{S}(X_3, \xi) - \tilde{S}(X_3, \tilde{\nabla}_{X_1}\xi) - \tilde{S}(\tilde{\nabla}_{X_1}X_3, \xi). \quad (4.5)$$

Using (2.3), (3.1) in (4.5), we get

$$(\tilde{\nabla}_{X_1}\tilde{S})(X_3, \xi) = -4(n-1)[g(X_1, X_3) - \eta(X_1)\eta(X_3)] - 2\tilde{S}(X_1, X_3) - \eta(X_1)\xi. \quad (4.6)$$

Comparing (4.4) and (4.6), we obtain

$$-4(n-1)[g(X_1,X_3)-\eta(X_1)\eta(X_3)]-2\tilde{S}(X_1,X_3)-\eta(X_1)\xi$$
$$=-2(n-1)[B_1(X_1)\eta(X_3)+B_3(X_3)\eta(X_1)]$$
$$+2\eta(X_1)B_2(X_3)-2\eta(X_3)[B_2(X_1)+B(X_1)]$$
$$+B_4(\xi)\tilde{S}(X_1,X_3)+2B(\xi)g(X_1,X_3). \quad (4.7)$$

Taking $X_1 = X_3 = \xi$,in (4.7), we have

$$-2(n-1)[B_1(\xi)+B_3(\xi)+B_4(\xi)]=0.$$

Since, this implies

$$B_1(\xi)+B_3(\xi)+B_4(\xi)=0. \quad (4.8)$$

In (4.2), we take $X_3 = \xi$ and get,

$$(\tilde{\nabla}_{X_1}\tilde{S})(\xi,X_4)=-2(n-1)[B_1(X_1)\eta(X_4)+B(X_4)\eta(X_1)]+2B_2(\xi)g(X_1,X_4)$$
$$-2\eta(X_4)[B_2(X_1)+B(X_1)]+2B(X_4)\eta(X_1)+B_3(\xi). \quad (4.9)$$

Also,

$$(\tilde{\nabla}_{X_1}\tilde{S})(\xi,X_4)=-4(n-1)[g(X_1,X_4)-\eta(X_1)\eta(X_4)]-2\tilde{S}(X_1-\eta(X_1)\xi,X_4). \quad (4.10)$$

Using (4.9) in (4.10) we obtain,

$$-4(n-1)[g(X_1,X_4)-\eta(X_1)\eta(X_4)]-2\tilde{S}(X_1-\eta(X_1)\xi,X_4)$$
$$=-2(n-1)[B_1(X_1)\eta(X_4)+B(X_4)\eta(X_1)]+2B_2(\xi)g(X_1,X_4)$$
$$-2\eta(X_4)[B_2(X_1)+B(X_1)]+2B(X_4)\eta(X_1)+B_3(\xi). \quad (4.11)$$

Setting $X_4 = \xi$ in (4.11), we get

$$-2(n-1)[B_1(X_1)+B_3(\xi)\eta(X_1)+B_4(\xi)\eta(X_1)]+2B_2(\xi)\eta(X_1)$$
$$+2B(\xi)\eta(X_1)-2[B_2(X_1)+B(X_1)]=0. \quad (4.12)$$

Take $X_1 = \xi$ in (4.11), we obtain

$$-2(n-1)[B_1(\xi)\eta(X_4)+B_4(X_4)+B_3(\xi)\eta(X_4)]$$
$$-2\eta(X_4)B(\xi)+2B(X_4)=0. \quad (4.13)$$

On replacing X_4 by X_1 in (4.13) we have

$$-2(n-1)[B_1(\xi)\eta(X_1)+B_4(X_1)+B_3(\xi)\eta(X_1)]$$
$$-2\eta(X_1)B(\xi)+2B(X_1)=0. \quad (4.14)$$

Adding (4.12) and (4.14) and using equation (4.8), we obtain

$$-2(n-1)[B_1(X_1)+B_4(X_1)+B_3(\xi)\eta(X_1)]$$
$$+2B_2(\xi)\eta(X_1)-2B_2(X_1)=0. \quad (4.15)$$

Substituting $X_1 = \xi$ in (4.7) we have,

$$-2(n-1)[B_1(\xi)\eta(X_3)+B_3(X_3)+B_4(\xi)\eta(X_3)]$$
$$+2B_2(\xi)\eta(X_3)+2B_2(X_3)=0. \quad (4.16)$$

Replacing X_3 by ξ,in (4.16), we get

$$-2(n-1)[B_1\xi)\eta(X_1)+B_3(X_1)+B_4(\xi)\eta(X_1)]$$
$$-2B_2(\xi)\eta(X_1)+2B_2(X_1)=0. \quad (4.17)$$

Adding (4.15) and (4.17) we obtain,

$$-2(n-1)[B_1(X_1)+B_3(X_1)+B_4(X_1)]=0,$$

which implies (since $n > 3$),

$$B_1(X_1)+B_3(X_1)+B_4(X_1)=0. \quad (4.18)$$

This proves the theorem.

WEAKLY RICCI SYMMETRIC KENMOTSU MANIFOLDS ADMITTING A SEMI-SYMMETRIC METRIC CONNECTION

Definition 5.1: A non-flat Kenmotsu manifold $M^n(n > 2)$ is said to be weakly Ricci symmetric with respect to the semi-symmetric metric connection $\tilde{\nabla}$ if $\exists$ 1-forms, A_1, A_2, A_3, not simultaneously zero and the Ricci tensor $\tilde{S}$ with respect to the semi-symmetric metric connection is not identically zero and satisfies

$$(\tilde{\nabla}_{X_1}\tilde{S})(X_2,X_3)=A_1(X_1)\tilde{S}(X_2,X_3)+A_2(X_2)\tilde{S}(X_1,X_3)$$
$$+A_3(X_3)\tilde{S}(X_2,X_1), \quad (5.1)$$

for all $X_1, X_2, X_3 \in \chi(M^n)$.

Theorem 5.1. The necessary condition for a Kenmotsu manifold with respect to the semi-symmetric metric connection $\tilde{\nabla}$ to be weakly Ricci symmetric with respect to $\tilde{\nabla}$ is that the sum of the associated 1-forms A_1, A_2, A_3 vanishes everywhere.

Proof: On replacing X_3 by ξ in (5.1), we obtain

$$(\tilde{\nabla}_{X_1}\tilde{S})(X_2,\xi)=A_1(X_1)\tilde{S}(X_2,\xi)+A_2(X_2)\tilde{S}(X_1,\xi)$$
$$+A_3(\xi)\tilde{S}(X_2,X_1), \quad (5.2)$$

which implies on using equation (4.7),

$$-4(n-1)[g(X_1,X_2)-\eta(X_1)\eta(X_2)]-2\tilde{S}(X_2,X_1-\eta(X_1)\xi)$$
$$=-2(n-1)[A_1(X_1)\eta(X_2)+A_2(X_2)\eta(X_1)]+A_3(\xi)\tilde{S}(X_1,X_2). \quad (5.3)$$

In (4.10), taking $X_1 = X_2 = \xi$ we get

$$A_1(\xi)+A_2(\xi)+A_3(\xi)=0. \quad (5.4)$$

Now, substituting $X_2 = \xi$ equation (5.4) becomes

$$A_1(X_1)=A_1(\xi)\eta(X_1). \quad (5.5)$$

Similarly, we can obtain

$$A_2(X_2) = A_2(\xi)\eta(X_2), \tag{5.6}$$

and

$$A_3(X_3) = A_3(\xi)\eta(X_3). \tag{5.7}$$

Taking the sum of (5.5), (5.6) and (5.7), we obtain

$$A_1(X_1) + A_2(X_1) + A_3(X_1) = 0. \tag{5.8}$$

This proves the theorem.

WEAKLY CONCIRCULAR SYMMETRIC AND WEAKLY CONCIRCULAR RICCI KENMOTSU MANIFOLDS ADMITTING A SEMI-SYMMETRIC CONNECTION

Definition 6.1. A Kenmotsu manifold $M^n(n > 2)$ is called a weakly concircular symmetric Kenmotsu manifold with respect to the semi-symmetric metric connection $\tilde{\nabla}$ if $\exists$ 1-forms (not simultaneously zero) B_1, B_2, B_3, B_4, B_5 such that

$$\begin{aligned}(\tilde{\nabla}_{X_1}\tilde{C})(X_2,X_3,X_4,X_5) &= B_1(X_1)\tilde{C}(X_2,X_3,X_4,X_5)\\ &+ B_2(X_2)\tilde{C}(X_1,X_3,X_4,X_5)+B_3(X_3)\tilde{C}(X_2,X_1,X_4,X_5)\\ &+ B_4(X_4)\tilde{C}(X_2,X_3,X_1,X_5)+B_5(X_5)\tilde{C}(X_2,X_3,X_4,X_1),\end{aligned} \tag{6.1}$$

where

$$\tilde{C}(X_2,X_3,X_4,X_5) = \tilde{R}(X_2,X_3,X_4,X_5) - \frac{\tilde{r}}{n(n-1)}[g(X_3,X_4)g(X_2,X_5) - g(X_2,X_4)g(X_3,X_5)]$$

is the concircular curvature tensor which is not identically zero.

In a weakly concircular symmetric Kenmotsu manifold admitting a semi-symmetric metric connection, $B_2 = B_3$ and $B_4 = B_5$. So (6.1) can be written as

$$\begin{aligned}(\tilde{\nabla}_{X_1}\tilde{C})(X_2,X_3,X_4,X_5) &= B_1(X_1)\tilde{C}(X_2,X_3,X_4,X_5)\\ &+ B_2(X_2)\tilde{C}(X_1,X_3,X_4,X_5)+B_2(X_3)\tilde{C}(X_2,X_1,X_4,X_5)\\ &+ B_4(X_4)\tilde{C}(X_2,X_3,X_1,X_5)+B_4(X_5)\tilde{C}(X_2,X_3,X_4,X_1).\end{aligned} \tag{6.2}$$

Substituting $X_2 = X_5 = E_i$ in (6.2) and taking summation over i, $1 \le i \le n$, we get

$$\begin{aligned}(\tilde{\nabla}_{X_1}\tilde{S})(X_3,X_4) - \frac{d\tilde{r}}{n}g(X_3,X_4) &= B_1(X_1)[\tilde{S}(X_3,X_4) - \frac{\tilde{r}}{n}g(X_3,X_4)]\\ &+B_2(X_3)[\tilde{S}(X_1,X_4) - \tfrac{\tilde{r}}{n}g(X_1,X_4)]\\ &+B_4(X_4)[\tilde{S}(X_3,X_1) - \frac{\tilde{r}}{n}g(X_3,X_1)]\\ &+B_2(\tilde{R}(X_1,X_3)X_4) + B_4(\tilde{R}(X_1,X_4)X_3)\\ &-\frac{\tilde{r}}{n(n-1)}[g(X_3,X_4)\{B_2(X_1) + B_4(X_1)\}\\ &-B_2(X_3)g(X_1,X_4) - B_4(X_4)g(X_1,X_3)].\end{aligned} \tag{6.3}$$

Taking $X_1 = X_3 = X_4 = \xi$, equation (6.3) reduces to

$$B_1(\xi) + B_2(\xi) + B_4(\xi) = \frac{dr}{\tilde{r} + 2n(n-1)}, \tag{6.4}$$

provided $\tilde{r} + 2n(n-1) \neq 0$.

Substituting X_1, X_3 by ξ in (6.3) and using (6.4), we have

$$B_4(X_4) = B_4(\xi)\eta(X_4). \tag{6.5}$$

Similarly, on substituting X_1, X_4 by ξ in (6.3) and using (6.4), we obtain

$$B_2(X_3) = B_2(\xi)\eta(X_3), \tag{6.6}$$

and taking $X_3 = X_4 = \xi$, in (57) and using equations (3.5), (6.4), (6.5) and (6.6) we get

$$B_1(X_1) = \frac{d\tilde{r}}{\tilde{r} + 2n(n-1)}[B_2(\xi) + B_4(\xi)]\eta(X_1). \tag{6.7}$$

This leads to the following theorem:

Theorem 6.1: In a weakly concircular symmetric Kenmotsu manifold admitting a semi-symmetric metric connection $\tilde{\nabla}$, the sum of the associated 1-forms B_1, B_2, B_4, is given by (6.7).

Definition 6.2: A Kenmotsu manifold $M^n(n > 2)$ is called a weakly concircular Ricci symmetric manifold with respect to the semi-symmetric metric connection $\tilde{\nabla}$ if $\exists$ 1-forms A_1, A_2, A_3, , not simultaneously zero such that the concircular Ricci tensor $\tilde{p}$ with respect to $\tilde{\nabla}$ given by

$$\tilde{P}(X_1,X_2) = \sum_{i=1}^{n}\tilde{C}(E_i,X_1,X_2,E_i) = \tilde{S}(X_1,X_2) - \frac{r}{n}g(X_1,X_2)$$

is not identically zero and satisfies

$$\begin{aligned}(\tilde{\nabla}_{X_1}\tilde{P})(X_2,X_3) &= A_1(X_1)\tilde{P}(X_2,X_3) + A_2(X_2)\tilde{P}(X_1,X_3)\\ &+ A_3(X_3)\tilde{P}(X_2,X_1),\end{aligned} \tag{6.8}$$

for all $X_1, X_2, X_3 \in \chi(M^n)$.

Suppose (6.8) holds. Then, we have

$$\begin{aligned}(\tilde{\nabla}_{X_1}\tilde{S})(X_2,X_3) - \frac{d\tilde{r}(X_1)}{n}g(X_2,X_3) &= A_1(X_1)\left[\tilde{S}(X_2,X_3) - \frac{\tilde{r}}{n}g(X_2,X_3)\right]\\ &+A_2(X_2)\left[\tilde{S}(X_1,X_3) - \frac{\tilde{r}}{n}g(X_1,X_3)\right]\\ &+A_3(X_3)\left[\tilde{S}(X_2,X_1) - \tfrac{\tilde{r}}{n}g(X_2,X_1)\right].\end{aligned} \tag{6.9}$$

On replacing X_1, X_2, X_3 by ξ, in (6.9), we obtain

$$A_1(\xi) + A_2(\xi) + A_3(\xi) = \frac{d\tilde{r}(\xi)}{\tilde{r}+2n(n-1)}, \quad (6.10)$$

provided $\tilde{r} + 2n(n-1) \neq 0$.

Taking $X_1 = X_2 = \xi$ in (6.9) and using (6.8), we get

$$A_3(X_3) = A_3(\xi)\eta(X_3). \quad (6.11)$$

Similarly, replacing X_1, X_3 by ξ,and using (6.10), (6.9) becomes

$$A_2(X_2) = A_2(\xi)\eta(X_2) \quad (6.12)$$

and replacing X_2, X_3 by ξ,in (6.9) and using (6.10), we get

$$A_1(X_1) = \frac{d\tilde{r}(X_1)}{\tilde{r}+2n(n-1)} + \left[A_1(\xi) - \frac{d\tilde{r}(\xi)}{\tilde{r}+2n(n-1)}\right]\eta(X_1), \quad (6.13)$$

provided $\tilde{r} + 2n(n-1) \neq 0$.

Adding equations (6.11), (6.12) and (6.13), we have

$$A_1(X_1) + A_2(X_1) + A_3(X_1) = \frac{d\tilde{r}(X_1)}{\tilde{r} + 2n(n-1)}, \quad (6.14)$$

provided $\tilde{r} + 2n(n-1) \neq 0$. This leads to the following theorem:

Theorem 6.2: The sum of the associated 1-forms A_1, A_2, A_3 in a weakly concircular Ricci symmetric Kenmotsu manifold which admits a semi-symmetric metric connection $\tilde{\nabla}$ is given by (6.14).

WEAKLY *m*-PROJECTIVELY SYMMETRIC KENMOTSU MANIFOLDS ADMITTING A SEMI-SYMMETRIC METRIC CONNECTION

Definition 7.1: A non *m*-projectively flat Kenmotsu manifold $M^n(n > 2)$ is said to be weakly *m*-projectively flat with respect to the semi-symmetric metric connection $\tilde{\nabla}$ if the *m*-projective curvature tensor $\tilde{M}$ with respect to the connection $\tilde{\nabla}$ given by

$$\tilde{M}(X_1, X_2)X_3 = \tilde{R}(X_1, X_2)X_3 - \frac{1}{2(n-1)}[\tilde{S}(X_2, X_3)X_1 - \tilde{S}(X_1, X_3)X_2 + g(X_2, X_3)\tilde{Q}X_1 - g(X_1, X_3)\tilde{Q}X_2], \quad (7.1)$$

is not identically zero and satisfies

$$(\tilde{\nabla}_{X_1}\tilde{M})(X_2, X_3, X_4, X_5) = A_1(X_1)\tilde{M}(X_2, X_3, X_4, X_5) + A_2(X_2)\tilde{M}(X_1, X_3, X_4, X_5) + A_3(X_3)\tilde{M}(X_2, X_1, X_4, X_5) + A_4(X_4)\tilde{M}(X_2, X_3, X_1, X_5) + A_5(X_5)\tilde{M}(X_2, X_3, X_4, X_1), \quad (7.2)$$

for all vector fields $X_1, X_2, X_3, X_4, X_5, \in \chi(M^n)$ and A_1, A_2, A_3, A_4, A_5 are 1-forms, not simultaneously zero.

In a weakly *m*-projectively symmetric Kenmotsu manifold admitting a semi-symmetric metric connection, $A_2 = A_3, A_4 = A_5$. So (7.2) can be written as

$$(\tilde{\nabla}_{X_1}\tilde{M})(X_2, X_3, X_4, X_5) = A_1(X_1)\tilde{M}(X_2, X_3, X_4, X_5) + A_2(X_2)\tilde{M}(X_1, X_3, X_4, X_5) + A_2(X_3)\tilde{M}(X_2, X_1, X_4, X_5) + A_4(X_4)\tilde{M}(X_2, X_3, X_1, X_5) + A_4(X_5)\tilde{M}(X_2, X_3, X_4, X_1). \quad (7.3)$$

From equation (7.1), we can obtain

$$\sum_{i=1}^{n} \tilde{M}(E_i, X_2, X_3, E_i) = \frac{n}{2(n-1)}\left[\tilde{S}(X_2, X_3) - \frac{\tilde{r}}{n}g(X_2, X_3)\right] = \frac{n}{2(n-1)}\tilde{W}(X_2, X_3), \quad (7.4)$$

where $\tilde{W}(X_2, X_3) = \tilde{S}(X_2, X_3) - \frac{\tilde{r}}{n}g(X_2, X_3)$.

Also,

$$\sum_{i=1}^{n} \tilde{M}(X_1, X_2, E_i, E_i) = 0, \quad (7.5)$$

$$\sum_{i=1}^{n} \tilde{M}(E_i, E_i, E_i, E_i) = 0. \quad (7.6)$$

Also, the *m*-projective curvature tensor $\tilde{M}$ with respect to $\tilde{\nabla}$ satisfies

$$\tilde{M}(X_1, X_2, X_3, X_4) + \tilde{M}(X_2, X_3, X_1, X_4) + \tilde{M}(X_3, X_1, X_2, X_4) = 0, \quad (7.7)$$

$$\tilde{M}(X_1, X_2, X_4, X_3) + \tilde{M}(X_2, X_3, X_4, X_1) + \tilde{M}(X_3, X_1, X_4, X_2) = 0. \quad (7.8)$$

NATURE OF THE SCALAR CURVATURE WITH RESPECT TO THE SEMI-SYMMETRIC METRIC CONNECTION

Let $\tilde{Q}$ be the Ricci operator with respect to the semi-symmetric metric connection $\tilde{\nabla}$defined by

$$g(\tilde{Q}X_1, X_2) = \tilde{S}(X_1, X_2).$$

Differentiating equation (7.7) covariantly along X_1 and using Bianchi identity, we get

$$(\tilde{\nabla}_{X_1}\tilde{M})(X_2,X_3,X_4,X_5)+(\tilde{\nabla}_{X_2}\tilde{M})(X_3,X_1,X_4,X_5)+$$
$$+(\tilde{\nabla}_{X_3}\tilde{M})(X_1,X_2,X_4,X_5)$$
$$=-\frac{1}{2(n-1)}[\{(\tilde{\nabla}_{X_1}\tilde{S})(X_3,X_4)-(\tilde{\nabla}_{X_3}S)(X_1,X_4)\}g(X_2,X_5)$$
$$+\{(\tilde{\nabla}_{X_2}\tilde{S})(X_1,X_4)-(\tilde{\nabla}_{X_1}\tilde{S})(X_2,X_4)\}g(X_3,X_5)$$
$$+\{(\tilde{\nabla}_{X_3}\tilde{S})(X_2,X_4)-(\tilde{\nabla}_{X_2}\tilde{S})(X_3,X_4)\}g(X_1,X_5)$$
$$+\{(\tilde{\nabla}_{X_1}\tilde{S})(X_2,X_5)-(\tilde{\nabla}_{X_2}\tilde{S})(X_1,X_5)\}g(X_3,X_4)$$
$$+\{(\tilde{\nabla}_{X_2}\tilde{S})(X_3,X_5)-(\tilde{\nabla}_{X_3}\tilde{S})(X_2,X_5)\}g(X_1,X_4)]. \quad (7.9)$$

Suppose the Ricci tensor $\tilde{S}$ is of Codazzi type, then

$$(\tilde{\nabla}_{X_1}\tilde{S})(X_2,X_3)=(\tilde{\nabla}_{X_2}\tilde{S})(X_1,X_3). \quad (7.10)$$

Using (7.10) in (7.9), we get

$$(\tilde{\nabla}_{X_1}\tilde{M})(X_2,X_3,X_4,X_5)+(\tilde{\nabla}_{X_2}\tilde{M})(X_3,X_1,X_4,X_5)+(\tilde{\nabla}_{X_3}\tilde{M})(X_1,X_2,X_4,X_5)=0. \quad (7.11)$$

Suppose (7.11) holds. Then, clearly the Ricci tensor $\tilde{S}$ is of Codazzi type. This leads to the theorem:

Theorem 7.1: In a weakly m-projectively symmetric Kenmotsu manifold, the Ricci tensor $\tilde{S}$ with respect to the semi-symmetric metric connection $\tilde{\nabla}$ is of Codazzi type if and only if the relation (7.11) holds.

Suppose the Ricci tensor $\tilde{S}$ is of Codazzi type. Then, (7.11) holds. Using (7.2) in (7.11), we get

$$\lambda(X_1)\tilde{M}(X_2,X_3,X_4,X_5)+\lambda(X_2)\tilde{M}(X_1,X_3,X_4,X_5)+\lambda(X_3)\tilde{M}(X_2,X_1,X_4,X_5)=0, \quad (7.12)$$

where, $\lambda(X_1)=A_1(X_1)-2A_2(X_1)$,

for all $X_1,X_2,X_3,X_4\in\chi(M^n)$.

Putting $X_2=X_5=E_i$ and taking summation over i, $1\le i\le n$, (7.12) reduces to

$$\frac{n}{2(n-1)}\left[\lambda(X_1)\tilde{S}(X_3,X_4)-\frac{\tilde{r}}{n}g(X_3,X_4)-\lambda(X_3)\tilde{S}(X_1,X_4)+\frac{\tilde{r}}{n}g(X_1,X_4)\right]=0. \quad (7.13)$$

Again, substituting $X_1=X_4=E_i$ in (7.12) and summing over i, $1\le i\le n$, we get $\lambda(\tilde{Q}X_3)=\frac{\tilde{r}}{n}\lambda(X_3)$, which implies that

$$\tilde{S}(X_3,X)=\frac{\tilde{r}}{n}g(X_3,X). \quad (7.14)$$

Thus, we have the theorem:

Theorem 7.2: If the Ricci tensor $\tilde{S}$ in a weakly m-projectively symmetric Kenmotsu manifold admitting a semi-symmetric metric connection $\tilde{\nabla}$ is of Codazzi type, then $\frac{\tilde{r}}{n}$ is an eigen value corresponding to the eigen vector X defined by $g(X_1,X)=\lambda(X_1)$.

Example: Let $M^3=\{(x,y,z)\in\mathbb{R}:x\neq 0\}$. Choose linearly independent vectors in M^3,

$$E_1=-x\frac{\partial}{\partial x},\quad E_2=x\frac{\partial}{\partial y},\quad E_3=x\frac{\partial}{\partial z}.$$

Let g be the Riemannian metric given by

$$g(E_1,E_1)=g(E_2,E_2)=g(E_3,E_3)=1,$$
$$g(E_1,E_2)=g(E_2,E_3)=g(E_3,E_1)=0.$$

Let $\varphi(E_1)=0$, $\varphi(E_2)=E_3$, $\varphi(E_3)=-E_2$ be the (1, 1) tensor field, and let the 1-form η be given by $\eta(X_3)=g(X_3,E_1)$ for any vector field $X_3\in\chi(M^3)$. Then, by linearity of φ and g, we have

$$\eta(E_1)=1,\qquad \varphi^2X_1=-X_1+\eta(X_1),$$
$$g(\varphi X_1,\varphi X_2)=g(X_1,X_2)-\eta(X_1)\eta(X_2),$$

for any vector fields $X_1,X_2\in\chi(M^3)$. So for $\xi=E_1$, (φ,ξ,η,g) is an almost contact structure on M^3. Let ∇ be the Levi-Civita connection with respect to g. Then, we have

$$[E_1,E_2]=-E_2,\qquad [E_2,E_3]=0,\qquad [E_1,E_3]=-E_3.$$

The Riemannian connection $\tilde{\nabla}$ of the metric g is given by Koszul's formula,

$$2g(\nabla_{X_1}X_2,X_3)=X_1g(X_2,X_3)+X_2g(X_1,X_3)-X_3g(X_1,X_2)$$
$$-g(X_1,[X_2,X_3])-g(X_2,[X_1,X_3])+g(X_3,[X_1,X_2]),$$

which yields

$$\nabla_{E_1}E_2=0,\qquad \nabla_{E_1}E_3=0,\qquad \nabla_{E_1}E_1=0,$$
$$\nabla_{E_2}E_3=0,\qquad \nabla_{E_2}E_2=-E_1,\qquad \nabla_{E_2}E_1=E_2,$$
$$\nabla_{E_3}E_3=-E_1,\qquad \nabla_{E_3}E_2=0,\qquad \nabla_{E_3}E_1=E_3.$$

From the above, it can be easily seen that (φ, ξ, η, g) is a Kenmotsu structure on M^3. Hence, $(M^3, \varphi, \xi, \eta, g)$ is a 3-dimensional Kenmotsu manifold. By using the above results we can easily obtain,

$$R(E_1,E_2)E_2 = -E_1, \quad R(E_1,E_3)E_3 = -E_1, \quad R(E_2,E_1)E_1 = -E_2,$$
$$R(E_2,E_3)E_3 = -E_2, \quad R(E_3,E_1)E_1 = -E_3, \quad R(E_3,E_2)E_2 = -E_3,$$
$$R(E_1,E_2)E_3 = -E_1, \quad R(E_3,E_2)E_1 = 0, \quad R(E_3,E_1)E_2 = 0.$$

The definition of Ricci tensor in a 3-dimensional manifold implies

$$S(X_1,X_2) = \sum_{i=1}^{n} g(R(E_i,X_1,X_2,E_i).$$

Using the components of the curvature tensor in the above equation we get

$$S(E_1,E_1) = -2, \quad S(E_2,E_2) = -2, \quad S(E_3,E_3) = -2,$$
$$S(E_1,E_2) = 0, \quad S(E_2,E_3) = 0, \quad S(E_3,E_1) = 0.$$

The semi-symmetric metric connection $\widetilde{\nabla}$ is given by (3.1) which gives

$$\widetilde{\nabla}_{E_1}E_2 = 0, \quad \widetilde{\nabla}_{E_1}E_3 = 0, \quad \widetilde{\nabla}_{E_1}E_1 = 0,$$
$$\widetilde{\nabla}_{E_2}E_3 = 0, \quad \widetilde{\nabla}_{E_2}E_2 = -2E_1, \quad \widetilde{\nabla}_{E_2}E_1 = 2E_2,$$
$$\widetilde{\nabla}_{E_3}E_3 = -2E_1, \quad \widetilde{\nabla}_{E_3}E_2 = 0, \quad \widetilde{\nabla}_{E_3}E_1 = 2E_3.$$

By using (3.2), we have

$$\tilde{R}(E_1,E_2)E_2 = -2E_1, \quad \tilde{R}(E_1,E_3)E_3 = -2E_1,$$
$$\tilde{R}(E_2,E_1)E_1 = -2E_2, \quad \tilde{R}(E_2,E_3)E_3 = -2E_2,$$
$$\tilde{R}(E_3,E_1)E_1 = -2E_3, \quad \tilde{R}(E_3,E_2)E_2 = -2E_3,$$
$$\tilde{R}(E_1,E_2)E_3 = -2E_1, \quad \tilde{R}(E_3,E_2)E_1 = 0,$$
$$\tilde{R}(E_3,E_1)E_2 = 0.$$

Using the components of the curvature tensor, we have

$$\tilde{S}(E_1,E_1) = -4, \quad \tilde{S}(E_2,E_2) = -6,$$
$$\tilde{S}(E_3,E_3) = -6, \quad \tilde{S}(E_1,E_2) = 0,$$
$$\tilde{S}(E_2,E_3) = 0, \quad \tilde{S}(E_3,E_1) = 0.$$

Using the above components of the curvature tensor with respect to and (4.18), we get

$$B_1(E_i) + B_2(E_i) + B_4(E_i) = 0, \quad \forall\, i = 1,2,3.$$

Also, using the above components of the Ricci tensor with respect to the semi-symmetric metric connection and (5.8), we get

$$A_1(E_i) + A_2(E_i) + A_3(E_i) = 0, \quad \forall i = 1,2,3.$$

Thus, this is an example of a 3-dimensional Kenmotsu manifold admitting a semi-symmetric metric connection which is weakly symmetric and weakly Ricci symmetric.

CONCLUSION

In this study, some geometric properties of weakly symmetric, weakly Ricci symmetric, weakly concircular symmetric, weakly concircular Ricci symmetric and weakly *m*–projectively symmetric Kenmotsu manifolds with respect to a semi-symmetric metric connection have been studied. The conditions for a Kenmotsu manifold to be weakly symmetric and weakly Ricci symmetric with respect to the semi-symmetric metric connection are obtained. Also, we derive the relation between the 1-forms in a weakly concircular symmetric and weakly concircular Ricci symmetric Kenmotsu manifold admitting a semi-symmetric metric connection. A necessary and sufficient condition for the Ricci tensor in a weakly *m*-projectively symmetric Kenmotsu manifold admitting a semi-symmetric metric connection to be Codazzi is obtained and the nature of the scalar curvature in this manifold is discussed.

REFERENCES

Amur K, Pujar SS (1978) On submanifolds of a Riemannian manifold admitting a metric semi-symmetric connection Tensor, N. S. 32: 35 - 38.

Blair DE (1976) Contact manifolds in Riemannian Geometry Lecture Notes in Math., Springer-Verlag, Berlin, New York.

Binh TQ (1990) On semi-symmetric connections Periodica Math. Hungar. 21(2): 101 –107.

De UC, Biswas SC (1997) On a type of semi-symmetric metric connection on a Riemannian manifold Publ. Inst. Math. 61(75): 90 - 96.

De UC, Ghosh GC (2005) On weakly concircular Ricci symmetric manifolds South East Asian J. Math. and Math. Sci. 3(2): 9 - 15.

Friedman A, Schouten JA (1924) Uber die Geometric der halbsymmetrischen Ubertragung Math. Zs. 21: 211 - 223.

Hayden HA (1932) Subspaces of space with torsion Proc. London Math. Soc. 34: 27 -50.

Kenmotsu K (1972) A class of almost contact Riemannian manifolds Tohuku Math. J. 24: 93 - 103.

Pokhariyal GP, Mishra RS (1971) Curvature tensor and their relativistic significance II,

Yokohama Math. J. 19: 97 - 103.

Prakasha DG, Vanli T, Bagewadi CS, Patil DA (2013) Some classes of Kenmotsu manifolds with respect to semi-symmetric metric connection Acta Math. Sinica, English Series 29(7): 1311 - 1322.

Prakasha DG, Vikas K (2015) On weak symmetries of Kenmotsu Manifolds with respect to quarter-symmetric metric connection Ann. Math. et Info. 45: 79-90.

Prvanovic M (1975) On pseudosymmetric metric semi-symmetric connections Pub. De L

Institut Math., Nouvelle Serie 18(32): 157 - 164.

Shaikh A, Hui SK (2009) On weakly concircular symmetric manifolds Ann. Sti. Ale. Univ. 30: 219 -224.

Tamassy L, Binh TQ (1992) On weakly symmetric and weakly projective symmetric Riemannian manifolds Coll. Math. Soc. J. Bolyai 56: 663 - 670.

Yano K (1970) On semi-symmetric metric connection Rev. Roum. Math. Pure Appl. 15: 1579 - 1586.

Science and Technology Journal, Vol. 7 Issue: I ISSN: 2321-3388

Artificially Intelligent Physics Solver: This AI Understands Newton's Law

V. Nirmala[1] and A. Rajagopal[2*]
[1]PG and Research Dept. of Physics, Queen Mary's College, Chennai
[2]IDRP, Indian Institute of Technology, IIT Madras, Chennai
E-mail: [1]gvan.nirmala@gmail.com, [2*]am18d301@smail.iitm.ac.in

Abstract—Artificial Intelligence (AI) is transforming many fields including science. At the intersection of physics and Artificial Intelligence, this paper explores if AI can understand the laws of physics? Specifically, this paper conceptualized and implemented a working prototype of a Deep Learning module that seem to understand Newton's third law of motion. The progress in AI is so fast, it has now exceeded human performance in specific tasks, mainly due to the progress in deep neural networks. In this paper, a Google BERT neural network model was trained using transfer learning technique on a synthetic dataset of simple physics problems within the scope of solving Newton's third law problems that requires understanding of concepts such as action and reaction, magnitude and direction forces, simple concepts of vectors in physics problems. The results are presented in this paper. Results demonstrate AI could solve simple physics problems within the specific context of Netwon's third law assuming certain boundaries on the language model of the word problems. A working prototype of this AI can be accessed at the given website. This paper also contributes the source code for reproducible results. This novel idea can be extended to more science topics. Applications of this interdisciplinary area of AI and physics have impact not just in areas of robotics and computational physics, but also in how science uses AI in the future. In future, more areas of science can benefit from the novel method contributed in this paper.

Keywords: Artificial Intelligence, Deep Learning, Computational Physics, Laws of Physics, Natural Language Understanding, Transfer Learning

INTRODUCTION

The progress in the field of Deep Learning in the recent few years is amazing. Artificial Intelligence (AI) is the new electricity, as per Prof Andrew Ng from Stanford University. AI is transforming many fields including science. Authored by 2018 Turing Award winners, Deep Learning (LeCun, 2015) is a seminal review of the potential of the AI technologies. The impact of AI on science is enormous. of the five most highly cited papers in Nature, three are related to AI in 2019 (Crew, 2019).

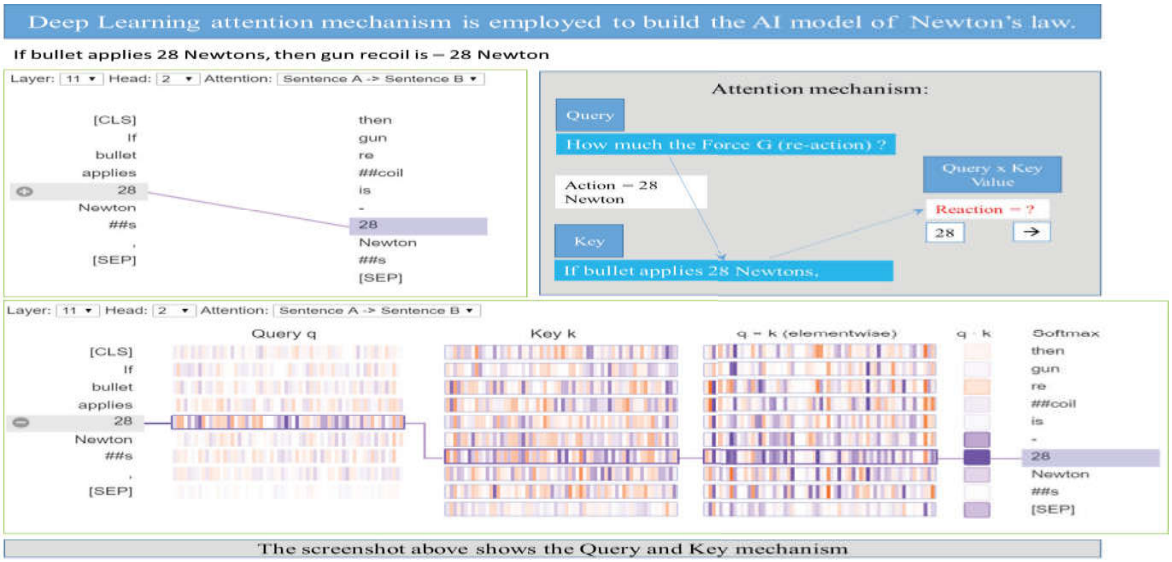

Fig. 1: Novel Method to Model Physics Problems as AI Models

http://doi.org/10.22232/stj.2019.07.01.03

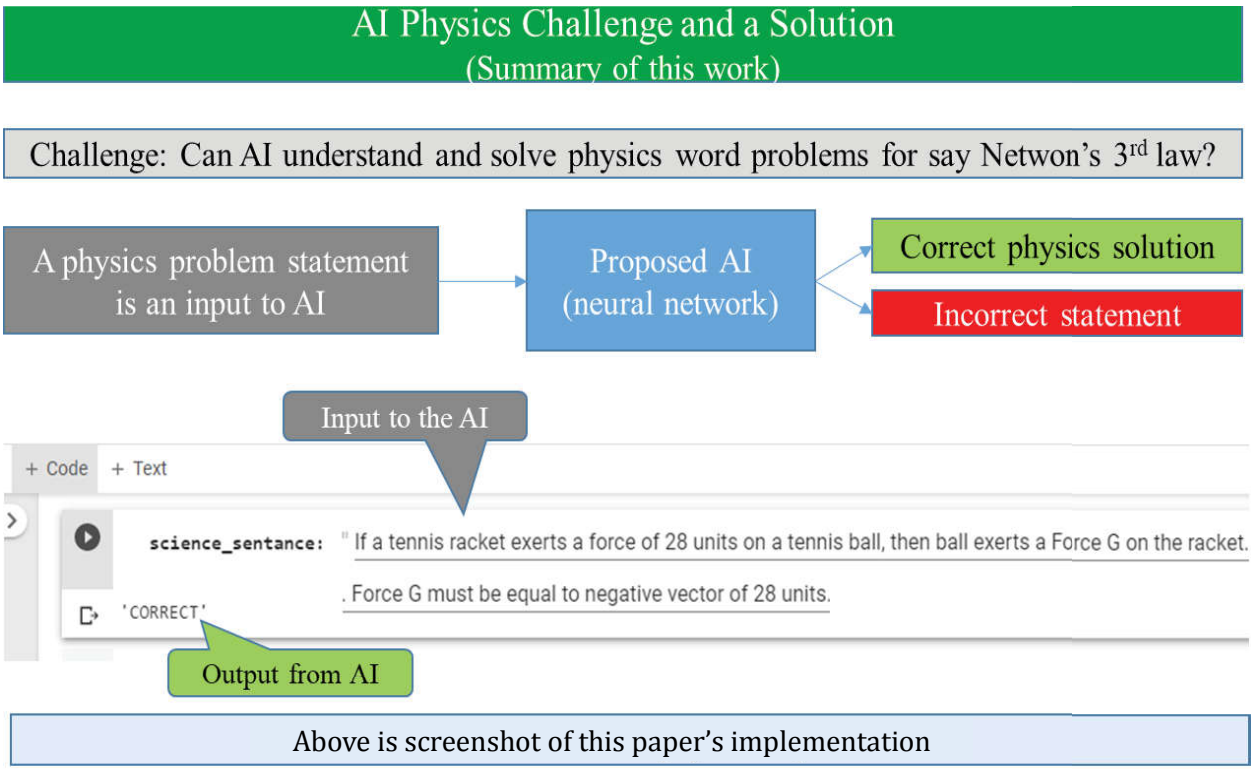

Fig. 2: Summary of this Paper's Contribution. Results Reproducible at URL

The Science of Learning Machines: Neural Networks and the Human Brain

Machines ability to learn like humans is a key trait inspired by how neurons in human brain works (Sarah, 2018). Deep Learning methods are apt in handling specific tasks rather than generic tasks. For instance Patel (2019) demonstrates AI progress in a specific task of medical image diagnosis. Both Mass (2019) and Levine (2019) demonstrates progress in understanding natural language.

Objective of the Paper: Can AI Understand Laws of Physics?

Nature physics paper (Buchanan, 2019) highlights the power of AI in physics. At the intersection of AI and physics, new themes are emerging such as Physics enhanced AI (O'Driscoll, 2019). While AI is being applied in science in many ways, this paper sets out to get an answer to this challenge: Is it possible for an AI to understand the laws of physics? Is it possible for an AI to understand word problems and solutions in a specific context of Newton's law? The specific challenge addressed in this paper is clearly presented in Figure 2.

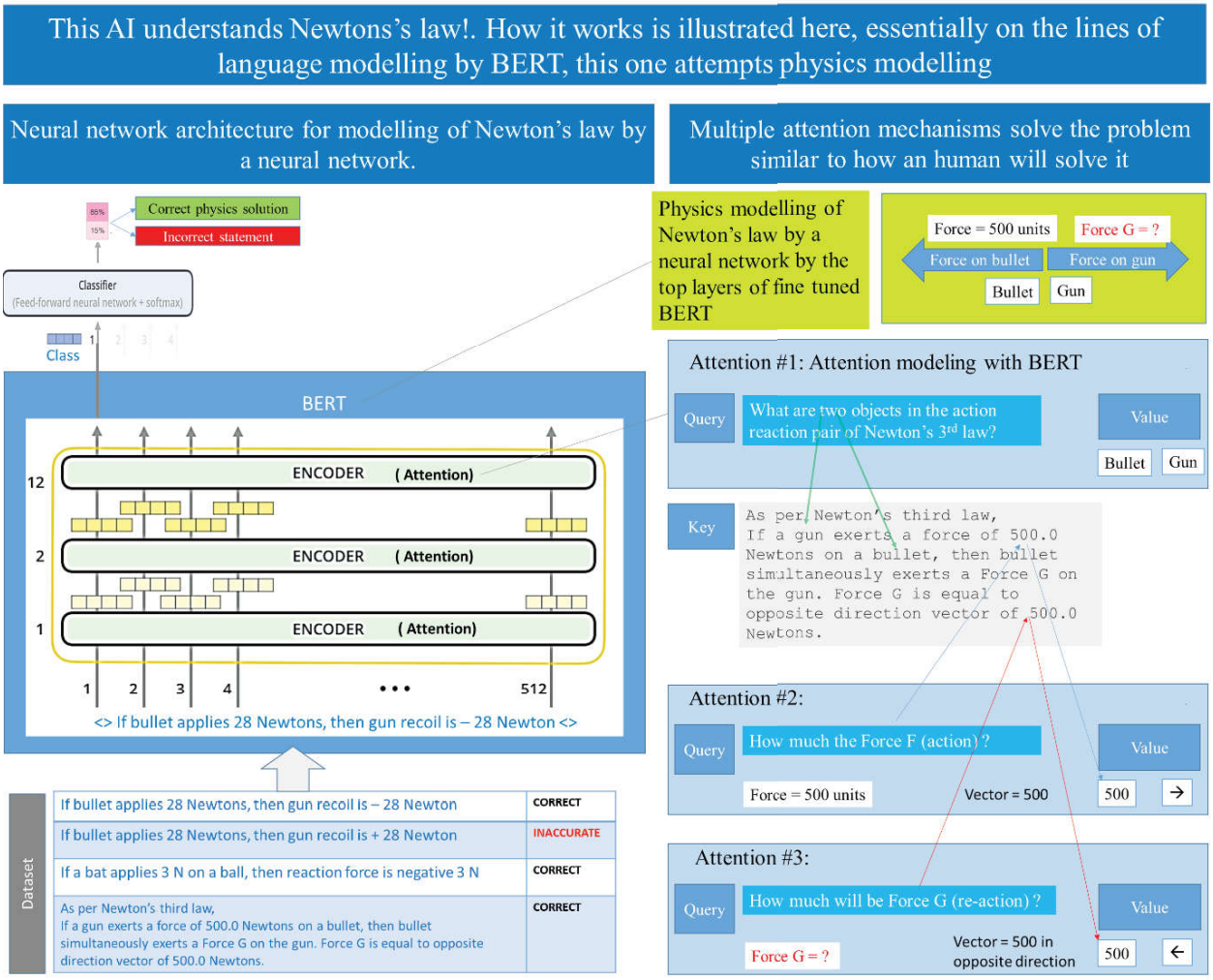

Fig. 3: Novel Method for Modelling Newton's Law as BERT Inspired AI Models is Proposed

METHODS

How to Solve the Challenge: Possibility of a Novel Method

How to build an AI that understands and solves problems in Newton's laws? For the challenge presented in section 1.2, this paper attempts with a novel approach: By mapping the challenge into a Deep Learning method of supervised classification task using state of art language modelling neural networks such as Google BERT (Devlin, 2018), a reasonable result is in the realm of feasibility.

Choice of Scope of Challenge: Why Newton's 3rd Law?

Given that Deep Learning has proven to be apt for specific tasks, a specific scope is considered for this experiment**.** A random choice of Newton's 3rd law is used in this experiment, though any law could be used. This paper aims to solve physics questions, that are simple yet challenging the fundamentals of modelling physics concepts using AI. For instance, can the proposed AI understand the concept of magnitude and direction of a force vector in Newton's 3rd law? The challenge is because the AI needs to understand the concepts involved in the law, the objects involved in the

context, and identify the action and reaction. The dataset listed in Figure 3 clearly scopes up the boundaries of the challenge taken in this paper.

Novel Method of Solving the Challenge: AI Attention can Model Science Questions!

Deep Learning based Attention models as a key technique to solve the science challenge is being proposed in this paper. Attention models (Vaswani, 2017) has demonstrated breakthrough results in the recent years such in Google translate (Ramati, 2018), Transformer networks (Mohamed, 2019), and more recently in Google BERT (Devlin, 2018). As shown in Figure 3, any science word problem can be handled as a text classification problem**.** The key technique now is to transform a neural network that understand natural english language (Jacob, 2018) into one that understands physics models. This transformation is realized using transfer learning method in this paper, as proposed in Figure 3. As proposed, Encoders in top of the BERT network would understand physics concepts and hence can model physics word problems. Figure 4 discusses the approach to design an AI model.

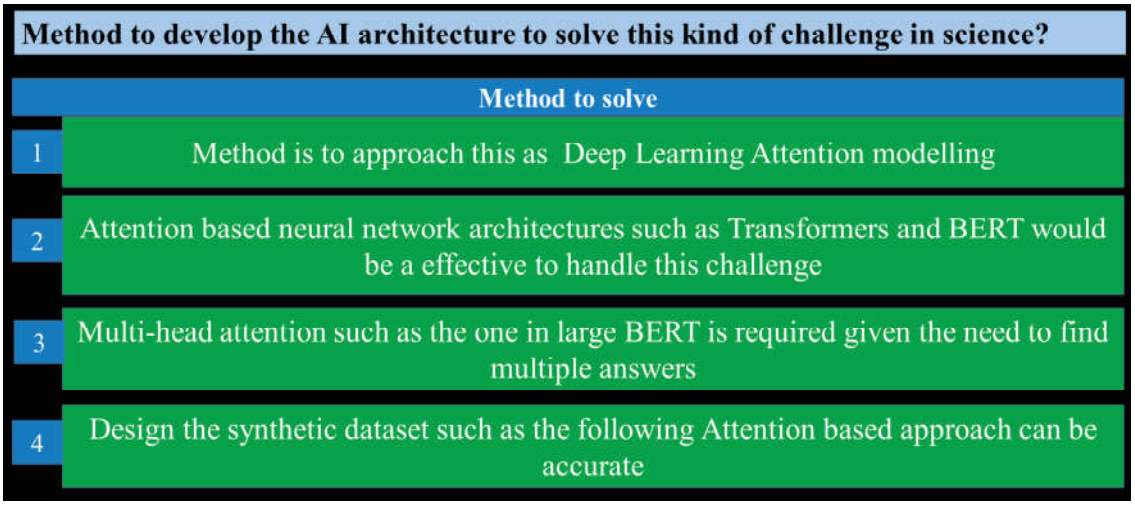

Fig. 4: Key Ideas in Designing the AI Model to Solve Word Problems in Science

RESULTS AND DISCUSSION

Results demonstrated in this paper are

1. It is feasible for an AI to solve the challenge in Figure 3 within scope listed in section 2.2.
2. Results & screenshots in Figure 5 are reproducible by readers at this URL.
3. Novel method for AI to learn Newton's law via BERT attention is established (Figure 3)

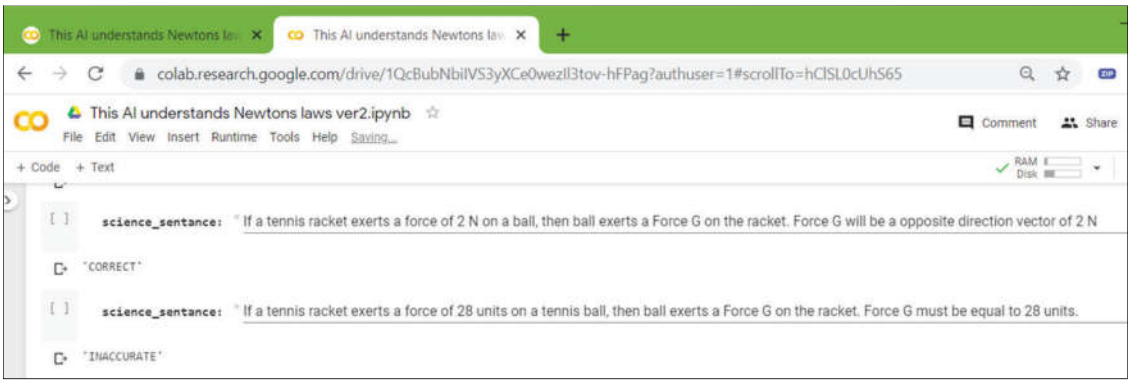

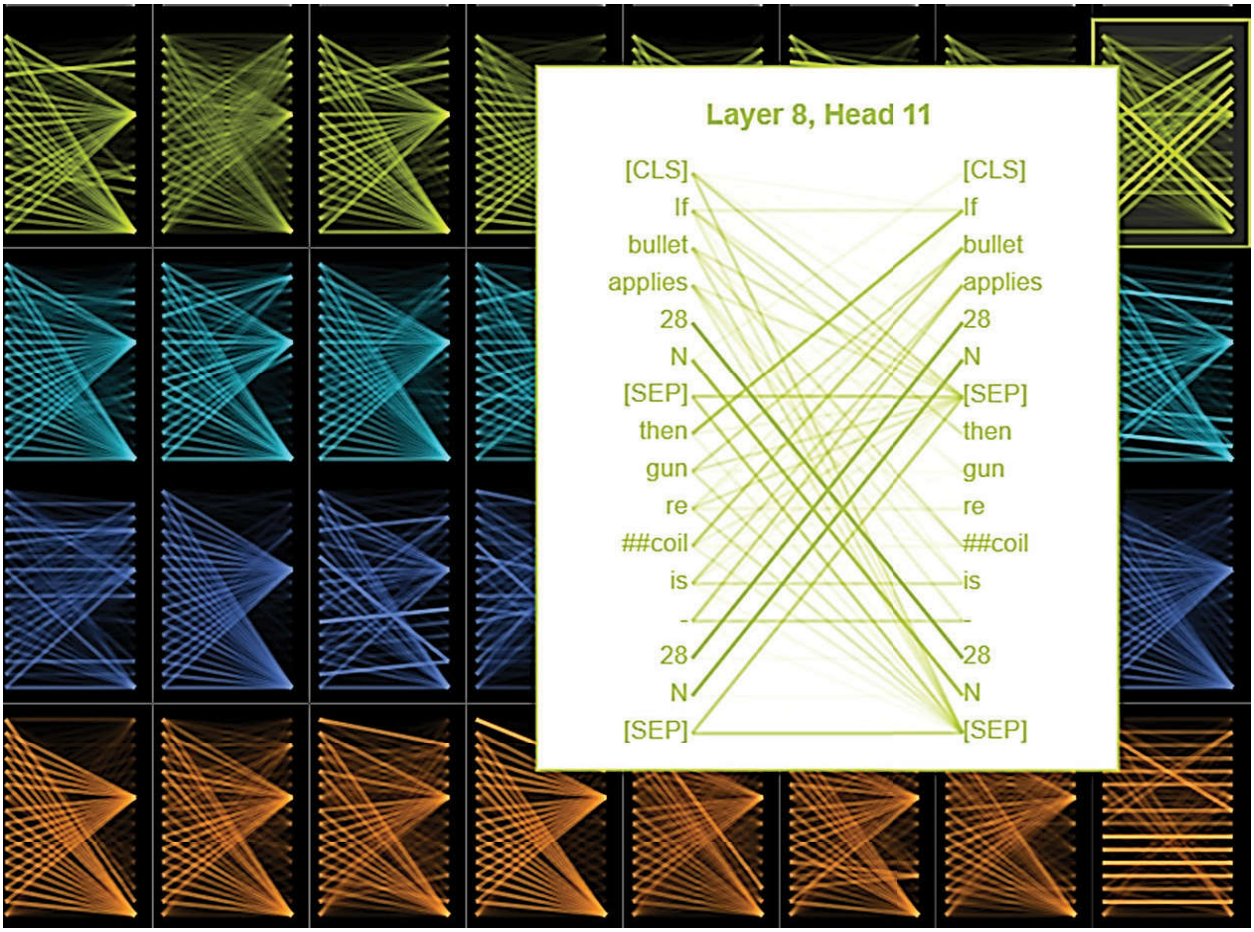

Fig. 5: Results of an AI Physics Classifier that Distinguishes Solutions as Right or Wrong

Contribution at Intersection of AI & Physics

This paper makes an important and new contribution at the intersection of Physics and AI**.** Specifically, as clearly presented in Figure 2, the core contribution is on how to develop a neural network that automatically learns physics laws by scanning through solved problems (provided as datasets in Figure 3). As demonstrated in Figure 3 and Figure 5, this AI can learn scientific laws, automatically deducing simple formulas between action and reaction, can understand and verify the correctness of magnitude and direction of the force vectors. This AI has been shown to be capable of identifying the pairs of objects interacting in Newton's law such as gun & bullet, tennis racket & ball pairs, as illustrated in Figure 3 and Figure 7.

Key Results: AI Attention Models Can Solve Simple Word Problems in Newton's Law!

Key result is development of breakthrough AI model that understands physics word problems. The results demonstrate that it is feasible for AI to understand physics laws and solve simple problems framed as simple sentences as depicted in Figure 5, within certain boundary conditions listed in section 3.4. By just looking at examples of solved problems, this AI can automatically learn physics concepts, understand the law of science, apply it solve simple problems in physics, and even apply the physics laws when a new problem set is presented. The novel method depicted in Figure 3 was implemented in TensorFlow. A live working demo of this AI is demonstrated in this URL**.** A specific screenshot of this working prototype is shown in Figure 2.

Source Code of the Novel Method

This AI is developed with Tensorflow Deep Learning framework using Keras. This source code can be accessed at this URL, https://sites.google.com/view/aiforphysics

Reproducibility of Results

To enable quick reproducibility of the results demonstrated in Figure 4, viewers are encouraged to visit to this URL, https://sites.google.com/view/aiforphysics. The experiments can be repeated and the results could be validated quickly.

Discussion on the Novel AI Method Contributed

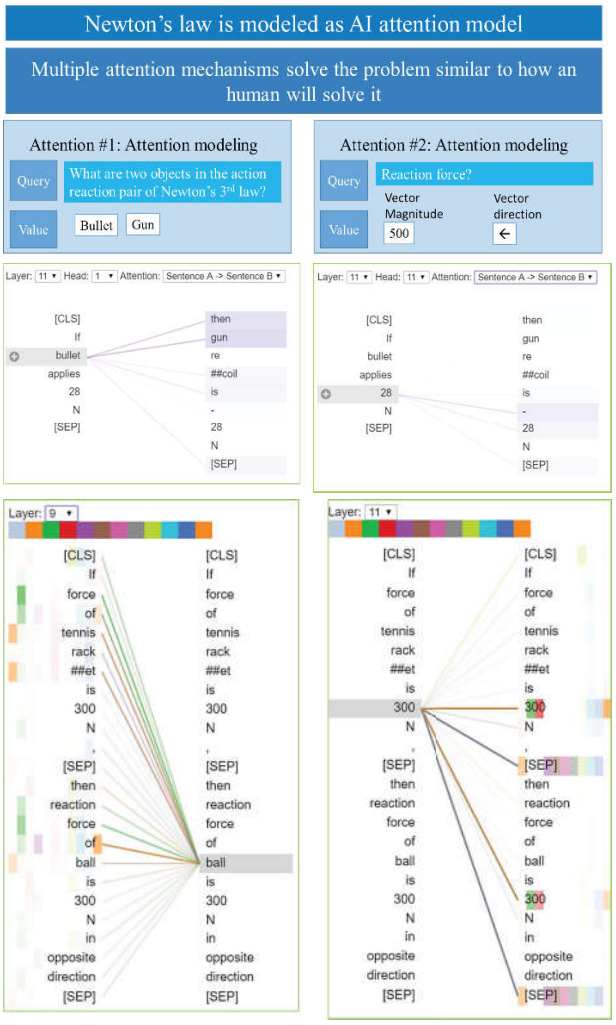

Fig. 6: Attention Modelling is at the Core of the Novelty

The core contribution is the novel to develop a neural network that automatically learn physics laws. The amazing result presented in section 3.2 was realized by the approach articulated in section 2.3. Deep Learning Attention models (Vaswani, 2017) is the heart of the method that produced this breakthrough result. This can be validated by observing the BERT visualization in Figure 1 and 6 for word problems in physics. One can observe in Figure 6, the head #1 of 11th encoder connects bullet to gun, while the head #11 of 11th encoder of BERT pays attention to the magnitude of applied force to compute the reaction force. Attention models learns with Query, Key mechanism, and this fundamental idea is brought out in Figure 1.

Discussion on Accuracy of AI and Assumptions

The boundary conditions were discussed in section 2.2. In addition, like other machine learning solutions, the test distribution and training distribution can't be different. In this specific case, the training dataset is synthesized programmatically, hence can be improved. Given programmatically created dataset, this binary text classifier based on BERT with 12 layers achieved a training accuracy over 95%. Validation accuracy could vary based on the test data's similarity to the training dataset.

CONCLUSION

The paper demonstrated the feasibility of developing a neural network that could understand, solve and validate certain type of word problems in physics laws. Attention models hold a key to understanding concepts of the physics laws, and Query Key mechanisms can attend to relevant values to validate the physics statements. While the result was demonstrated with one of the Newton's laws, it could be extended to model more topics in science. This paper contributed by conceptualizing the challenge, designing a novel method to model physics laws with attention based neural networks, and demonstrated with a working prototype. The novel AI technique implemented in source code is contributed online for reproducibility. Readers are encouraged to visit the online website, https://sites.google.com/view/aiforphysics to check out a live demo of AI that understands Newton's 3rd law.

REFERENCES

Buchanan M. (2019). The power of machine learning. Nature Physics. 15: 1208.

Crew B. Google Scholar reveals its most influential papers for 2019. Nature Index; 2019 [cited 21 Dec 2019] https://www.natureindex.com/news-blog/google-scholar-reveals-most-influential-papers-research-citations-twenty-nineteen

Devlin J, Chang M, Lee K, Toutanova K (2018). Bert: Pre-training of deep bidirectional transformers for language understanding. arXiv:1810.04805.

LeCun Y, Bengio Y , Hinton G (2015) Deep learning. Nature 521: 436–444

Levine Y, Lenz B, Dagan O, Padnos D, Sharir O, Shalev SS, Shashua A, Shoham Y. (2019) Sensebert: Driving some sense into bert. arXiv:1908.05646.

Mass Y, Roitman H, Erera S, Rivlin O, Weiner B, Konopnicki D (2019) A Study of BERT for Non-Factoid Question-Answering under Passage Length Constraints. arXiv:1908.06780.

Mohamed A, Okhonko D, Zettlemoyer L (2019) Transformers with convolutional context for ASR. arXiv:1904.11660.

O'Driscoll P , Lee J, Fu B (2019) Physics Enhanced Artificial Intelligence. arXiv:1903.04442.

Patel BN, Rosenberg L, Willcox G, Baltaxe D, Lyons M, Irvin J, Rajpurkar P, Amrhein T, Gupta R, Halabi S (2019) Human–machine partnership with artificial intelligence for chest radiograph diagnosis. Nature Partner Jounral Digital Medicine 2(1) : 1-10.

Ramati I, Pinchevski A (2018) Uniform multilingualism: A media genealogy of Google Translate. New Media & Society 20.7: 2550-2565.

Vaswani A, Shazeer N, Parmar N, Uszkoreit J, Jones L, Gomez AN, Kaiser L, Polosukhin I (2017) Attention is all you need, Advances in neural information processing systems. 31st Conference on Neural Information Processing Systems; NIPS 2017, CA, USA. 5998-6008.

Webb S (2018) Deep learning for biology. Nature: 554, 555-557.

Science and Technology Journal, Vol. 7 Issue: 1 ISSN: 2321-3388

New Taxon of Fungal Endophytes from *Phrynium capitatum* Willd: A Promising Ethnomedicinal Plant in Northeast India and its Systematic and Phylogenetic Analysis

Richa Sharma[1], Sumpam Tangjang[2] and Amritesh C. Shukla[3*]
[1,2]Department of Botany, Rajiv Gandhi University, Rono Hills, Doimukh,
Itanagar–791112 Arunachal Pradesh, India
[1,3]Department of Botany, University of Lucknow, Lucknow–226007, Uttar Pradesh, India
E-mail: [3*]amriteshcshukla@gmail.com

Abstract—The findings of the current study deal with the first time report on the diversity of fungal endophyte from the ethnomedicinal plant- *Phrynium capitatum* Willd., **(**Marantaceae). The plant is growing wildly in the forest of Papum Pare, Arunachal Pradesh, India, and traditionally been used for anti-diabetic, antihyperglycemic or analgesic effects. During the investigation, samples of the plant parts, viz., leaves, stem, and roots were collected for isolation of endophytic spp. The endophytic spp were identified based on the morphological, cultural, and reproductive structures (hyaline, ellipsoidal, aseptate, pycnidia, beta conidia, perithecia, asci, and ascospores). Further, the phylogenetic analysis of the isolated species was made, using the sequences of 5.8S and 28S rDNA internal transcribed spacer sequence 1 and 4. The largest number of fungal endophytes (39%) were isolated from the leaves, followed by the roots (31%) and stems (30%). Overall 35 fungal species have been isolated, out of which, thirty-four belongs to the class Ascomycetes, and one from the class zygomycetes. The highest species richness and frequency of colonization were recorded in the leaf. The observations show that *Pestalotiopsis longiseta* was the most dominant endophytic species followed by *Diplodina* microsperma*, Nodulisporium hinnuleum, Aspergillus flavus* , *Diaporthe* sp., *Nigrospora oryzae* and *Lasiodiplodia viticola*. However, *Pestalotiopsis neglecta, Sordaria fimicola, Diplodina microsperma, Fusarium incarnatum, Preussia* sp., *Diaporthe* sp., *Aureobasidium* sp.were common fungal endophytes isolated from *P. capitatum*

Keywords: Biodiversity, Colonization Frequency, Endophyte, Internal Transcribed Spacer, Medicinal Plant, Arunanchal Pradesh

INTRODUCTION

De Barry (1866) coined the term 'endophyte' to detect fungi that live intercellulary and intracellularly in plants tissues causing no harm to the plant (Compant *et al.,* 2017; Jeewon *et al.,* 2017). Further, based on their interactions with host plants, fungal endophytes may be divided into three groups: commensalists, parasites, and mutualists (Jia *et al.,* 2016, Kirschner 2018)**.** In mutualism, definite fungal endophytes give tolerance to abiotic and biotic stresses on their host plants, improve their growth, and restrain diseases (Redman 2002, Rodriguez 2008). These Endophytes protect their hosts from infectious agents and adverse conditions by secreting bioactive secondary metabolites (Nath *et al.,* 2012; Nongalleima *et al.,* 2013). Endophytic fungi were reported in almost all the plants spp. algae, ferns, mosses and mainly in gymnosperms, angiosperms reported from various parts of the world (Radic and Strukelj 2012; Doilom *et al.,* 2017). Many researchers have proven that endophytes are the potential source of novel natural products for exploitation in modern medicine, agriculture and industry (Kaul *et al.,* 2013). To date, it has been found that taxol can be produced by endophytic fungi *Metarhizium anisopliae* and *Cladosporium cladosporioides* (El-Maali *et al.,* 2018). However, fungal endophytes can be easily grown in labs under routine culture techniques, and hence the potential for discovering a virtually inexhaustible supply of metabolites is high. Fungal endophytes can

http://doi.org/10.22232/stj.2019.07.01.04

produce compounds similar to their host plants and are capable of preserving the world's diminishing biodiversity (Bender *et al.,* 2016; Mane *et al.,* 2017).

Studies on fungal endophytes concentrated on medicinal plants have shown that the curative property of the medicinal plant is not only because of the chemicals present in the plant but also because of the fungal endophytes that present in the plant (Verma 2011; Suryanarayanan 2013). Thus there is a need to isolate and identify several fungal endophytes and explore the potency of their secondary metabolites. Although, number of studies have already been reported in the association of fungal endophytes with medicinal plants from India viz., *Clerodendron serratum, Pongamia, Ashwagandha, Taxus brevifolia, Azadirachta indica, Terminalia arjuna, Trigonella, foenum graecum, Labelia nicotinifolia, Adhatoda zeylanica, Bauhinia phoenicea,Catharanthus roseus, Parthenium hysterophorus, Ficus religiosa, Coffea Arabica, Crataeva magna, Silybum marianum, Allium sativum, Mamordica chaeantia, Azadarichata indica* and *Nothapodytes nimmoniana, (*Tejesvi *et al.,* 2005; Mane *et al.,* 2017; Mane and Vedamurthy 2018), but there is no such report on fungal endophytic association with *P. capitatum*.

MATERIALS & METHODS

Study Area

The study area Papum Pare is located at the N 26°56′11″ to 27°35°44″ and E 93°12′45″ to 94°13′30″ is one of the important hotspots in the world, ranked 25th (Chowdhery 1999), and among the 200 globally important eco-regions (Olson and Dinerstein 1998). It covers an area of 2875 sq. km, having an annual rainfall of 2694 mm. Major part (75%) of this district is covered by thick forest which has a sub-tropical, deciduous and humid type of vegetation (Fig.1-a).

Plant & Sample Collection

The selected plant, *P. capitatum* is a semi-evergreen herb with creeping rootstock and is wildly growing in forest area (Papum Pare) in Arunanchal Pradesh (Fig. 1-b). Leaves oblong, acuminate, base rounded or obtuse, to 30 x 18 cm; petiole to 60 cm long, spike globose, sessile on the petiole, 4-6 cm across**.** Inner bracts ovate**-**oblong, fimbriate at the apex, corolla yellow, outer petaloid staminodes orange-red, lip with a pendulous appendage, ovary tomentose (Anon 2019).

Samples of leaves, stems, and roots were collected during (Dec 2016- Dec 2018) from the healthy plant of *P. capitatum* in sterile bags and brought to the laboratory for processing within 24 hours after sampling.

Surface Sterilization and Isolation

The samples thus collected were washed gently in running tap water to remove the soil and debris. Further, isolation of fungal endophytes was determined, using the method of Suryanarayanan *et al.,* (1998). Samples were cut into small pieces of (0.5-1.0 cm). The pieces were then surface-sterilized by dipping them serially in 70% ethanol for 5 sec and 4% NaOCl for 90 sec; finally rinsed in sterile distilled water for 10 sec. Now, 150 segments of the samples were selected randomly and plated on Potato Dextrose Agar (PDA) medium (supplemented with 150 mg/L chloramphenicol) contained in Petri dishes (7.5 cm diam). Petri dishes were incubated (12 h dark: 12 h light cycle) for 25 days at 25± 2°C, to observe the growth of endophytes, following the method of Suryanarayanan (1992). The hyphal tips which grew out from the segments were isolated and subcultured on PDA medium and preserved at 4°C for further investigation.

Further, the colonization frequency (CF) was calculated, using the following formula (Suryanarayanan *et al.,* 2003):

$$CF\% = \frac{\text{Number of segments colonized by fungal endophytes}}{\text{Total number of segment observed}} \times 100$$

However, the density of colonization (rD%) of a single endophyte species was calculated, using the method of Fisher and Petrini (1987).

$$rD\% = (Ncol/Nt) \times 100$$

Where,

Ncol = Number of segments colonized by each fungus

Nt = Total number of segments inoculated

Morphological Identification

We identified the endophytes thus isolated based on their macroscopic and microscopic characteristics viz., the morphology of fruiting structures and spore morphology (Sutton 1980; Subramanin 1983 and Nagmani 2005).

MOLECULAR IDENTIFICATION

DNA Extraction and PCR Amplification of rDNA

Genomic DNA was extracted from fresh fungal mycelia growing on PDA plates (at 25± 2°C and 5 to 8 days old), using a Qiagen microbial extraction kit. Fragments of 18S rRNA gene were amplified by PCR, using forward ITS1 (5'-TCCGTAGGTGAACCTGCGG-3') and reverse ITS4 (5'-TCCTCCGCTTATTGATATGC-3') primer (White *et al.,* 1990). Each PCR amplification reaction was performed in a final volume of 25 µL containing 25 ng template DNA, 10X PCR buffer (10 mM Tris-HCl, 50 mM KCl, pH 8.3), 1.5 mM MgCl2, 200 µM of each dNTP, 50 pM of each primer, 1 unit of Taq polymerase (Genei, Banglore) and distilled water (Sigma, USA). The conditions of the PCR was initial denaturation at 95°C for 5 minutes followed by 35 cycles for 45 sec, annealing at 56 °C for 1 minute (35 cycles) and primer extension at 72 °C for 1 minute (again 35 cycles), final extension at 72 °C for 7 minutes (1 cycle) and hold (cooling) at 4 °C. PCR products were checked on 1.2 % Agarose gel in Tris–acetate-EDTA buffer (TAE) at pH 8.0, stained with ethidium bromide (0.3 g/mL) and visualized under UV light by using Gel documentation system. Sequencing was done by GeNei Labs Private Limited, Bengaluru using PRISM® BigDyeTM Terminator Cycle Sequencing Kits with AmpliTaq® DNA polymerase, as per the manufacturer instructions. Obtained Sequences were subjected to BLAST (Basic Local Alignment Search Tool). All obtained sequences were submitted and awarded access numbers in GenBank of NCBI (Table 1).

PHYLOGENETIC ANALYSIS

The primer pairs ITS1/ITS4 (White *et al.,* 1990) were used to amplify ITS-rDNA and partial. The reaction mixture and thermal cycling conditions were the same as described by Karimi *et al.* (2016). The data thus sequenced was subjected to BLAST (Basic Local Alignment Search Tool), for homology search and multiple sequence alignments were made by ClustalW. Phylogenetic relationship of all fungal species; drawn their phylogenetic relationship. Further, it was analyzed using Neighbor-Joining methods of MEGA 5 (Tamura *et al.,* 2011); and the robustness of the inferred phylogeny was assessed using bootstrap value at 1,000 replications.

RESULTS

The findings of the present investigation deal with the isolation of endophytic fungi, from *P.capitatum*; an ethnomedicinal plant commonly used to treat various ailments in human beings. The samples of the plants were collected randomly from the study area (Papum Pare). Out of total of 15 plant materials of *P. capitatum*, 150 segments were processed (including root, stem and leaves plant parts); for the isolation of endophytic fungi. The observations recorded total of 127 isolates of endophytic fungi; which belong to 35 fungal spp. The maximum number of fungal isolates were recorded from leaves (39%), followed by roots (31%) and stems (30%) [Fig. 1-c], respectively; however, the colonization frequency rate was recorded highest in leaves (80%) followed by roots (70%) and stem (59.61%). Total of 35 fungal endophytes were isolated, which belongs to 25genera.The observations show that *Pestalotiopsis longiseta* was the most dominant endophytic fungi, isolated from the selected plant (*P.capitatum*); followed by *Diplodina microsperma, Nodulisporium hinnuleum, Aspergillus flavus*, etc. However, *Pestalotiopsis neglecta, Sordaria fimicola, Diplodina microsperma, Fusarium incarnatum, Preussia* sp., *Diaporthe* sp. and *Aureobasidium* sp. were the common fungal endophytes recorded from all the plant parts viz., leaf, stem, and roots. While, isolating the organ-based fungal endophytes; it was recorded highest in leaves viz., *Biscogniauxia mediterranea, Nodulisporium hinnuleum, Corynespora cassiicola, Scopulariopsis brevicaulis, Aspergillus nidulans* and *A. fischeri*; followed by *Curvularia borreriae, Nigrospora oryzae, Lasiodiplodia pseudotheobromae, L. viticola* and *Chaetomium globosum* from the stem as well as *Mucor hiemalis, Bipolaris bicolor* and fungal Endophyte sp., from the roots. Besides, the density of colonization (rD%) was recorded in the chronology of *P. longiseta* (14%) < *D. microsperma* (6%) < *N. hinnuleum* (5.33%) < *S. fimicola* (4%), and 0.66% to 4.00% for the remaining endophytes (Table 1; Fig. 2).

The analysis of fungal taxonomy of all the isolated 35 fungal endophytes shows that 14 endophytic fungi belong to class- Sordariomycetes; 13 belongs to the class Dothideomycetes; 06 belongs to the class Eurotiomycetes; 01 belong to the class Zygomycetes and 01 could not identify properly. While categorizing up to the order level; it was observed that *C. borreriae, C. spicifera, C. cassiicola, Alternaria* sp. *B.bicolour, P. chartarum, Preussia* sp., *Phoma* sp. and *P. brabeji* belongs to the order Pleosporales;

A.niger, A. flavus, A. nidulans, A. fischeri, A. fumigates and *P. chrysogenum* belongs to the order Eurotiales; *D. microsperma, F. merismoides* and *F. incarnatum* belongs to the order Hypocreales; *P. longiseta, B. mediterranea, N. hinnuleum* and *Eutypa* sp.belongs to the order Xylariales; *S. fimicola* and *C. globosum* belongs to order *Sordariales; L. pseudotheobromae* and *L. viticola* belongs to order Botryosphaerial; *C. fructicola* and *C. gloeosporioides* belongs to the order Glomerellales; *Dothidea* sp., *Aureobasidium* sp. belongs to the order Dothideales; Besides this, 02 fungal endophytes belong to order Mucorales viz., *M. hiemalis, S. brevicaulis;* 01 fungal endophyte *N. oryzae* belongs to the orders Trichosphaeriales, and one *Diaporthe* sp. belongs to the orders Diaporthales, respectively.

Samples of the fungal endophytes thus isolated (35 samples) were used for extraction of the DNA and its molecular characterization and submitted to the NCBI and got the accession number (Table 1). Further, phylogenetic analyses based on the ITS1-ITS4 sequencing data of the isolated fungal endophytes were also recorded. The observations of the neighbor-joining tree as constructed based on the sequence-structure alignment, and recorded in figure two; shows the structure alignment clearly in five well-separated groups. Group 'A' consisted of *L. viticola, Alternaria* sp., *P.brabeji, P.chrysogenum, F.incarnatum, Aureobasidium* sp., *P. longiseta*, and *C. cassiicola* where only *P. brabeji* and *P.chrysogenum* show strong bootstrap value. Similarly, Group 'B' consisted of *C. globosum, C. spicifera, S.brevicaulis*, *A. fumigates* and *Phoma* sp. Group 'C' contains *F. merismoides, Preussia* sp., *B. bicolor, L. pseudotheobromae A.fischeri*, *C.gloeosporioides, B. mediterranea.* Group 'D' contains *S. fimicola*, *A.niger, Eutypa* sp., *Diaporthe* sp., *C. fructicola.* .However, group 'E' consisted *P. longiseta, Dothidea* sp., Fungal Endophyte sp., *D. microsperma*, *C.borreriae, N.hinnuleum, M. hiemalis*, *P. chartarum, A. flavus, N. oryzae* (Fig. 3).

The findings also show that there is not any such type of report on the isolation of endophytic fungi from *P. capitatum* as investigated in the current study; it indicates itself the uniqueness of the work as the first report.

DISCUSSION

Literature reveals that diversity of fungal endophytes have already been reported from several medicinal plants viz., *Aspergillus candidus, Nigrospora oryzae, Cladosporium cladosporioides* and *Rhizoctonia solani* reported from *Ananas comosus* (Krishnamurthy *et al.,* 2008); *Fomitopsis* sp. *Penicillium* sp., *Diaporthe* sp., *Arthrinium* sp. *Phomopsis* sp. and *Schizophyllum* sp. have been reported from *Garcinia mangostana* and *G .parvifolia* (Sim *et al.,* 2010); *Mortierella minutissima, N. sphaerica, Acremonium strictum, Humicola Grisea, Mortierella hyaline, Oidiodendron echinulatum, O. griseum, Humicola fuscoatra* and *Arthroderma tuberculatum* reported from *Elaeocarpus sphaericus* (Shukla *et al.,* 2012); *Phoma tropica, Cladosporium sphaerospermum, Xylaria* sp., *Phomopsis archeri,* and *Tetraploa aristata* from *Opuntia ficus-indica* (Bezerra *et al.,* 2012); *Phomopsis* spp, *Diaporthe* spp, *Schizophyllum* spp, *Penicillium* spp, *Fomitopsis* spp and *Arthrinium* spp from *Cinchona* spp. (Maehara *et al.,* 2013); *A. alternata, Phomopsis* sp. and *Fomitopsis* sp. from *Miquelia dentate* (Shweta *et al.,* 2013); *F. oxysporum,Talaromyces radicus* and *Eutypella* spp. From *Catharanthus roseus* (Kuriakose *et al.,* 2016); *Altenaria alternata, C. capsici, and C. taiwanense from Passiflora incarnate* (Seetharaman *et al.,* 2017); *Penicillium sp., P. griseofulvum, A. flavus, Mycoleptodiscus terrestris, Trichoderma* sp., *C. gloeosporioides* and *Shiraia* sp. from *Huperzia serrata* (Su *et al.,* 2017); *P.citrinum, A. alternate, A. niger, Cladosporium* sp., *Rhizopus* sp., *C.vermiformis* reported from *Helicteres isora* (Gayathri and Chandra 2017); *Periconia hispidula, Allomyces arbuscula, N. sphaerica, A. falciforme, P. chrysogenum Aureobasidium sp. Chaetomium sp. from Litsea cubeba (Deepanwita and Dhruva 2018); and Fusarium spp*, *Aspergillus sp.*,, *Chaetomium sp.*,, *Penicillium sp., Setosphaeria rostrata*, *F.solani*, *Bipolaris maydis, D.phaseolorum, Rhizoctonia bataticola,* and *Macrophomina phaseolina* reported from *Chlorophytum borivilianum* (de Carvalho *et al.,* 2019) as well as *A. alternata, A. terreus, Alpestrisphaeria reported from Vitex rotundifolia* (Yu-Hung Yeh and Roland Kirschner 2019). However, there are no such reports of the fungal endophytes on *P. capitatum*; as recorded in the present investigation.

In the current study, overall 127 species of endophytic fungi; which belong to 35 fungal spp have been isolated from the plant parts including leaves (39%), followed by roots (31%) and stems (30%), respectively [Fig. 1c]. Further, it was observed that *Pestalotiopsis longiseta* was the most dominant endophytic fungi followed by *Diplodina microsperma, Nodulisporium hinnuleum, Aspergillus flavus* and others. However, *Pestalotiopsis neglecta, Sordaria fimicola, Diplodina microsperma, Fusarium incarnatum, Preussia* sp., *Diaporthe* sp. and *Aureobasidium* sp.were the common fungal endophytes recorded from all the plant parts viz., leaf, stem and roots as well as the density of colonization (rD%) was recorded for *P. longiseta* (14%) < *D. microsperma* (6%) < *N. hinnuleum* (5.33%) < *S. fimicola* (4%), and 0.66% to 4.00% for the remaining endophytes

(Table 1; Fig. 2). Furthermore, the fungal taxonomy of all the isolated 35 fungal endophytes was also recorded. Sordariomycetes was the class represented the maximum endophytes (14), however, Zygomycetes was the class with the least representation (01). Besides this, extraction of the DNA and its molecular characterization as well as phylogenetic analyses based on the ITS1-ITS4 sequencing data of the isolated thirty-five fungal endophytes, have also been investigated and recorded in Table -1.

Furthermore, literature also reveals that fungal endophytes mimic the plants behavior and function and also are capable to produce bioactive compound/ secondary metabolites as novel compounds having antimicrobial, anticancer, antioxidants, insecticidal, anti-malaria, anti-tuberculosis, anti-diabetes mellitus and cure cancer and cytotoxic activity (Das *et al.,* 2012; Desale 2016; Kumar and Mongolla, 2018). Biology of fungal endophytes has useful in several clinical applications with molecular approaches and fungal endophytes may assist to improve the activity of drug research area. Fungal endophytes nanoparticles may be used to improve plant growth, as bio- fertilizers, enhance crop yield and soil fertility (Netala *et al.,*, 2016; Mohamed *et al.,* 2019). Secondary metabolites produced by fungal endophytes used various field of food, and pharmaceutical, agricultural and other related industries (Das *et al.,* 2012; Desale 2016; Netala *et al.,* 2016; Kumar and Mongolla, 2018; Mohamed *et al.,* 2019). Similarly, in the present study, some of the endophytic fungi have also been recorded to have antimicrobial efficacy.

ACKNOWLEDGEMENTS

The authors are thankful to the tribal peoples of Arunanchal Pradesh, for providing ethnomedicinal information about the particular plant and its uses for various ailments. Further, authors are also thankful to the Head Department of Botany, Rajiv Gandhi University, Arunanchal Pradesh as well as to the Head Department of Botany, the University of Lucknow for providing various facilities during the present study. Besides this, one of the authors is thankful to the MHRD, Govt of India; for providing financial support.

REFERENCES

Anon (2019). India Biodiversity Portal, Species https://indiabiodiversity.org/biodiv/species/show/258439

Bender SF, Wagg C,Van Der, Heijden MGA(2016) An underground revolution: biodiversity and soil ecological engineering for agricultural sustainability. Trends Ecol Evol 31(6): 440-452.

Bezerra JD, Santos MG, Svedese VM, Lima DM, Fernandes MJ, Paiva LM, Souza-Motta CM (2012) Richness of endophytic fungi isolated from *Opuntia ficus-indica* Mill. (*Cactaceae*) and preliminary screening for enzyme production. World J Microbiol Biotechnol 28:1989–1995

Chowdhery HJ (1999) Arunachal Pradesh; in Floristic diversity and conservation strategies in India, Vol. II: In the context of states and Union Territories (eds.) V Mudgal and PK Hajra Kolkata: Botanical Survey of India - pp 1059.

Compant S, Saikkonen K., Mitter B, Campisano A, Mercado-Blanco J (2017) Editorial special issue: soil, plants and endophytes. Plant Soil 405(1–2):1–11.

Das K, Das S and Tiwari RKS (2012). Bioprospecting of Endophytic Fungi for Bioactive Natural Products: Recent Trends and Future Perspectives. Microbiology Application (eds) pp. 346-364.

Desale MG (2016). Bioprospecting of Endophytic Fungi From Certain Medicinal Plants. PhD Thesis, Bharati Vidyapeeth Deemed University, Pune.

De Barry A (1866) Morphologie und physiologie der pilze, flechten, und myxomyceten, (Vol. II), Hofmeister's Handbook of Physiological Botany, Leipzig, Germany.

de Carvalho CR et al (2019) Bioactive compounds of endophytic fungi associated with medicinal plants. In: Yadav A, Singh S, Mishra S, Gupta A (eds) Recent Advancement in White Biotechnology Through Fungi. Fungal Biology. Springer, Cham.

Deepanwita D and Dhruva KJ (2018) Antimicrobial activity of Endophytic Fungi from leaves and barks of *Litsea cubeba* Pers., a Ttaditionally Important Medicinal Plant of North East India, Jordan Journal of Biological science pp 73-79.

Doilom M, Manawasinghe IS, Jeewon R, Jayawardena RS, Tibpromma S, Hongsanan, S, Meepol W, Lumyong S, Jones EBG, Hyde KD (2017) Can ITS sequence data identify fungal endophytes from cultures? A case study from *Rhizophora apiculata*. Mycosphere 8:1869–1892.

El-Maali N, Mohrram A, El-Kashef H, Gamal K (2018) Novel resources of Taxol from endophytic and entomopathogenic fungi: isolation, characterization and LC-Triple mass spectrometric quantification. Talanta 190: 466–474.

Fisher PJ and Petrini O (1987) Location of fungal endophytes in tissues of *Suaeda fruticosa*: A preliminary study. Trans. Brit. mycol. Soc 89:246-249.

Gayathri Pai and Chandra M (2017) Screening of Phytochemicals and Isolation of Endophytic Fungi from Medicinal plant *Helicteres isora* L." IOSR Journal of Pharmacy (IOSRPHR), vol. 7:12, pp. 01- 05.

Jeewon R, Wanasinghe DN, Rampadaruth S, Puchooa D, Zhou LG, Liu AR, Wang HK (2017). Nomenclatural and identification pitfalls of endophytic mycota based on DNA sequence analyses of ribosomal and protein genes phylogenetic markers: a taxonomic dead end? Mycosphere 8(10): 1802–1817.

Jia ML, Chen HL, Xin CJ, Zheng K, Rahman T, Han and LP, Qin (2016) A Friendly Relationship between Endophytic Fungi and Medicinal Plants: A Systematic Review. Front. Microbiol 7: 906.

Karimi K, Khodaei S, Rota-Stabelli O, Arzanlou M, Pertot I (2016) Identification and Characterization of two new Fungal Pathogens of Polygonatum odoratum (Angular Solomon's seal) in Italy. J Phytopathol 164: 1075-1084.

Kaul S, Ahmed M, Zargar K, Sharma P, Dhar MK (2013) Prospecting endophytic fungal assemblage of digitalis lanata Ehrh, (foxglove) as a novel source of digoxin: a cardiac glycoside, Biotechnology 3:335-40.

Kirschner R (2018) Fungi on the leaf—a contribution towards a review of phyllosphere microbiology from the mycological perspective. Biosyst. Ecol. Ser 34:433–448

Krishnamurthy YL, Naik SB, Jayaram S (2008) Communities in herbaceous medicinal plants from the Malnad region, Southern India. Microbes and Environments 23(1):24-28.

Kumar CG and Mongolla P (2018) Bioprospecting of Endophytic Fungi for Bioactive Compounds. In: Gehlot P, Singh J (eds) Fungi and their Role in Sustainable Development: Current Perspectives. Springer, Singapore.

Kuriakose GC, Palem PP, Jayabaskaran C (2016) Fungal vincristine from *Eutypella* spp-CrP14 isolated from *Catharanthus roseus* induces apoptosis in human squamous carcinoma cell line-A431. BMC Complement Altern Med 16.

Maehara S, Simanjuntak P, Maetani Y et al (2013) Ability of endophytic filamentous fungi associated with Cinchona ledgeriana to produce Cinchona alkaloids. J Nat Med 67: 421–423.

Mane and Vedamurthy (2018) The fungal endophytes: Sources and future prospects, J Med Plants Stud 6(2): 121-126.

Mane RS, Shinde MB, Wagh PR, Malkar HM (2017) Isolation of endophytic microorganisms as a source of novel secondary metabolite producers against Tuberculosis. IJSART 3: 1267-1269.

Mohamed NH, Ismail1 MA, Abdel-Mageed WM and Shoreit AAM (2019). Antimicrobial activity of green silver nanoparticles from endophytic fungi isolated from *Calotropis procera* (Ait) latex. Microbiology 165(9): https://doi.org/10.1099/mic.0.000832.

Nagmani AI, Kunwar Manoharachary KC (2005) Hand book of soil fungi. I. K. International Pvt. Ltd.

Nath A, Raghunatha P, Joshi SR (2012) Diversity and biological activities of endophytic fungi of *Emblica officinalis*, an ethnomedicinal plant of India. Mycobiology 40: 8-13.

Netala VR, Kotakadi VS, Bobbu P, Gaddam SA, Tartte V. Endophytic fungal isolate mediated biosynthesis of silver nanoparticles and their free radical scavenging activity and anti microbial studies. 3 Biotech. 2016;6(2):132. doi:10.1007/s13205-016-0433-7

Nongalleima KH, Dey A, Deb L, Singh C, Biseshwori T, Devi HS and Devi SI (2013) Endophytic fungus isolated from *Zingiber zerumbet* (L.) Sm. inhibits free radicals and cyclooxygenase activity. International Journal of Pharm Tech Research 5: 301-307.

Olson DM, Dinerstein E (1998) The Global 200: A representation approach to conserving the Earth's most biologically valuable ecoregions. Conserv Biol 12: 502–515.

Radic N, Strukelj B (2012) Endophytic fungi- the treasure chest of antibacterial substances. Phytomedicine 19:1270–1284.

Redman RS, Sheehan KB, Stout RG, Rodriguez RJ and Henson JM (2002) Thermotolerance conferred to plant host and fungal endophyte during mutualistic symbiosis. Science 298:1581.

Rodriguez RJ, Henson J, Volkenburgh EV, Hoy M, Wright L, Beckwith F, Kim YO and Redman RS (2008) Stress tolerance in plants via habitat-adapted symbiosis. ISME J 2:404–416.

Seetharaman P, Gnanasekar S, Chandrasekaran R *et al.* (2017) Isolation and characterization of anticancer flavone chrysin (5,7-dihydroxyflavone)-producing endophytic fungi from *Passiflora incarnata* L. leaves. Ann Microbiol 67:321–331.

Shukla AK, Yongam Y and Tripathi P (2012) Distribution of endophytic fungi in different parts of Rudraksh (*Elaeocarpus sphaericus*) plants. In: Microbes: Diversity & Biotechnology pp. 37-42.

Shweta S, Bindu JH, Raghu J et al (2013) Isolation of endophytic bacteria producing the anticancer alkaloid camptothecine from *Miquelia dentata* Bedd (Icacinaceae). Phytomed 20:913–917.

Sim JH, Khoo CH, Lee LH and Cheah YK (2010) Molecular diversity of fungal endophytes isolated from *Garcinia mangostana* and *Garcinia.parvifolia*. J.Microbiol. Biotechnol 20: 651-658..

Su J, Liu H, Guo K *et al* (2017) Research advances and detection methodologies for microbederived acetylcholinesterase inhibitors: a systemic review. Molecules 22.

Subramanian CV (1983) Hyphomycetes, Taxonomy and Biology, Academic Press London, Vol I & II 930.

Suryanarayanan TS (1992) Light-incubation: a neglected procedure in mycology. Mycologist 6: 144.

Suryanarayanan TS (2013) Endophyte research: going beyond isolation and metabolite documentation. Fungal Eco 6: 561-568.

Suryanarayanan TS, Kumaresan V, Johnson JA (1998) Foliar fungal endophytes from two species of the mangrove *Rhizophora*. Canadian Journal of Microbiology .44: 1003–1006.

Suryanarayanan TS, Venkatesan G, Murali TS (2003) Endophytic fungal communities in leaves of tropical forest trees: Diversity and distribution patterns. Current Science 85(4), 489 – 492

Sutton and Brian (1980) The coelomycetes. Commonwealth mycological institute kew, surrey, Engaland.

Tamura KD, Peterson N, Peterson G, Stecher M, Nei S Kumar (2011) MEGA5: Molecular Evolutionary Genetics Analysis using Maximum Likelihood, Evolutionary Distance, and Maximum Parsimony Methods. Mol Biol Evol 28: 2731- 2739.

Tejesvi MV, Mahesh B, Nalini MS, Prakash HS, Kini KR., Subbiah V and Hunthrike SS (2005) Endophytic fungal assemblages from inner bark and twig of *Terminalia arjuna* W. and A. (Combretaceae). World J Microbiol Biotechno l 21: 1535–1540.

Verma VC, Gond SK, Kumar A, Kharwar RN, Boulanger LA and Strobel GA (2011) Endophytic fungal flora from roots and fruits of an Indian neem plant *Azadirachta indica, A. Juss* and impact of culture media on their isolation. Ind.J.of Microbiol 51:469-476.

White TJ, Bruns T, Lee S, Taylor J (1990) Amplification and direct sequencing of fungal ribosomal RNA genes for phylogenetics. In: Innis MA, Gelfand DH, Sninsky JJ, White TJ, editors. PCR protocols: a guide to methods and applications. New York: Academic Press, 315–322.

Yu-Hung Yeh and Roland Kirschner (2019) Diversity of Endophytic Fungi of the Coastal Plant *Vitex rotundifolia* in Taiwan, Microbes Environ Vol. 34: (1) 59-63.

Table 1: Fungal Endophytes Isolated from *P. capitatum*, its Frequency (CF %), Density (rD%) and Accession Number

S. N.	Isolated of Fungal Endophytes	Plant parts			CF (%)	rD (%)	NCBI Accession No.
		Leaf	Stem	Root			
1	*Pestalotiopsis longiseta*	Leaf	Stem	Root	42	14.0	MK299129
2	*Sordaria fimicola*	Leaf	Stem	Root	12	4.00	MK299157
3	*Curvularia borreriae*	---	Stem	---	10	3.33	MK299132
4	*Biscogniauxia mediterranea*	Leaf	---	---	4	1.33	MK398255
5	*Colletotrichum fructicola*	---	Stem	Root	10	3.33	MK299145
6	*Diplodina microsperma*	Leaf	Stem	Root	18	6.00	MK332492
7	*Nodulisporium hinnuleum*	Leaf	---	---	16	5.33	MK299151
8	*Mucor hiemalis*	---	---	Root	6	2.00	MK299138
9	*Aspergillus niger*	Leaf	---	Root	12	4.00	MK248610
10	*Nigrospora oryzae*	---	Stem	---	14	4.66	MK299154
11	*Corynespora cassiicola*	Leaf	---	---	6	2.00	MK299155
12	*Dothidea sp.*	Leaf	Stem	---	8	2.66	MK299156
13	*Penicillium chrysogenum*	Leaf	---	Root	6	2.00	MK299147
14	*Fusarium merismoides*	Leaf	Stem	---	10	3.33	MK299158
15	*Alternaria sp.*	Leaf	Stem	---	8	2.66	MK332475
16	*Aspergillus flavus*	Leaf	---	Root	16	5.33	MK332476
17	*Bipolaris bicolor*	---	---	Root	2	0.66	MK332477
18	*Curvularia spicifera*	Leaf	---	Root	8	2.66	MK332478
19	*Pithomyces chartarum*	Leaf	Stem	---	2	0.66	MK299154
20	*Lasiodiplodia pseudotheobromae*	---	Stem	---	8	2.66	MK248599
21	*Scopulariopsis brevicaulis*	Leaf	---	---	10	3.33	MK299149
22	*Colletotrichum gloeosporioides*	---	Stem	---	6	2.00	MH752465
23	*Eutypa sp.*	Leaf	Stem	---	8	2.66	MK299142
24	*Aspergillus nidulans*	Leaf	---	---	12	4.00	MK299125
25	*Fungal Endophyte sp*	---	---	Root	4	1.33	MK248607
26	*Fusarium incarnatum*	Leaf	Stem	Root	8	2.66	MK299134
27	*Lasiodiplodia viticola*	---	Stem	---	14	4.66	MK398249
28	*Aspergillus fischeri*	Leaf	---	---	10	3.33	MH748593
29	*Preussia sp.*	Leaf	Stem	Root	4	1.33	MK398250
30	*Phoma sp.*	---	Stem	---	6	2.00	MK398251
31	*Pseudocamarosporium brabeji*	Leaf	---	Root	2	0.66	MK398252
32	*Aspergillus fumigatus*	---	Stem	root	8	2.66	MK398253
33	*Diaporthe sp.*	Leaf	Stem	Root	16	5.33	MK398254
34	*Aureobasidium sp.*	Leaf	Stem	Root	10	3.33	MK398283
35	*Chaetomium globosum*	---	Stem	---	2	0.66	MK398256

--- indicates absences of the fungal endophytes.

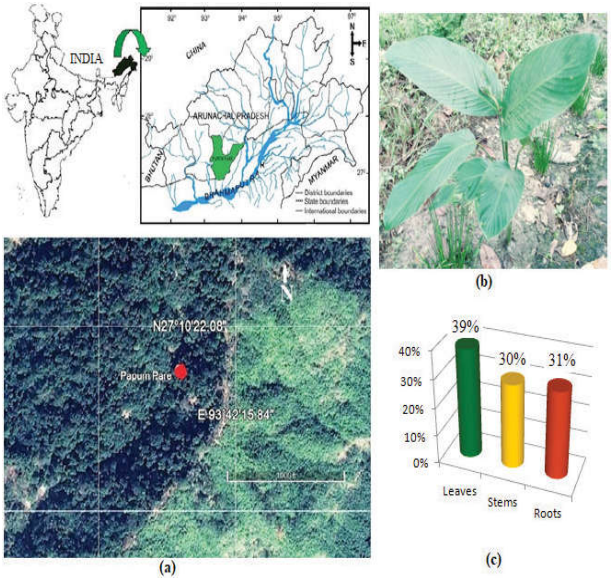

Fig. 1: Sample Collection Site of *P. capitatum*, in Arunachal Pradesh, India (Satellite Image), where, Red Circle Indicates Collection Site (b) Ethnomedicinal Plant *P. capitatum*, an Overview (c) Fungal Endophytes Isolated from Different Parts of *P. capitatum*

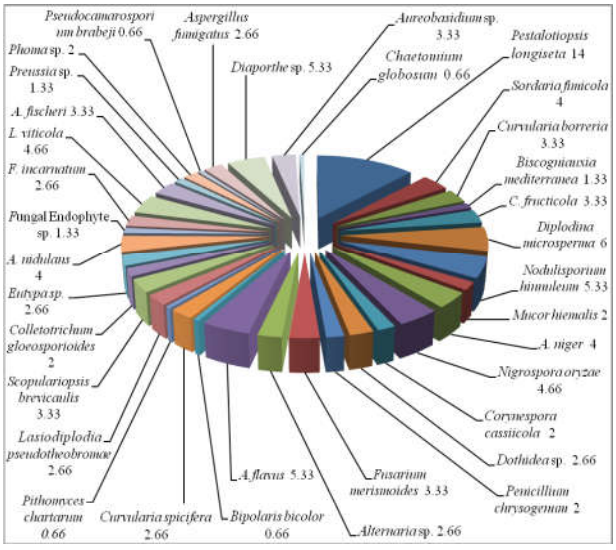

Fig. 2: Isolated Fungal Endophytes and its rD (%) from *P. capitatum*

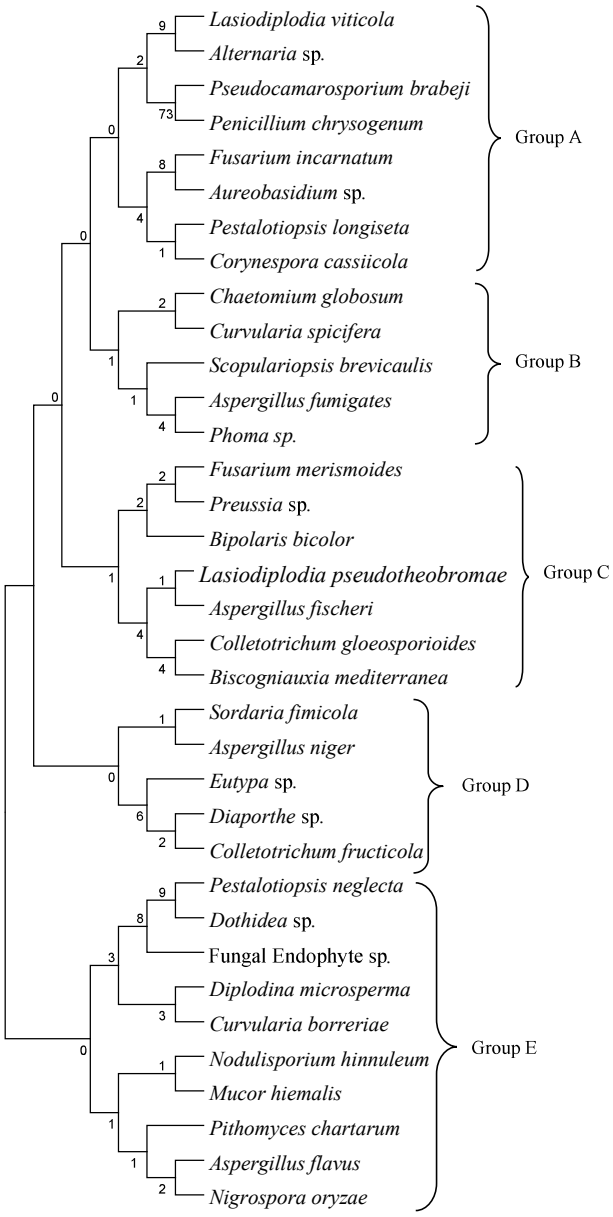

Fig. 3: Phylogenetic Analysis based on Neighbor-joining Tree based on ITS rDNA Sequences of the Isolated 35 Fungal Endophytes. Numerical Values Indicate Bootstrap Percentile from 1000 Iterations

Science and Technology Journal, Vol. 7 Issue: 1 ISSN: 2321-3388

Interactive Color Image Segmentation using HSV Color Space

D. Hema[1] and Dr. S. Kannan[2]
[1]Assistant Professor, Department of Computer Science, Lady Doak College, Madurai
[2]Professor, Department of Computer Applications, School of Information Technology, Madurai Kamaraj University, Madurai
E-mail: [1]hemamku17@gmail.com, [2]skannanmku@gmail.com

Abstract—The primary goal of this research work is to extract only the essential foreground fragments of a color image through segmentation. This technique serves as the foundation for implementing object detection algorithms. The color image can be segmented better in HSV color space model than other color models. An interactive GUI tool is developed in Python and implemented to extract only the foreground from an image by adjusting the values for H (Hue), S (Saturation) and V (Value). The input is an RGB image and the output will be a segmented color image.

Keywords: Color Spaces, CMYK, HSV, Segmentation

INTRODUCTION

Image Processing

Human eyes can perceive and understand the objects in an image. In order to design a machine that can understand like a human, it requires appropriate algorithm and massive training. An image is a visual representation of any real world object that can be manipulated computationally. Image Processing is an extensive area of research that gains attention in many applications including Vehicle detection where the author (Kaur 2017) has implemented Image Enhancement, Morphological operations, Segmentation, Otsu Threshold and Edge Detection to detect vehicles from satellite images, Fabric defect Detection (Tamil Selvi and Nasira 2017) is performed where Artificial Neural Networks (ANN) and Support Vector Machines (SVM) have been used to classify fabrics with defects. Image processing involves processing of data where input and output are images.

Digital Image processing processes the image using pixel values and is deployed in Machines. Low-level Image processing techniques are noise reduction, contrast enhancement and image sharpening. Mid-level Image processing techniques are segmentation, image classification, object description and recognition. The High-level Image processing techniques are image analysis and cognitive functions to emulate the human vision. Computer vision is another branch of research where Digital Image processing plays a vital role to learn, make inferences and perform actions based on visual inputs.

Color Models and Spaces

A color model is an abstract mathematical model in which colors are represented as tuples of numbers either three or four values or color components. When the color model is associated with an accurate description of how the components are to be inferred and the conditions are viewed, the set of resulting colors is called "color space." Color space can also describe the ways in which human color vision can be modeled. In few instances, color space and color models are significantly equal. There are different color spaces like RGB, NTSC, YCbCr, HSV, CMY, CMYK and HSI. Given an RGB image, converting it into any other color space is performed using any transformative functions. RGB Color space is the basic form of image representation, but some applications may find it more convenient to use other color spaces as well.

RGB

The default color model of an image is RGB (Red, Green, and Blue). In this model, an image is an I x J x 3 array of color pixels,

http://doi.org/10.22232/stj.2019.07.01.05

where each pixel is a triplet of three colors red, green and blue at a spatial location (I, J). These three color components can be viewed as a stack of three individual layers. Every pixel in an image will have a red layer, blue layer and green layer that will result in a RGB image. All these color components can be viewed as a 3-D model. In additive color mixing, when all three color channels have a value of zero, it means that light is not emitted hence, resulting color is black. When all three color channels are set to their maximum values i.e., 255, then the resulting color is white. Television Monitors are very good examples which uses the concept of additive color mixing.

HSV

HSV (Hue, Saturation, Value) color space is considerably closer to RGB color space in which humans describe color sensations and perceive colors. Hue is the dominant color observed by humans. Saturation is the amount of white light assorted with hue. Value is the brightness/ Intensity. In short form, Hue refers to tint, Saturation refers to shade and Value refers to tone. A HSV color space can be viewed as a geometric cylinder, where the angular dimension represents Hue(H), starting at the primary red at 0°, and moving to primary green at 120° and primary blue at 240°, and then finally wrapping back to red at 360°.The distance from the central axis of HSV cylinder corresponds to Saturation(S). A saturation value moving towards the outer edge means that the colorfulness value is at the maximum for the color defined by the hue. The central vertical axis of HSV color space is the Value (V), ranging from black at the bottom with lightness or value 0, to white at the top with a lightness or value 1.

CMYK

The CMYK color space involves subtractive primary colors like Cyan(C), Magenta (M), Yellow(Y) and Black (K). A large range of colors seen by humans can be obtained by combining cyan, magenta and yellow transparent inks on a white substrate. A fourth ink, black is added to enhance the reproduction of some dark colors. The cyan color absorbs red light but it transmits green and blue color. The magenta color absorbs green light but transmits red and blue color, and the yellow color absorbs blue light but transmits red and green color. The white color reflects the transmitted light back to the viewer. CMYK color space is mainly used for printers and for photographs.

NTSC

The NTSC color space is used in television. In this color space, gray-scale information is separated from color data, hence the single signal can be used for both color and monochrome television sets. In this color space, an image is represented as three components such as luminance, hue and saturation. Luminance is the gray-scale information whereas the other two components are the color information of a TV signal.

SEGMENTATION

Image Segmentation is the process of dividing an image into its constituent regions or objects. The level of subdividing an image depends on the problem being solved. Segmentation process can stop when the objects of interest is isolated for further processing. There is wide range of applications which require image segmentation. Based on the area of image application, appropriate Segmentation techniques can be used. There is an evolutionary process of region immigration and deportation along with watershed algorithm (Roohollah and Kazem 2017). Image segmentation is very helpful in the field of medical applications to detect breast cancer (Samson 2015), liver diseases (Pandey 2018)etc. There also has been a hybridization of Otsu method and median filter to segment the desired image (Firas and Fawzi 2013). The color images are segmented using a combination of grab cut and color spaces for foreground extraction (Dina 2014). Watershed algorithm and region merging (Ji and Harris 1998) using artificial neural networks is also used for color image segmentation. In this research work, we have developed an interactive tool that has 3 Control bars for Hue, Saturation and Value. When an input image is given, the GUI interface is opened, and the Control bars will be displayed for H, S and V with minimum and maximum limits. The User can interactively drag the control bars towards left and right and witness the changes that happen in the image. When the desired result is obtained, the process of adjusting the HSV values can be stopped and the procedure can be repeated for multiple images under study.

COLOR IMAGE SEGMENTATION USING HSV

Color image segmentation is frequently used for human skin color detection. Skin color detection (Hanaa and salma 2018) using all three color spaces like RGB, HSV and YCbCr is carried out as a segmentation step. A new color image segmentation method (Gustavo 2016) such as split & merge and region growing, and the combination of the

RGB and HSV color representation models was reviewed. In our work, the foreground object from the given image is segmented for detecting and recognizing the object. This is performed as a two-step algorithm. The first step is to select the Region of Interest (ROI) from the given image and the second step is to adjust HSV values in the ROI to extract the foreground image.

In the first step, an RGB image is converted to HSV image. Each component Hue, Saturation and Value is separated, and its value is represented in a range using a GUI developed in Python. The HSV values are chosen interactively by adjusting the GUI based track bar for each component Hue, Saturation and Value. The Hue is in the range of 0-179 whereas Saturation and Value is in the range of 0-255.By dragging the track bar and adjusting its value over it, an optimum value for all H, S and V is identified. Hereby, the background is masked and only the objects of interest are found. A single H, S and V may not be applicable for all kind of images. But by using an interactive tool, the user will have a provision to select the H, S and V values for different category of images. When the selected object of interest is segmented completely, the HSV adjustments can be stopped and the foreground image can be saved for further processing. The process flow for this technique to segment only the foreground image is given in Fig.1.

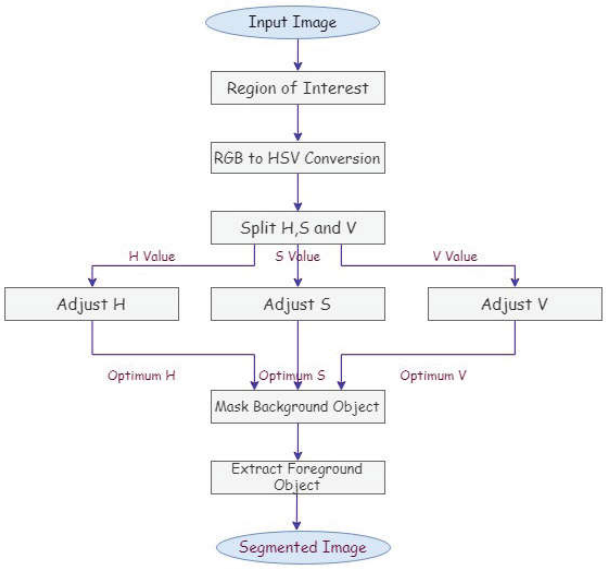

Fig. 1: Color Image Segmentation Technique using HSV

RESULTS & DISCUSSION

The object of interest is based on the application in which it requires further high-level image processing techniques like Object recognition, Scene classification etc. The Color image segmentation using HSV is achieved until the object to be processed is extracted. Each object is segmented for different HSV values. The same HSV values are not applicable for all images under study. Hence, the HSV values are adjusted in the track bar to find the optimum value for each set of images. The Experimental results of this segmentation process is given in Fig.2. The different set of Original image like human face, bird, flower, bottle and chair is Fig. 2(a), Region of Interest is Fig.2 (b), segmented image using HSV is Fig.2(c) and manually segmented image is Fig.2 (d). The images obtained as a result of this HSV segmentation technique can be used for further process of feature extraction and classification techniques.

STRUCTURAL SIMILARITY INDEX

To evaluate the performance of the HSV color image segmentation technique deployed in this work, a metric called Structural Similarity Index (SSIM) is calculated between the HSV segmented images and manually segmented images. SSIM is a metric widely used to measure the similarity between two images. The SSIM has a value that ranges from 0 to 1. The maximum value of 1 indicates that the two images to be compared are structurally similar while a value of 0 indicates no structural similarity between two images. The SSIM value for the 5 set of images is given in Table 1.

From the SSIM values, it can be visualized that the images segmented using HSV technique and manually segmented images are more or less similar. When the images are seen through human eyes, there is a negligible difference that can be seen between the set of images in Fig. 2(d) and Fig. 2. (c).

(a) (b) (c) (d)

Fig. 2: Original Image (a), ROI (b), Segmented Image using HSV(c) and Manually Segmented Image (d) for Human Face, Bird, Flower, Bottle and Chair

Table 1: SSIM Values between HSV Segmented and Manually Segmented Images

Image	SSIM
Human face	0.4932
Bird	0.8608
Flower	0.6132
Water bottle	0.6513
Chair	0.8769

CONCLUSION

Image Segmentation can either be low-level or high level processing and it is based on the needs of the user who is incorporating the ideas. In this paper, we have focused on color image segmentation for object detection and learning. Sometimes it can also be a major research area which requires large scale image processing techniques and automatic classification of image. To the best of my knowledge, most of the papers have implemented color space segmentation for only single set of object class. But in

this paper, color image segmentation is performed to extract not only human skin color but also for other objects from background. To enhance this segmentation process, the segmented images can be followed by or integrated with any other morphological operations.

REFERENCES

Noorpreet Kaur Gill, Anand Sharma (2017) Vehicle Detection from Satellite Images in Digital Image Processing. International Journal of Computational Intelligence Research 13: 697-705.

S. Sahaya Tamil Selvi, G. M. Nasira (2017) An Effective Automatic Fabric Defect Detection System using Digital Image Processing. Journal of Environmental Nanotechnology 6: 79-85.

Roohollah Aslanzadeh,Kazem Qazanfari, Mohammad Rahmati (2017) An Efficient Evolutionary Based Method For Image Segmentation

Samson Nivins (2015) Breast cancer detection of ultrasound image using watershed technique. International Journal of Engineering Science and Research 3:88-93

Pandey, Ram & Vasan, Ashwin & Ramakrishnan, A. (2018). Segmentation of Liver Lesions with Reduced Complexity Deep Models.

Firas Ajil Jassim, Fawzi H. Altaan (2013). Hybridization of Otsu Method and Median Filter for Color Image Segmentation. International Journal of Soft Computing and Engineering 3:69-74

Dina Khattab, HalaMousher Ebied, Ashraf Saad Hussein, Mohamed Fahmy Tolba (2014). Color Image Segmentation Based on Different Color Space Models Using Automatic GrabCut. Scientific World Journal.

S. Ji and C. Harris. Image segmentation of color image based on region coherency. Proceedings of International Conference on Image Processing; 1998.

Hanaa Mohsin & Salma Hameedi Abdullah (2018). Human Face detection using Skin Color Segmentation and Morphological Operations. Journal of Al-Nisour University college 7.

Gustavo Scheleyer, Claudio Cubillos, Gastón Lefranc, Román Osorio-Comparán, Ginno Millán. A new colour image segmentation. proceedings of 6th International Conference on Computers Communications and Control;2016.

Science and Technology Journal, Vol. 7 Issue: I ISSN: 2321-3388

Impact of Optical Booster to Enhance the Gain Bandwidth for Dense Optical Communication System

Ghanendra Kumar[1] and Chakresh Kumar[2]*
[1]Department of Electronics and Communication Engineering
National Institute of Technology, Delhi–110040, India
[2]University School of Information, Communication & Technology,
Guru Gobind Singh Indraprastha University, New Delhi–110078, India
E-mail: *chakreshk@gmail.com

Abstract—This paper explains how the combination of RAMAN amplifier and PARA-METRIC amplifier using non-linear fiber components increases the gain bandwidth. Two kinds of configuration of amplifier are demonstrated with gain associated and bit error rate is seen. 15dB gain is measured and flat gain of 5 dB is measured.

Keywords: FWM, OPC, RZ, NRZ, DWDM, OBP, XPM, EDFA, Mach-Zehnder Modulator

INTRODUCTION

In recent years, the most attracting technology is the RAMAN amplifier, which allows high-capacity data signals for long distance in the optical fiber communication. RAMAN amplifying device is in the research process due to its small size and high compact high energy pumping laser availability. Thus, both non-linear process fiber RAMAN Amplifier (FRA) and Optical PARA-METRIC Amplifier (OPA) hybrid is used to develop wide bandwidth amplifying device [1-5]. RAMAN amplification technology demonstrates the increase in transmitting capacity and span length. FRA output showed results of ultra-wide BW, lower noise and suppressing non-linearity. Discrete RAMAN Amplifier (DRA) using Dispersion compensating fiber (DCF)/Highly non-linear fiber (HNLF) have good noise output and better signal budget. PARA-METRIC amplifier uses highly productive four-wave mixing in fiber optics. We can get a gain value around 49 dB and bandwidth of 200 nm by proper design of HNLF [6]. The demand of large bandwidth, less noise figure and also less gain ripple values makes both FRA's and OPA's more attractive over tradition EDFA [7]. Studies have concluded that RAMAN assisted EDFA having configuration of hybrid yielding low noise figure (NF) and optical to signal ratio. Flat gain characteristics over C and L band are used in RAMAN/ EDFA hybrid amplifier. But, bandwidth gets restricted by Er ions. FRA design laser problem of quandary of pump interaction. A lot of compact amplifier are used the minimum of noise signal or gain fluctuation will be multiplied several times in te end. E Golo Vehecnko, Hsieh and Freitas have tried to increase gain-enhancing effect on the coupling of two non-linear process. In this paper we see a way of combining FRA and HNLF to achieve gain around or over 15dB and a gain ripple within 5dB [8-12].

MATHEMATICAL MODEL

Mathematical model is divide into two parts-A. Power Pump evalutation for co- propagation para-metric and counter propagating RAMAN pump. B. Net signal gain A. If both the amplifier interact using RAMAN effect, thus the coupling equation used in RAMAN effect can be represented as

$dP/dz = g\lambda R/A_{eff} * P_R P_P - \&_p P_P$

$dP_R/dz* = - w_R/w_P A_{eff} * g\lambda R P_R P_P - \&_R P_R$

A_{eff} – Effective mode area

P_R- RAMAN effective power

P_P- PARA-METRIC effective power, $\&_R$- Attenuation coefficient (RAMAN), $\&_p$- Attenuation coefficient (PARA-METRIC), Thus, initially P_P (l=0) = $P_{P@0}$ [w] while P_P (L km) = $P_{R@L}$[W]

http://doi.org/10.22232/stj.2019.07.01.06

Now the solution can be obtained by dividing the wire into small lengths of delta z with constant light power. Also iterating using fourth order Range- Kutta method power output can be calculated.

B. The net gain by RAMAN pump and the PARA-METRIC pump are represented by

$$g_R(\lambda,L) = [\, g_R(\lambda,\beta_1)\, g_R(\lambda,\beta_2).....g_R(\lambda,\beta_n)]$$

$$g_P(\lambda,L) = [g_P(\lambda,\beta_1)\, g_P(\lambda,\beta_2).....g_p(\lambda,\beta_n)]$$

Where $g_R(\lambda,L)$ and $g_p(\lambda,L)$ are gain of each segment in both the pumps respectively.

RAMAN Gain in Each Segment

The pump power level may be derived as

$$dP_s/dz = g\lambda R/A_{eff} * P_R P_s - \&_s P_s$$

$$dP_R/dz* = -\&_R P_R$$

Where, P_S is power output by the signal. Thus, solving this equation using the small valued gain assumption over delta z length gives the total gain as-

$$g_R(\lambda, \text{delta z}) = EXP[\, g_R P_R(\text{delta z})/ A_{eff} \&_R * (e^{\& R^{\text{delta z}}} - 1) - \&_S P_S)$$

Calculating PARA-METRIC Gain in Each Segment (delta z)

According to small signal theory, there is a PARA-METRIC gain which amplifies the signal with idler rising at wp= 2wp+ws.

Therefore, small power gain at the length delta z

$$g_p(\lambda, \text{delta z}) = 1+ [\, \lambda P_p(\boldsymbol{\delta} z)/g_p \sinh(g\boldsymbol{\delta} z)]$$

The PARA-METRIC gain g is given by,

$$g^2 = -\boldsymbol{\Delta} k_o\, (\boldsymbol{\Delta k}_o/4 + \boldsymbol{\gamma} P_p(\boldsymbol{\delta} z)]$$

$\boldsymbol{\Delta k}_o$ is linear phase mismatch.

$$\boldsymbol{\Delta k}_o = - 2\pi c/ (\lambda_o)^2 * dD/d\lambda\, (\lambda_p - \lambda_0)\, (\lambda_{p\_} \lambda_s)^2$$

thus, the net gain is given by $G_{net,}$

$$G_{net}(\lambda,L) = 10\log[\, g_R(\lambda,L) + 10 \log[\, g_p(\lambda,L)]$$

Gnet = Net signal gain due to two pumps for the length (L)

$$G_{ON/OFF} = Gnet((\lambda,L)) + |\, L_T|$$

$G_{ON/OFF}$ = on/off gain = sum of total component losses (LT)

EXPERIMENTAL SETUP

By employing two different arrangements namely. Tandem and Unison, we observe the plausible gain BW increment of the amplifier. Fig.1 (a) shows the unison configuration. In this arrangement both the gains occur in the same HNLF. Para-metric pump source is a DFB laser (λ = 1603nm) which is a combination of 580-660 MHz RF frequencies centred at around 1603nm frequency. Although a high power EDFA is used to amplify/ pump the para-metric pump (OPA), PARA-METRIC nonlinear interaction can be better generated by using high power LD with low noise. ASE noise is filtered by 1 nm wide passband filter. Signal source is a tunable laser whose power is kept constant at -3dBm. The modulation OSF, The signal beam was done using the LiNbo3 Mach Zehnder Dimension Modulator (MZM), which is powered by the enhanced output of a pattern generator, which produces 10 Gbps NRZ pseudo bit stream and bit stream behaviour is randomly. (PRBS: 10-31). The para-metric pump (λ = 1601) and the signal then went through a 1452 nm/ C and L band Wavelength Division multiplexer (WDM) before they were launched in 550 m long HNLF fiber. The HNLF that has a smallest dispersion wavelength λ'=1590nm, an effective area Aeff = 16 into 10–12 m2A, a loss occurs of 0.7 dB/km, length L=550m and a non-linear coefficient $\boldsymbol{\gamma}$=5.7 into 10–3W–1 m-1. A 1452 nm/C+L coupler connects to the HNLF, A counter-propelled RAMAN pump focuses on 1452 nm, in which the full width of 2nm is half the maximum (FWHM) bandwidth. The signal passes through an edge filter with 1dB insertion loss for wavelength shorter than 1593nm and level of blocking is about 40dB for wave-lengths greater than 1600nm. The signal is analyzed, when Edge and 12822 AO/ E convert and use the sample oscilloscope to pass through the edge filter using the optical spectrum analyzer (OSA) in time and Wavelength's domain. BERT analyzer was used for bit error rate analysis.

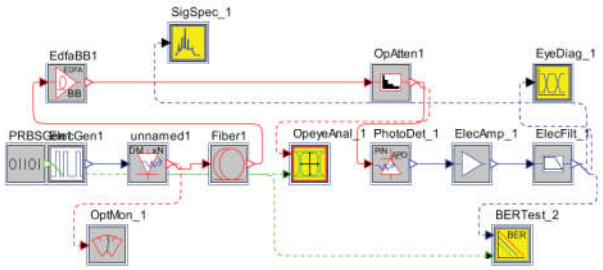

(a)

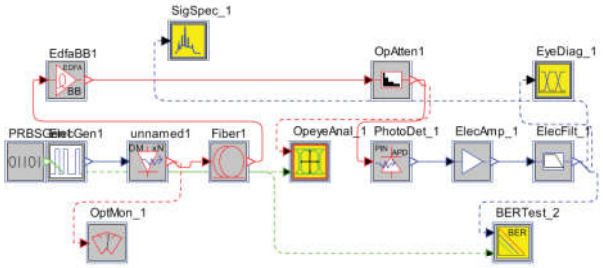

(b)

Fig. 1(a): Experimental Setup for Unison Structure of Hybrid RAMAN/Optical Fiber Amplifier, Figure 1(b): Exploratory Setup for Tandem Structure of the Hybrid Amplifier

Fig. 1(b) show the tandem configuration. Two separate 550nm long HNLF fiber are used for each of these processes. The signal and PARA-METRIC pump were coupled using 70/30 coupler, from where it is launched into the primary segment holding the PARA-METRIC process. At the end of this segment, edge filter allows the signal to pass through, neglecting 1603nm signal. Two 1450nm/C+L coupler holds the second segment. The second coupler joins the RAMAN pump to the HNLF, while the first dumps the RAMAN pump. Resulting signal which is allowed to pass through these couplers are observed for their spectral and temporal characteristics also error analyzer was used to give bit rate analysis.

EXPLORATORY RESULT

A. Ranging of the Gain Bandwidth 1st independent individual characterisation of both the processes was observed. The on/off gain ($G_{ON/OFF}$) is defined as –

$$G_{ON/OFF} - P_{Sig\_out(pump\text{-}on)} - P_{sig\_out(pump\text{-}off)}$$

Where, $P_{sig\_out(pump\text{-}on)}$ and $P_{Sig\_out(pump\text{-}off)}$

Variables used are wavelength and power level of pumps. The wavelength is varied over C+L band. For each of nonlinear pumps, two plots of the on/off gain curves were obtained against the variations.

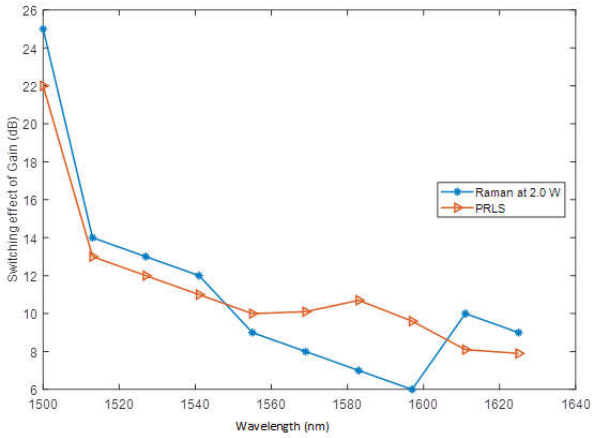

Fig. 2

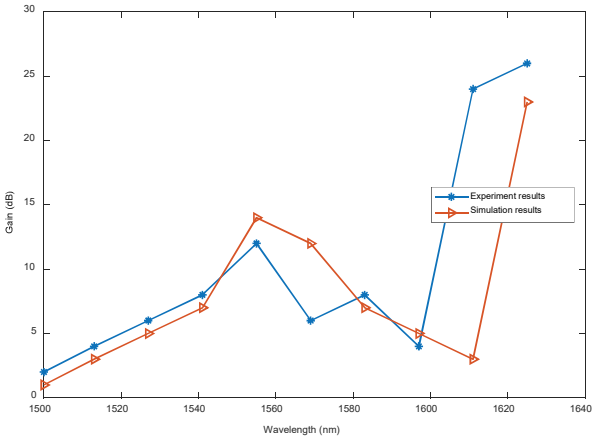

Fig. 3

Fig (2) and Fig (3) For RAMAN only pump at 1.6W, the on/off gain max (15.2dB) was observed at 1555nm and with increase with wavelength into L, declined gradually. For PARA-METRIC, only pump the maximum (14.5dB) on/off gain was obtained at 1584nm. Now for hybrid effect, both pump were on with the same power level and variations of wavelength into C-L band. It was noted that there is a significant increase in the gain for the PARA-METRIC region while the gain decreases in the RAMAN region with the wavelength tuning from 1615 to 1580nm. The RAMAN dump port explains this phenomenon. It was found that when wavelength was coordinated with the RAMAN region, with RAMAN pump tune at 1.6w and PARA-METRIC pump at 0.69w, there was about 15% of power transfer from the RAMAN pump power to the PARA-METRIC pump. This suggests that in UNISON configuration leads to power transfer from RAMAN pump to PARA-METRIC pump. Therefore, there is an increase in PARA-METRIC gain coupled with a decrease in RAMAN gain.

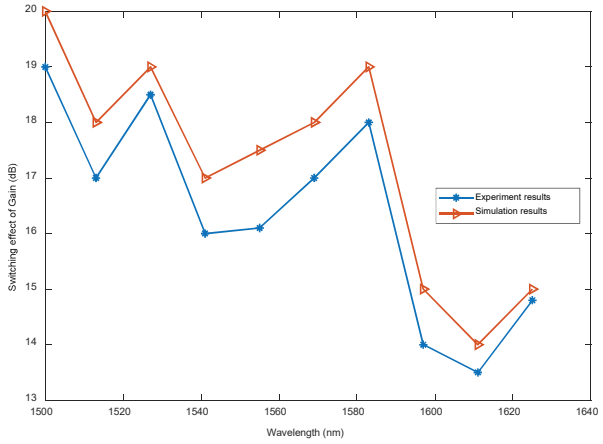

Fig. 4

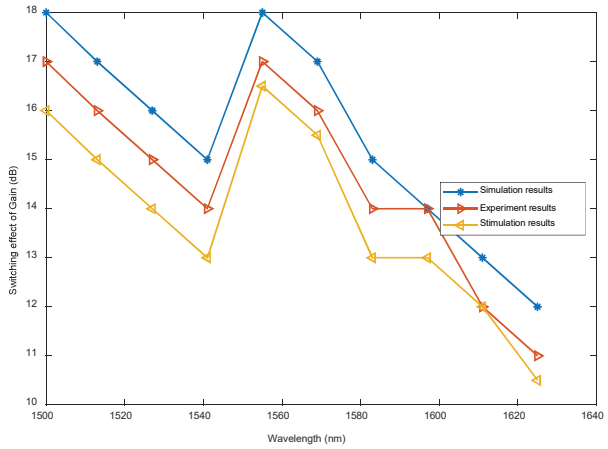

Fig. 5

Reconfiguration of independent variables leads to most favourable condition of the pumps (RAMAN pump tune at 1.6w, para-metric pump at 0.38w. For these set values, gain deviation of 5.4dB, on gain and off gain (maximum) is examined of 14dB. It was noted the polarizations of these signal impacts the gain compute in this region of powerful para-metric gain on a major level in comparison to the para-metric pump producing polarization. Two polarization controllers (PC), one each in PARA-METRIC pump and signal path control the relative polarization. The amplification is a two stage process. First HNLF segment amplifies the signals within the parametric gain system while as signal in RAMAN gain region get amplified by first HNLF segment. Both pumps (PARA-METRIC and RAMAN) amplify wavelength in region 1570-1580nm. By adjusting overlapping gain region, the gain variation can be minimized as well as optimized. Adjustments of pump with power helps to obtain the flat gain. The experimental data fares well the simulation that with relative error (max) at 12% with RAMAN region, while 10% in para-metric region of gain.

For Tandem & Unison configuration, the noise figure can be expressed using -

$$NF_S = 2P_{PF+}/\eta\ \omega_S BG_S + 1/G_s$$

For single PARA-METRIC pump lowest NF values are 3.7, 3.8 and 4.2dB from fig. 4 and fig. 5. Limited OPA pump source power, phase modulator and insertion loss compels for usage of EDFA . ASE is generated due to this and can be terminated by using a number of lower insertion filter.

Relative noise intensity also gets generated from SBS in the PARA-METRIC process. Signal with these (ASE and SBS) noise sources get onto second RAMAN amplification stage. Amplified spontaneous scattering by RAMAN process due to higher RAMAN pump (1.63W) is also a noise. Tandem NF value is -34dB greater than unison configuration value. Increased NF value of signal is due to increased ASE noise. This causes higher power at RAMAN pump. Usage of multiple lower power RAMAN pumps can solve the problem with a slight change in HNLF length, but the gain characteristics must be kept equivalent. while for unison configuration RAMAN region NF are lower than PARA-METRIC region value. ASE gets transferred, reduced by almost 6dB from its RAMAN region peak while PARA-METRIC pump ASE is increased by the same amount. This transfer is controlled by para-metric pump wave-length. Selection of PARA-METRIC pump where RAMAN pair is maximum leads to large NF variations i.e. 7.3 dB – 21 dB. In regions of smaller RAMAN pair para-metric pump choice has reduced the NF variation 7.9dB to 13.7 dB.

THE STUDIES OF TIME DOMAIN

For this time, study of the time domain, consolidate the configuration by keeping the RAMAN pump at 1.534 and the PARA-METRIC pump at 0.34W. BER performance (assuming Gaussian noise) was calculated by observing optical power over a range of varied wavelengths. Q-parameter is calculated as

$$Q = (-0.167+\sqrt{(0.028 - \log((BER/0.217)+3.92)}$$

Power penalty is observed at 1.58nm wavelength due to increased NF and SBS noise. In unison configuration, the 15% of total of power of RAMAN is transferred to para-metric pump causing SBS noise. In Tandem configuration, SBS remains low due to no transfer of power between any pumps thus producing only 1dB power penalty.

CONCLUSION OF THE EXPERIMENT

Conclusion It turns out that by combining the PARA-METRIC and RAMAN process in one unit, practically and in principle, we can increase the BW by increasing the profit area to get RAM benefits. We come across the features like gain, BW, noise figure and error in bit rate for two non-linear processes. Two different ways to achieve the flat gain bandwidth are Unison and Tandem. The mathematics shows that tuning the two pump, wavelength give improved gain flatness. Multiple RAMAN amplifier and proper HNLF length are used to reduce noise properties. In the RAMAN gain area (1545 nm-1570 nm), a negligible power penalty is produced for both Unison and Tandem. We configure that substantial increase can be seen in the gain region if we are provided with experimental flexibility. We mainly focus on the increase of gain BW and not on optimized parameters used in the combined RAMAN and Para-metric amplifiers.

REFERENCES

Pinto A M R, Frazão O, Santos J L, Lopez Amo M (2010) Multiwavelength fiber laser based on a photonic crystal fiber loop mirror with cooperative Rayleigh scattering: Appl. Phys. B, Lasers Opt. 99: 391–395.

Zhang L , Xu Y , Gao S, Saxena B , Chen L, Bao X (2018) Multiwavelength coherent Brillouin random fiber laser with ultrahigh optical signalto-noise ratio: IEEE J. Sel. Topics Quantum Electron 24: 0900308.

Du X, Zhang H, V X, Wang X, Zhou P, Liu Z (2015) Multiwavelength Raman fiber laser based on polarization maintaining fiber loop mirror and random distributed feedback: Laser Phys. Lett. 12: 045106.

Sugavanam S, Tarasov N, Shu X, Churkin D V (2013) Narrow-band generation in random distributed feedback fiber laser: Opt. Express 21: 16466–16472.

Pang M, Xie S, Bao X, Zhou D P, Lu Y, Chen L (2012) Rayleigh scattering-assisted narrow linewidth Brillouin lasing in cascaded fiber: opt. Lett. 37: 3129–3131.

Zhu T, Huang S, Shi L, Huang W, Liu M, Chiang K (2014) Rayleigh backscattering: A method to highly compress laser linewidth: Chin. Sci. Bull 59: 4631–4636.

Babin S A, Zlobina E A, Kablukov S I, Podivilov E V (2016) High-order random Raman lasing in a PM fiber with ultimate efficiency and narrow bandwidth: Sci. Rep. 6: 22625.

Zlobina E A, Kablukov S I, Babin S A (2015) Linearly polarized random fiber laser with ultimate efficiency: Opt. Lett. 40: 4074–4077.

Wu H, Wang Z N, Churkin D V, Vatnik I D, Fan M Q, Rao Y J (2015) Random distributed feedback Raman fiber laser with polarized pumping: Laser Phys. Lett. 12: 015101.

Xu J (2017) Near-diffraction-limited linearly polarized narrow-linewidth random fiber laser with record kilowatt output: Photon. Res. 5: 350–354.

Li T (2018) Power scaling of narrow-linewidth fiber amplifier seeded by Yb-doped random fiber laser: IEEE J. Sel. Topics Quantum Electron 24: 0903208.

Jin X, Lou Z, Zhang H, Xu J, Zhou P, Liu Z (2016) Random distributed feedback fiber laser at 2.1 μm: Opt. Lett. 41: 4923–4926.

Science and Technology Journal, Vol. 7 Issue: I ISSN: 2321-3388

A Comparative Study between Pre-construction and Construction Phases of Champhai-Zokhawthar Road Construction, Mizoram: Air Quality and Noise Quality Assessments

Lalventluanga[1]* and H. Lalramnghinglova[2]
[1,2]Department of Environmental Science, Mizoram University, Aizawl–796004, Mizoram, India
E-mail: *venalushai@gmail.com

Abstract—In recent years, Mizoram has made immense progress in various sectors and initiated developmental programmes for its economic growth. An important contributing factor to this development and growth is the transport connectivity projects. Although connectivity projects can boost economic growth, its negative effects cannot be neglected. In view of this, the present research studies the impacts of Champhai – Zokhawthar road construction on the air quality and noise quality of the region. This comparative study of the impact on the quality of air and noise pollution in the pre-construction phase and construction phase provide a clear-cut example of the negative impacts caused by road construction and provide a fresh outlook for formulation of improved management plans. Air quality assessment was carried out using High Volume Air Sampler and the following parameters were monitored – suspended particulate matter (SPM), respirable suspended particulate matter (RSPM), nitrogen dioxide (NO_2) and sulphur dioxide (SO_2). The results indicate that mean SPM concentration was increased by 22.82 μg/m^3; RSPM concentration by 14.67 μg/m^3; NO_2 concentration by 4.08 μg/m^3; and SO_2 concentration was increased by 0.06 μg/m^3 from the pre-construction phase to construction phase. Noise quality assessment was carried out at three sites – Zotlang, Melbuk and Zokhawthar by using Lutron SL-4001 Sound Level Meter and Leq, Lmax and Lmin were recorded and calculated. The mean noise level at Zotlang wasincreased by 8.72 dB (A) and at Melbuk the mean noise level was increased by 9.35 dB (A). However, at Zokhawthar, there was a decrease in mean noise level by 0.13 dB (A). From the present study, it is evident that road construction poses a threat to the air quality and noise quality of the study area and improved measuresneed to betaken to curb its negative impacts.

Keywords: Environmental Impact Assessment, Air Quality, Noise Quality, Road Construction, Champhai

INTRODUCTION

Roads are an integral part of the transport system and play an important role in the socio-economic growth of a community, state or nation. The overall performance and social functioning of a community is largely influenced by developed and maintained road networks. Roads enhance mobility, exposure from isolation and therefore poverty (Seiler 2001). The state of Mizoram has also made tremendous improvement in road infrastructure with Government of India taking initiatives to improve its road network in North-Eastern States of India. Mizoram being a state which greatly depends on roads for transportation will benefit immensely from these road improvement plans. Although the positive impacts of roads are greatly acknowledged, its negative impacts mainly to the environment are neglected and underestimated (Newman *et al.,* 2012). Therefore, awareness on these negative impacts needs to be focused on with proper and effective mitigation measures before decision-making is done in any road construction project.

Road construction activities include land clearing, operation of machines and wide scale demolition works which generate high levels of dust which can disperse over long distances if not properly monitored (Gray, 2018). Such heavy machineries and vehicles emit a variety of pollutants– carbon dioxide, carbon monoxide, oxides of nitrogen, oxides of Sulphur, particulate matter, hydrocarbons and heavy metals,

http://doi.org/10.22232/stj.2019.07.01.07

all of which have serious effects on flora, fauna and people. Stunted growths in plants near highways, photosynthetic and catalytic complexities, and even abrupt increase in species composition have been recorded (Spellerberg and Morrison, 1998). Emission of dust and other particulate matter have a serious toll in people as it penetrates into the lungs and causes respiratory illness, asthma, bronchitis and even cancer. Besides dust generation, the most common effect of road construction is noise pollution since construction equipment and heavy machineries are operated daily for long durations of time. Exposure to high noise levels has been found to alter activity patterns in animals with increase in heart rate and production of stress hormones. In human beings, exposure to high noise levels associated with road construction work can adversely affect human health causing stress, sleep disturbance, high blood pressure and even hearing loss (Gray, 2018). These detrimental effects render effective monitoring of road construction activities mandatory.

Environmental Impact Assessment (EIA) is a widely employed and effective tool to check the degradation caused by developmental projects including road constructions. It is defined as the systematic identification and evaluation of the potential impacts (effects) of proposed project plans, programmes or legislative actions relative to the physical, chemical, biological, cultural and socio-economic components of the total environment (Canter 1996). EIA as a mandatory regulatory procedure originated in the early 1970s, with the implementation of the National Environmental Policy Act (NEPA) in the United States of America (Glasson *et al*., 2012). In India, the foundation of EIA was laid in 1976–77 and formalized when Government of India enacted the Environment (Protection) Act on 23rd May 1986 (Mukherjee 2012).

In this study, the environmental impacts of road construction on air quality and noise quality are assessed to highlight the extent of degradation caused by the road project. The results generated are then compared with the baseline data of its pre-construction phase provided by EIA report of Champhai–Zokhawthar Road Construction 2014 by STUP Consultants Pvt. (Anon. 2014). The overall results obtained will provide useful information on the effects of air and noise pollution caused by road construction and hopefully prompt legislators to take necessary actions to reduce wildlife hazards and protect human environment.

MATERIALS AND METHODS

Study Site

Champhai is one of the eight Districts in Mizoram which came into existence in the year 1998. It is the third largest of the 8 (eight) districts in Mizoram in terms of size and population. The district lies in the eastern part of Mizoram between 93.21°E longitude and 23.26°N latitude (Mizoram District Profile 2017). It has 80 km long international boundary with Myanmar in the east and Myanmar border is about 8 km from the District headquarters Champhai. The district is bounded by Manipur state in the north, Serchhip District in the west and Aizawl District in the north-west. The minimum and maximum temperature is 0°C to 20°C during winter and 15°C to 30°C during summer (Census of India 2011).

The road construction and up-gradation of the Champhai – Zokhawthar road is a development project under the Mizoram State Roads Project – II (MSRP – II). It is an environmental category "A" developmental project as per World Bank Policy as well as Government of India (GOI), Ministry of Environment, Forest & Climate Change (MoEF&CC). The existing *Champhai – Zokhawthar* Road (C-Z Road) is 28.0 km long. The designed length of the road is 27.247 km including spur road (short road forming a branch from a longer road) of 2.53 km length. The *Champhai –Zokhawthar* Road passes through villages viz; *Khankawn, Zotlang, Ruantlang, Mualkawi,Melbuk & Zokhawthar*. The road project map is depicted in Figure 1.

Fig. 1: Champhai to Zokhawthar Road Project Map Alongwith Diversions (Anon. 2014)

Air Quality

The ambient air quality was assessed at Zokhawthar village (main construction zone during assessment period) from September 2016 to August 2018 quarterly at 3 months interval employing High Volume Air Sampler. Sampling was carried out for 16 hours at a four hours interval from 6a.m to 10p.m. The absorbing reagents and filter papers were then taken back to the laboratory for analysis. Handbook of Methods in Environmental Studies: Air, Noise, Soil and Overburden Analysis (Maiti 2003) and Manual on Environmental Analysis (Aery 2010) were mainly used for analysis of air quality parameters. Suspended Particulate Matter (SPM >10µm) was determined using highvolume method and the cyclonic flow technique was employed for determination of Respirable Suspended Particulate Matter (RSPM<10 µm). Jacob & Hochheiser modified (sodium arsenide) method was used for determination of nitrogen dioxide, NO_2 (Merryman *et al*., 1973)and the modified West and Gaeke method was used for determination of Sulphur dioxide, SO_2 (West and Gaeke 1956). The air quality parameters are then compared with the standards set by Central Pollution Control Board – National Ambient Air Quality Standards (NAAQS) vide Notification dated 11th April 1994 (Central Pollution Control Board 1994) and National Ambient Air Quality Standards (NAAQS) vide Notification dated 18th November 2009 (Central Pollution Control Board 2009).

Noise Quality

Noise sampling was carried out at three sites i.e. Zotlang (Residential), Tarmat Base Camp (Residential area) and Zokhawthar (Residential area) from June 2016 to May 2018. The instrument used for sampling was Lutron SL-4001. The operational function of data recording was done by switching on the device at "A" weighing scale and "slow" response (CPCB 2015). The numerical values displayed on LCD were recorded. After recording of all the readings, Lmax, Lmin and Leq were calculated and the results were compared with the level of the standards of Noise Pollution (Regulation and Control) Rules 2000 (Ministry of Environment Forests & Climate Change 2000).

RESULTS AND DISCUSSION

Air Quality

Table 1: The Results for Air Quality Assessment and NAAQS

Sampling Period	SPM (µg/m³)		RSPM (µg/m³)		NO_2 (µg/m³)		SO_2 (µg/m³)	
	Mean	NAAQS	Mean	NAAQS	Mean	NAAQS	Mean	NAAQS
Sept – Nov 2016	112.13	200	51.21	100	25.42	80	6.67	80
Dec – Feb 2017	162.12		67.89		31.26		7.71	
Mar – May 2017	92.31		28.65		8.94		5.32	
June – Aug 2017	76.18		24.76		11.92		4.66	
Sept – Nov 2017	143.72		71.26		23.78		5.88	
Dec – Feb 2018	133.78		77.61		14.34		6.87	
Mar – May 2018	105.34		31.02		17.45		4.45	
June – Aug 2018	121.04		48.98		15.56		4.67	
Overall mean construction	**118.32**		**50.17**		**18.58**		**5.76**	
Overall mean pre-construction	**95.5**		**35.5**		**14.5**		**5.7**	

The analysis of variance (ANOVA) showed that there was no significant variation in air quality between the seasons during the assessment period – 0.960 (at 5%). The average SPM concentration ranged from 76.18 to 162.12 µg/m³ with a total mean concentration of 118.32 µg/m³. The average RSPM concentration ranges from 24.75 to 77.61 µg/m³ with a total mean concentration of 50.17 µg/m³. High SPM and RSPM concentration lead to increased dust generation which mainly consists of fumes, smoke and dust (ENVIS 2018); andhave deleterious consequencesin humans such as asthma attacks, bronchitis, high blood pressure, heart attack, strokes and premature death (Reddy *et al.,* 2015). The

average NO_2 concentration ranges from 8.94 to 31.26 µg/m^3 with a total mean concentration of 18.58 µg/m^3. The average SO_2 concentration ranges from 4.45 to 7.71 µg/m^3 with total mean concentration of 5.76 µg/m^3. High concentrations of NO_2 and SO_2 can cause damage to plant and materials, and cause complications in human respiratory system such as bronchitis (Chen *et al.,* 2007).

Although the values of all calculated parameters in all seasons did not exceed the permissible limits of NAAQS for Residential areas at 24 hours sampling, the duration of exposure to such concentrations may prove detrimental to human health. Also, the concentrations of measured parameters peaked during the dry seasons (September–February) and showed lesser concentration during monsoon period (March–August). Dry conditions coupled with unmetalled roads produce heavy dust movements in the study area. Slope cutting and dumping of soil in nearby areas contributed immensely to the increase in concentration during the dry period. The seasonal variations of the measured parameters are shown in Figure 2.

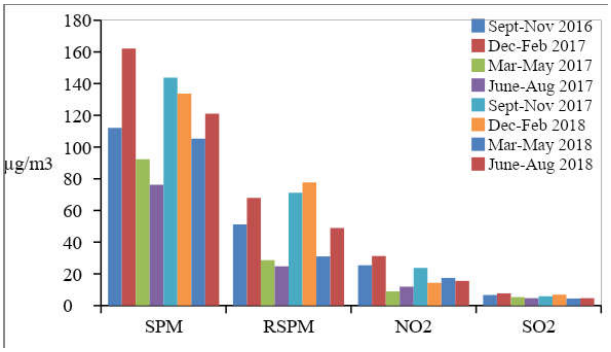

Fig. 2: Seasonal Variation of Air Quality Parameters

Comparison of Air Quality Between Pre-Construction Phase and Construction Phase

Analysis of variance (ANOVA) shows there were no significant changes between the pre-construction phase and construction phase at 0.758 (P<0.05). However, the overall mean values show that the concentrations of the parameters have increased. The mean SPM concentration increased by a value of 22.82 µg/m^3 i.e. 95.5 µg/m^3 to 118.32 µg/m^3, RSPM concentration increased by a value of 14.67 µg/m^3 i.e. 35.5 µg/m^3 to 50.17 µg/m^3, NO_2 concentration increased by a value of 4.08 µg/m^3 i.e. 14.5 µg/m^3 to 18.58 µg/m^{3}and SO_2 concentration increased by a value of 0.06 µg/m^3 i.e. 5.7 µg/m^3 to 5.76 µg/m^3. As mentioned earlier heavy dust movements mainly due to operation of heavy machineries for construction activities have rendered the area arenaceous and the air unclean. During sampling period many residents were spotted wearing masks and seen sprinkling water around the premises of their homes as a precautionary measure. Variation in air quality parameters between the two phases are depicted in Figure 3.

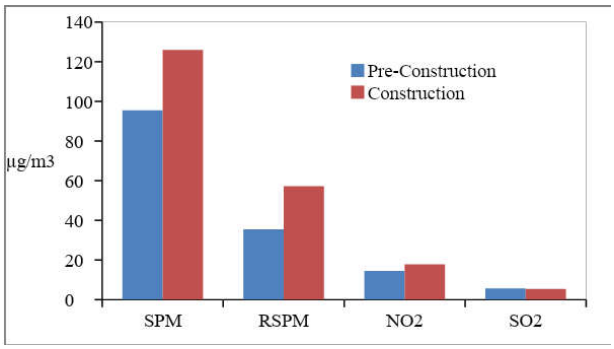

Fig. 3: Variation in Air Quality Parameters between the Pre-construction Phase and Construction Phase

Noise Quality

Table 2: The Results for Noise Quality Assessment at Zotlang, Melbuk and Zokhawthar

Season	Parameters	Permissible Limit (Residential)	Zotlang (dB)	Melbuk (dB)	Zokhawthar (dB)
Jun – Aug 2016	*Leq*	55 dB	75.3	57.8	58.3
	Lmax		78.3	60.4	59.8
	Lmin		45.4	42.7	46.1
Sep – Nov 2016	*Leq*		57.9	79.4	78.5
	Lmax		60.6	81.1	78.2
	Lmin		43.8	50.4	54.5

Table 2 (Contd.)...

...Table 2 (Contd.)

Season	Parameters	Permissible Limit (Residential)	Zotlang (dB)	Melbuk (dB)	Zokhawthar (dB)
Dec – Feb 2017	*Leq*	55 dB	64.5	70.9	74.1
	Lmax		66.6	71.9	76.6
	Lmin		54.3	55.2	49.6
Mar – May 2017	*Leq*		75.6	77.1	50.7
	Lmax		76.5	80.5	49
	Lmin		64.8	66.9	42.1
Jun – Aug 2017	*Leq*		74.1	59.7	52.8
	Lmax		76.3	60.7	54
	Lmin		60.7	48.8	42.1
Sep – Nov 2017	*Leq*		69.7	77.6	57.8
	Lmax		70.7	78	58.9
	Lmin		57	63.7	45
Dec – Feb 2018	*Leq*		69.6	76.9	65.1
	Lmax		69.5	76.3	66.5
	Lmin		56.3	63	44.8
Mar – May 2018	*Leq*		75.6	77.1	50.6
	Lmax		76.5	80.5	49
	Lmin		64.8	66.9	42.1
Overall mean Construction			70.28	72.06	60.98
Overall mean Pre-Construction			61.56	62.71	61.11

ANOVA showed that there was no significant variation in noise quality between the seasons during the study period at 0.9 ($P<0.05$). At Zotlang area, the average noise level ranged from 57.9 to 75.6 dB (A) with a mean value of 70.28 dB (A). At Melbuk area, the average noise level ranged from 57.8 to 79.4 dB (A) with a mean value of 72.06 dB (A). At Zokhawthar area, the average noise level ranged from 50.6 to 78.5 dB (A) with a mean value of 60.98 dB (A). The noise levels in the three study areas in all seasons exceeded the permissible limits as per the Noise Pollution (Regulation and Control) Rules 2000 except for Zokhawthar area.

Noise pollution usually do not cause direct impacts or losses, but rather indirect impacts causing problems and complications in humans and wildlife over a period of time, it is difficult to express its health effects as well as economic loss in a short period of time (Jacyna *et al.,* 2017). Still, exposure to high noise levels can cause cardiovascular diseases and lead to acute or chronic changes of the physiological stress hormone regulation in humans (Ising and Kruppa, 2004) and a certain number of physiological and behavioural changes in birds (Bottalico *et al.,* 2015). Seasonal variations in noise quality in the three assessment sites are shown in Figure 4.

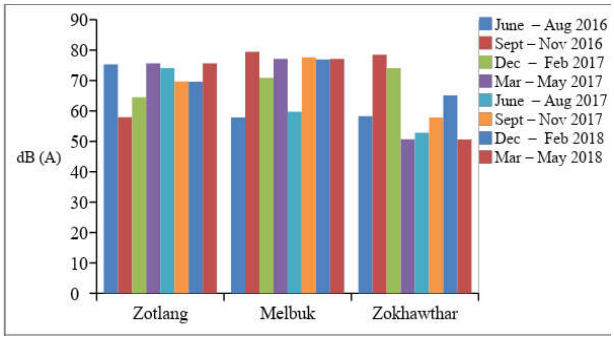

Fig. 4: Seasonal Variation of Noise Quality in the Three Sampling Sites

Comparison of Noise Quality between Pre-Construction Phase and Construction Phase

ANOVA showed that there were no significant changes in noise level between pre-construction phase and construction phase at 0.18 ($P<0.05$). However, the overall mean noise level at Zotlang and Melbuk areas during construction phase is much higher in comparison to noise level during pre-construction phase. The mean noise level

at Zotlang increased by 8.72 dB (A) i.e. 61.56 dB (A) to 70.28 dB (A) and at Melbuk the mean noise level increased by 9.35 dB (A) i.e. 62.71 dB (A) to 72.06 dB (A). However, at Zokhawthar, there was a decrease in mean noise level by 0.13 dB (A) i.e. 61.11 dB (A) to 60.98 dB (A). Although Zotlang is a residential area, the diversion road cuts through the locality and noise is mainly detected from vehicles passing through the area as well heavy machinery operating in the area. The Contractor's base camp is located at Melbuk area and heavy machinery were continuously in construction during the study period. However, the mean noise level at Zokhawthar during construction phase is lower compared to the noise level during pre-construction phase which may be due to the fact that construction work/activities were inconsistent during study period and there was a halt in construction during rainy seasons. Variation in mean noise levels between the two phases are depicted in Figure 5.

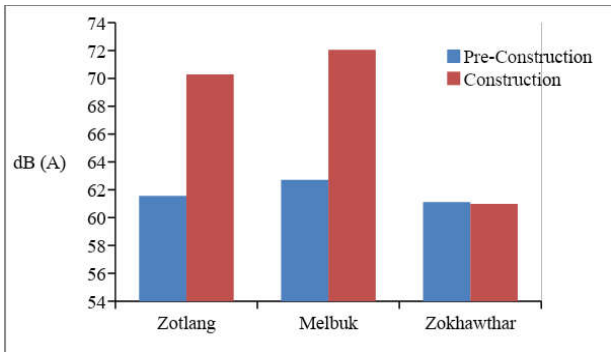

Fig. 5: Variation in Noise Quality between the Pre-Construction Phase and Construction Phase

CONCLUSION

The present study has revealed that the extensive use of heavy machinery and other construction equipment in road construction activities causes degradation to air quality as well as noise quality. Although environmental degradations are bound to occur during construction work, taking into account the baseline environmental conditions of the area, the level of degradation caused over a span of few years is notable. Alteration of landscape, topography and use of heavy machineries has led to air and noise quality degradation in the region. Taking into consideration the level of increase in air and noise pollution, better planning and proper execution of the construction work is imperative with strict implementation of mitigating measures proposed by environmental consultants and impact guidelines.

Therefore, the present study indicates the range of effects of road construction activities but the extent or magnitude of such effects still require more research. The Champhai–Zokhawthar road, in the near future will be an important gateway for trade and tourism for the country, therefore, it is mandatory to uphold and conserve the environmental stability of the area and minimize air and noise pollution to its permissible limits.

REFERENCES

Aery NC (2010) Manual on Environmental Analysis. 1st Edn. Ane Books Pvt. Ltd., New Delhi.

Anonymous (2014) Environmental Impact Assessment Report for Widening to 2-lane, Re-alignment and Geometric Improvement of Champhai-Zokhawthar Road. Public Works Department, Government of Mizoram.

Anonymous (2014) Environmental Management Plan for Widening to 2-lane, Re-alignment and Geometric Improvement of Champhai-Zokhawthar Road. Public Works Department, Government of Mizoram.

Bottalico P, Spoglianti D, Bertetti CA, Falossi M (2015) Effect of Noise Generated by Construction Sites on Birds. In Burroughs C (edn). Implementing Noise Control Technology. 44th International Congress and Exposition on Noise Control Engineering (InterNoise); Aug 9-12; San Francisco, California. Institute of Noise Control Engineering: Curran Associates Inc; pp. 1419 – 1425.

Canter LW (1996) Environmental Impact Assessment. 2nd Edn. McGraw-Hill Inc., New York.

Census of India (2011) District Census Handbook: Champhai (2011). Directorate of Census Operations, Mizoram.

Cental Pollution Control Board (1994) National Ambient Air Quality Standards. CPCB, New Delhi.

Cental Pollution Control Board (2009) National Ambient Air Quality Standards. CPCB, New Delhi.

Cental Pollution Control Board (2015) Protocol for Ambient Level Noise Monitoring. CPCB, New Delhi.

Chen TM, Kuschner WG, Gokhale J, Shofer S (2007) Outdoor Air Pollution: Nitrogen Dioxide, Sulfur Dioxide, and Carbon Monoxide Health Effects. ***Am J Med Sci*** 333: 249-256.

Directorate of Economics and Statistics (2017) Mizoram District Profile 2017. Directorate of Economics and Statistics, Government of Mizoram.

ENVIS (2018) Suspended particulate matter. Ministry of Environment, Forests and Climate Change (MoEF&CC); 2018 [cited 2018 Sept 23]. www.nbrienvis.nic.in.

Glasson J, Therivel R, Chadwick A (2012) Introduction to Environmental Impact Assessment. 4th Edn. Taylor & Francis Ltd, London.

Gray J. Pollution from construction. United Kingdom: Sustainable Build; 2018 [cited 2018 October 24]. http://www.sustainablebuild.co.uk/PollutionFromConstruction.html

Ising H, Kruppa B (2004) Health effects caused by noise: Evidence in the literature from the past 25 years. *Noise Health* 6: 5 – 13.

Jacyna M, Wasiak M, Lewczuk K, Karon G (2017) Noise and environmental pollution from transport: Decisive problems in developing ecologically efficient transport systems. *J Vibroeng* 19: 5639-5655.

Maiti SK (2003) Handbook of Methods in Environmental Studies, Volume 2: Air, Noise, Soil and Overburden Analysis. 1st Edn. ABD Publishers, Jaipur.

Merryman EL, Spicer CW, Levy A (1973) Evaluation of arsenite modified Jacobs Hochheiser procedure. *Environ Sci Technol* 7: 1056–1059.

Ministry of Environment Forests & Climate Change (2000) Noise Pollution (Regulation and Control) Rules. MoEF & CC, New Delhi.

Mukherjee P (2012) EIA Scams: Decaying the EIA Legal Regime in India. *J Environ Res Develop* 6: 507 – 513.

Newman P, Hargroves C, Desha C (2012) Reducing the Environmental Impact of Road Construction. Sustainable Built Environment National Research Centre, Australia.

Reddy YBR, Reddy SM, Reddy CBS (2015) Determination of Respirable Suspended Particulate Matter, Non Respirable Suspended Particulate Matter and Total Suspended Particulate Matter in Piduguralla Industrial Area India. *Int Res J Environ Sci* 4: 45-51.

Seiler A (2001) Ecological Effects of Roads. Swedish University of Agricultural Sciences (SLU), Uppsala.

Spellerberg IF, Morrison T (1998) The ecological effects of new roads: a literature review. Department of Conservation, Wellington, New Zealand.

West PW, Gaeke GC (1956) Fixation of SO2 as sulfi-tomercurate (II) and subsequent colorimetric estimation. *Anal Chem* 28: 1816–1819.

Science and Technology Journal, Vol. 7 Issue: I ISSN: 2321-3388

Avian Diversity in Mizoram University Campus, Aizawl, Mizoram

Lalawmawia Sailo[1], G.S. Solanki[2]* and C. Lalhruaizela[3]
[1,2]Department of Zoology, Mizoram University
[3]Department of Journalism & Mass Communication, Mizoram University
E-mail: *gssolanki02@yahoo.co.in

Abstract—We conducted an avian survey to assess the avian diversity of Mizoram University campus, Aizawl for a period of 24 months. During the study a total of 3,555 no of individuals of 189 species of birds belonging to 43 families were recorded. The family Muscicapidae represented the highest species composition with 28 species followed by family Timaliidae and Cuculidae with 19 and 13 species respectively. Avian profile of university campus, 1419(74.5%) are known to be resident of MZU campus and its adjacent area, 31 (16.4%) species are winter visitors, 15 (7.9%) species are summer visitor, and two species namely, Hooded pitta (*Pitta sordid)* and Forest wagtail (*Dendronanthus indicus*) are passer migrants. The variation in avian species recorded in university campus across the seasons is significant ($P<0.05$), variation between the seasons was also significant ($P<0.01$). University campus exhibited high avian diversity. Shannon Wiener diversity index (H') value calculated was 3.286 and species evenness index was 0.62. The detailed of avian fauna of campus recoded and the need of conservation actions are discussed in length.

INTRODUCTION

Mizoram falls within the northeast bio-geographical zone and is a part of Indo-Mynmar biodiversity hotspot; encompasses rich biodiversity. Several factors and variability within habitat such as topographical, climatic, and forest category have contributed to avian species diversity and richness. Wilderness species in Mizoram has been reported to have a very wide taxonomic range, with respect to the enormous diversity of ecosystem and geographical conditions. However, in the last few decades, human activities and infrastructure developmental projects are the primary factors liable for reduction of biodiversity and also resulted in reduced carrying capacity of the environment (Gaston *et al.*, 2003). Human induced disturbances are causing subtle to major landscape changes. Rapid deforestation of tropical forest and large scale human disturbances has increased concern about their effect on vegetation structure and composition, and animal communities in general (Schutle and Niemi, 1998).

Birds are more sensitive to such changes and are considered good predictors of habitat quality, as they relate to changes in their associated habitat in numerous ways (Shankar Raman *et al.* 1998, Chettri *et al.* 2001, Shankar Raman, 2011) because they respond to habitat structure (MacArthur and MacArthur, 1961) and represent several trophic groups or guilds (Steele *et al.* 1984). Mizoram has a great variety of wild flora and fauna due to its location within Indo-Myanmar Hotspot region. Bird community plays an important role in forest ecosystem. Although population studies can be used for monitoring the long term change in the ecosystem (Weins, 1989), knowledge of the diversity of bird in a particular area is important for determining the health of the ecosystem. The requirement for bird's habitat is food, water, space and cover (US Fish and Wildlife Service (2002). So, the study of the avian community of a particular habitat can be a determinant of the health of that habitat. Mizoram University campus is lush green campus with high biological diversity. Since campus is relatively new and vibrant due to various infrastructural and anthropogenic activities. Landscape and natural forest transformation is undergoing rapidly that is affecting natural fauna. A study was undertaken to develop a profile and assess avian community on the campus that will give a baseline data for further studies on monitoring and evaluation of avian fauna when university campus will grow further and witness more such activities.

http://doi.org/10.22232/stj.2019.07.01.08

MATERIALS AND METHOD

Study Area

Study was carried out inside the Mizoram University (MZU) campus, 15 Km away from Aizawl town. Mizoram University campus encompasses roughly 980 acres of land area and geographically located between 23^0 73'94" N and 92^0 66'51" E elevation ranges from 300 m to 880 m above mean sea level. Number of steams flows through the campus namely Setlak lui, Rultawi lui, Hradawng lui, Lalmangkhawng lui, Lungsumazau lui, Kel lui and Chengkawl lui flows through campus and joins the main Tlawng river (Zothanpui, 2019). The vegetation type is mainly tropical wet evergreen to semi evergreen including a protected forest and a small biodiversity park. The area was covered with lush green vegetation with mostly evergreen trees of 384 species of vascular plants which belongs to 290 genera and 107 families (Lalchhuanawma, 2008) interspersed with tall grass.

The bird survey was conducted inside the University campus and its adjacent forest by walking the forested path. Opportunistic sampling was also considered to strengthen the species composition. The survey path were walked mostly in the morning (0500–0830hrs) and evening (1400 –1700hrs) for 24 months during 2017and 2018. Frequency of observing birds was maintained one day per week and four days in a month. For each survey, DSLR Camera (Nikon D5100 and Canon 760D) was used for photography and binocular (Nikon Aculon15x50) was used for observation and identification of birds, For identification of birds, colored plates of Grimmett *et al.* (2013) were used. A book on Popular Birds of Mizoram (Lalthanzara and Kasambe, 2015) was referred for local name of birds. Variation in avian diversity across the seasons was tested by Analysis of Variance (ANOVA) and comparison of diversity between the seasons was tested by student's 't' test using SPSS ver. 17. Shannon Weaver's diversity and Simpson evenness index was calculated as per Mugurran (1985).

OBSERVATIONS AND DISCUSSION

Mizoram lies at the Indo-Myanmar Biodiversity hotspot, a biodiversity rich area, however the works on avian community is very scanty. Lepage (2018) recorded 652 species of bird from this hilly state of Mizoram including 26 globally threatened species. Choudhury (2008) listed 479 species with an additional 140 uncertain species from Mizoram. The Zoological Survey of India (2007) recorded 370 species and 317 species by BNHS-ENVIS.The MZU campus is observed an abode for total of 189 species of birds belonging to 43 families (Table 1). The family Muscicapidae has the highest species composition with 28 species recorded inside the campus followed by family Timaliidae and Cuculidae with 19 and 13 species respectively. The families-Zosteropidae, Fringilidae, Rhipiduridae, Aegithinidae, Artamidae, Pittidae, Eurylaimidae, Coraciidae, Podargidae, Caprimulgidae, Upupidae, Rallidae, and Turnicidae has a single species representative (Fig. 1).

The high species composition of the family Muscicapidae is recorded, it might be due to the higher adaptability of members of the family in areas of various anthropogenic disturbances and tolerant of various threats. Their habits of foraging in the top canopy, open shrub and near human settlements are also believed to increase the species count in the present study. It may be also due to the diverse habitat occupied by various species under the family Muscicapidae which allows the species to thrive well and survive under the dynamic ecosystem in MZU campus with ongoing diverse anthropogenic activities.

A total of 3,555 no of individuals of bird belonging to 189 different species recorded during total observation period indicate high degree of avian diversity that is also reflected in Shannon Wiener diversity index (H) of 3.287. There thirteen families which are represented by single species is another indicator of species diversity. Distribution of species evenness was high with 0.62. This high diversity of bird species in a roughly 980 acres of land was remarkably high. The result of evenness clearly depicts the occurrence of individuals of different species which in turn indicates the suitability of the habitat for a great variety of bird species. 141 species were identified as resident, 31 species were winter visitors (table 2), 15 were summer visitor (table 3), and two species were recorded as passer migrants, Hooded pitta (*Pitta sordid)* and Forest wagtail (*Dendronanthus indicus*) (table 4). A photoplate of some birds is also enclosed. Variation of avian species across the seasons was found to be significant ($P<0.05$) and species recorded between seasons was compared and also found significant ($P<0.01$). The present record of 189 species at MZU campus is more than the record elsewhere in similar habitat. Chakdar *et al.* (2016) recorded 73 species of birds in the Assam University Campus of Silchar, Assam. Dey *et al.* (2013) recorded 76 species of birds from 234 acre campus

area of Maharaja Bir Bikram College, Agartala, Tripura. Mizoram University is a potential habitat for avian diversity in comparison to other such organizations in this region.

In Dampa Tiger Reserve (DTR), 215 species of birds was claimed to be present by the official website of Environment, Forest and Climate Change Department, Government of Mizoram. The renowned Murlen National Park (MNP) is known to be haven for more than 150 species of birds while Lalawmawia and Lalthanzara (2015) recorded 146 species of birds from Lengteng Wildlife Sanctuary. Meanwhile, Vanlalsawmi *et al.* (2011) also reported 54 species of birds only from DTR in a short study period. The avian species diversity of MZU campus is higher than the Phawngpui National Park (PNP) where 108 species are recorded by Ghose (1999). However inter species and inter generic variations may be higher in Phawngpui nationa Park being a protected area.

Among the recorded avian species, 75% are resident of MZU campus and its adjacent area and 25% of birds are visitors (Fig. 2). The grassy patch which interspersed the evergreen forest traversed by the wet and dried streams provide safe haven for these large congregation of diverse avian species. High percentage of resident species clearly depicts the richness of MZU campus in terms of avian diversity make this area very important for conservation and rehabilitation of birds. The authors encounter with some local hunters inside the MZU campus that is distressing for birds, and need immediate intervention of the University authorities. In view of the high number of resident species as well as seasonal visitors, the campus area needs to be well preserved and protected from the onslaught of external and internal threats which are deleterious to the wildlife and their habitat.

Table 1: Check List of Birds Recorded on Mizoram University Campus

Family	English Name	Scientific Name	Local Name(Mizo)
Phasianidae	Red Jungle Fowl	*Gallus gallus*	Ram-ar
	Kalij Pheasant	*Lophura leucomelanos*	Vahrit
	Mountain Bamboo Partridge	*Bambusicola fytchii*	Vahlah
Turnicidae	Barred Button Quail	*Turnix suscitator*	Vahmim
Falconidae	Amur Falcon	*Falco amurensis*	Sialsir
	Common Kestrel	*Falco tinnunculus*	Mu te
Accipitridae	Crested Serpent Eagle	*Spilornis cheela*	Muvanlai
	Oriental Honey Buzzard	*Pernis ptilorynchus*	Khuaimu
	Crested Goshawk	*Accipiter trivirgatus*	Muningaldang
	Shikra	*Accipiter badius*	Mute
	Japanese Sparrowhawk	*Accipiter gularis*	Mute
	Besra	*Accipiter virgatus*	Mute
	Rufous-bellied Eagle	*Lophotriorchis kienerii*	Mu-ar la
	Common Buzzard	*Buteo buteo*	Munibuang
	Black Baza	*Aviceda leuphotes*	Mu kelrang

Table 1 (Contd.)...

...Table 1 (Contd.)

Family	English Name	Scientific Name	Local Name(Mizo)
Rallidae	Slaty-legged Crake	*Rallina eurizonoides*	Kang-kang
Culumbidae	Pin-tailed Green Pigeon	*Treron apicauda*	Huipui
	Orange-breasted Green Pigeon	*Treron bicinctus*	Vahui
	Wedge-tailed Green Pigeon	*Treron sphenurus*	Vahui
	Barred Cuckoo Dove	*Macropygia unchall*	Thumimeisei
	Emerald Dove	*Chalcophaps indica*	Ramparva
	Spotted Dove	*Stigmatopelia chinensis*	Thuro
	Oriental Turtle Dove	*Streptopelia orientalis*	Thumi
	Thick-billed Green Pigeon	*Treron curvirostra*	Huifek
Psittacidae	Red-breasted Parakeet	*Psittacula alexandri*	Kiteng
	Vernal Hanging Parrot	*Loriculus vernalis*	Run vaki/Vaki te
Strigidae	Himalayan Wood Owl	*Strix leptogrammica*	Chingpirinu
	Collered Owlet	*Glaucidium brodiei*	Hrangkir
	Collared Scops Owl	*Otus lettia*	Chhimbuk
	Oriental Scops Owl	*Otus sunia*	Chhimbuk
	Asian-barred Owlet	*Glaucidium cuculoides*	Chhimbuk te
	Spot-bellied Eagle Owl	*Bubo nipalensis*	Chhimbukpui
Cuculidae	Greater Coucal	*Centropus sinensis*	Lalruangasehnawt
	Lesser Coucal	*Centropus bengalensis*	Lalruangasehnawt
	Green-billed Malkoha	*Rhopodytes tristis*	Vazun/va uk
	Large Hawk Cuckoo	*Hierococcyx sparverioides*	Kiltheihrawk
	Common Hawk Cuckoo	*Hierococcyx varius*	Kiltheihrawk
	Asian Koel	*Eudynamys scolopaceus*	Mitthi ar
	Jacobin Cuckoo	*Clamator jacobinus*	
	Chestnut-winged cuckoo	*Clamator coromandus*	

Table 1 (Contd.)...

...Table 1 (Contd.)

Family	English Name	Scientific Name	Local Name(Mizo)
	Banded Bay Cuckoo	*Cacomantis sonneratii*	Thangfenpabawp
	Asian Emerald Cuckoo	*Chrysococcyx maculatus*	
	Lesser Cuckoo	*Cuculus poliocephalus*	Thangfenpabawp te zawk
	Hodgson's Hawk Cuckoo	*Hierococcyx nisicolor*	Kiltheihrawk
	Violet Cuckoo	*Chrysococcyx xanthorynchus*	Mawntaipirtliak
Meropidae	Blue-bearded Bee-eater	*Nyctyornis athertoni*	Tlakawrh
	Chestnut-headed Bee-eater	*Merops leschenaulti*	Fuanhawr
Upupidae	Common Hoopoe	*Upupa epops*	Chhuangtuar/Vaseek
Ramphastidae	Blue-throated Barbet	*Megalaima asiatica*	Tukloh
	Great Barbet	*Megalaima virens*	Tawllawt
Picidae	Greater Yellownape	*Picus flavinucha*	Thlohlupar
	Lesser Yellownape	*Picus chlorolophus*	Thlohlupar
	White-browed Piculet	*Sasia ochraceae*	Luangtubeuh
	Speckled Piculet	*Picumnus innominatus*	Luangtubeuh
	Grey-capped Pygmy Woodpecker	*Dendrocopos canicapillus*	Thlohte
	Fulvous-breasted Woodpecker	*Dendrocopos macei*	Thlohte
	Bay Woodpecker	*Blythipicus pyrrhotis*	Mauthloh
	Rufous Woodpecker	*Micropternus brachyurus*	Fanghmir thloh
	Eurasian Wryneck	*Jynx torquilla*	Valeisei
	Grey-headed Woodpecker	*Picus canus*	Thloh hring
Hirundinidae	Nepal House Martin	*Delichon nipalense*	Vamurte
	Asian Palm Swift	*Cypsiurus balasiensis*	Vamur
	Brown -backed Needletail	*Hirundapus giganteus*	Murpui
	Fork-tailed Swift	*Apus pacificus*	Murpui
	Striated Swallow	*Cecropis striolata*	Vamur Ngumsen

Table 1 (Contd.)...

...Table 1 (Contd.)

Family	English Name	Scientific Name	Local Name(Mizo)
Motacillidae	Grey Wagtail	*Motacilla cinerea*	Lailen
	White Wagtail	*Motacilla alba*	Lailen var
	Tree Pipit	*Anthus triavilis*	Chip
	Forest Wagtail	*Dendronanthus indicus*	Sehnungzui/Ngawkar Lailen
Campephagidae	Scarlet Minivet	*Pericrocotus speciosus*	Bawng
	Long-tailed Minivet	*Pericrocotus ethologus*	Bawng
	Ashy Minivet	*Pericrocotus divaricatus*	Bawngte
	Large Woodshrike	*Tephrodornis gularis*	Thlekbur
	Large Cuckooshrike	*Coracina macei*	Irliak
	Black-winged Cuckooshrike	*Coracina melaschistos*	Changde
Pycnonotidae	Red-vented Bulbul	*Pycnonotus cafer*	Tlaiberh
	Red-whiskered Bulbul	*Pycnonotus jacosus*	Thlangvaberh/Phaitlaiberh
	Black-crested Bulbul	*Pycnonotus flaviventris*	Tukkhumvilik
	White-throated Bulbul	*Alphophoixus flaveolus*	Dawkek
	Ashy Bulbul	*Hemixos flavala*	Kawlrit
	Flavescent Bulbul	*Pycnonotus flavescens*	Setawt
	Black Bulbul	*Hypsipetes leucocephalus*	Hmuisen/Kesen/Liandorit
Caprimulgidae	Grey Nightjar	*Caprimulgus jotaka*	Valambawk
Podargidae	Hodgson's Frogmouth	*Batrachostomus hodgsoni*	Valambawk/Vabak
Coraciidae	Indian Roller	*Coracias benghalensis*	Vapui
Eurylaimidae	Long-tailed Broadbill	*Psarisomus dalhousiae*	Thizil
Pittidae	Hooded Pitta	*Pitta sordida*	Buarchawm lu uk
Artamidae	Ashy Wood swallow	*Artamus fuscus*	Lengder
Aegithinidae	Common iora	*Aegithina tiphia*	Zairumva
Laniidae	Long-tailed Shrike	*Lanius scach*	Chhemhur
Halcyonidae	Brown Shrike	*Lanius cristatus*	Chhemhur uk

Table 1 (Contd.)...

...Table 1 (Contd.)

Family	English Name	Scientific Name	Local Name(Mizo)
	Burmese Shrike	*Lanius collurioides*	Chhemhur sen uk
	Grey-backed Shrike	*Lanius tephronotus*	Chhemhur(vut buak)
	White-throated Kingfisher	*Halcyon smyrnensis*	Kaikuangral
	Black-capped Kingfisher	*Halcyon pileata*	Kaikuangral ludum
Dicruridae	Bronzed Drongo	*Dicrurus aeneus*	Changkak
	Ashy Drongo	*Dicrurus leucophaeus*	Thlanthla
	Lesser Racket-tailed Drongo	*Dicrurus remifer*	Thlanthla changhlawi
	Greater Racket-tailed Drongo	*Dicrurus paradiseus*	Vakul changhlawi
	Hair-crested Drongo	*Dicrurus hottentottus*	Kulherh
Oriolidae	Slender-billed Oriole	*Oriolus tenuirostris*	Vamaitai
	Black-naped Oriole	*Oriolus chinensis*	Vamaitai
	Maroon Oriole	*Oriolus trailii*	Changsen
Rhipiduridae	White-throated Fantail	*Rhipidura albicollis*	Changarh
Monarchidae	Black-naped Monarch	*Hypothymis azurae*	Zumzek/Thangthlengral
	Asian Paradise Flycatcher	*Terpsiphone paradisi*	Thlehhniar
Corvidae	Eastern Jungle Crow	*Corvus macrorynchos*	Choak
	Common Green Magpie	*Cissa chinensis*	Dawntliang
	Rufous Treepie	*Dendrocitta vagabunda*	Bemkawng
	Grey Treepie	*Dendrocitta formosae*	Bemkawng
Cisticolidae	Common Tailorbird	*Orthotomus sutorius*	Daikat/hnahkhawr
	Plain Prinia	*Prinia inornata*	Zirziak
	Striated Prinia	*Prinia crinigera*	Changdawt
	Black-throated Prinia	*prinia atrogularis*	Changdawt awr dum
	Rufescent Prinia	*Prinia rufescens*	Zirziak
Sylviidae	Yellow-browed Leaf Warbler	*Phyloscopus inornatus*	Chivit/Saivate/Chilim/ Chhawlchhaih

Table 1 (Contd.)...

...Table 1 (Contd.)

Family	English Name	Scientific Name	Local Name(Mizo)
	Grey-crowned Warbler	*Seicercus burkii*	Chivit/Saivate/Chilim/ Chhawlchhaih
	Yellow-vented Warbler	*Phylloscopus cantator*	Chivit/Saivate/Chilim/ Chhawlchhaih
	Thick-billed Warbler	*Phragamaticola aedon*	Hmunchhe arpuilian
	Common Stonechat	*Saxicola torquatus*	Tep
	Grey Bushchat	*Saxicola ferreus*	Terzik
Timaliidae	Puff-throated Babbler	*Pellorneum ruficeps*	Valeisawt
	Rufous-capped Babbler	*Stachyridopsis ruficeps*	Vate lusen
	Pin-striped Tit Babbler	*Macronous gularis*	
	Chestnut-capped Babbler	*Timalia pileata*	Vatelusen
	Rufous-fronted Babbler	*Stachyridopsis rufifrons*	Vatelusen
	Grey-throated Babbler	*Stachyris nigriceps*	Vatekawngkan
	Spot-breasted Scimitar Babbler	*Pomatorhinus erythrocnemis*	Ngalvapual awmtial
	Coral-billed Scimitar Babbler	*Pomatorhinus ferruginosus*	Ngalvapual
	White-crested Laughingthrush	*Garrulax leucolophus*	Koro
	Greater-necklaced Laughingthrush	*Garrulax pectoralis*	Vazar/Zarpuithiawrh
	Lesser-necklaced Laughingthrush	*Garrulax monileger*	Vazar/Zarfek
	Rufous-necked Laughingthrush	*Garrulax ruficollis*	Vachawm
	White-browed Shrike Babbler	*Pteruthius flaviscapis*	Kawl vasir
	Brown-cheeked Fulvetta	*Alcippe poioicephala*	Mau va
	Nepal Fulvetta	*Alcippe nipalensis*	Ngawkar mitval
	Yellow-eyed Babbler	*Chrysomma sinense*	
	Striated Yuhina	*Staphida castaniceps*	Tehhek
	White-bellied Erpornis	*Erpornis zantholeuca*	Vate lungleng
	Greater Rufous-headed Parrotbill	*Psittiparus ruficeps*	Vahnanghlai chikhat

Table 1 (Contd.)...

...Table 1 (Contd.)

Family	English Name	Scientific Name	Local Name(Mizo)
Muscicapidae	White-capped Redstart	*Chaimarrornis leucocephalus*	Vachalde
	Rufous-gorgeted Flycatcher	*Ficedula strophiata*	Terzik nghawngsen
	Little Pied Flycatcher		Ter pa
	Verditer Flycatcher	*Eumyias thalassinus*	Vapawl
	Taiga Flycatcher	*ficedula albicilla*	Ter
	Blue Whistling Thrush	*Myophonus caeruleus*	Thangfenpabawp
	Orange-headed Thrush	*Zoothera citrina*	Vakhuang
	Scaly Thrush	*Zoothera dauma*	Ram chippui
	Grey-sided Thrush	*Turdus faea*	Tiau
	Blue Rock Thrush	*Monticola solitarius*	Va-in-ro nghak
	Long-billed Thrush	*Zoothera monticola*	Ramchippui hmuisei
	Dark-sided Thrush	*Zoothera marginata*	Ramchippui
	Siberian Rubythroat	*Luscinia calliope*	Tawktawk awrsen
	White-tailed Rubythroat	*Luscinia pectoralis*	Tawktawk awrsen(a chang var)
	Himalayan Bluetail	*Tarsiger rufilatus*	
	Oriental Magpie Robin	*Copsychus saularis*	Khawmual chinrang
	White-rumped Shama	*Copsychus malabaricus*	Vatelal
	Black Redstart	*Phoenicurus ochruros*	
	Blue-fronted Redstart	*Phoenicurus frontalis*	
	Black-backed Forktail	*Enicurus immaculatus*	Chinrang
	Spotted Forktail	*Enicuruc maculatus*	Chinrang
	White-tailed Robin	*Myiomela leucura*	Pi-tuibur-kei-ve/Pi tuibur dil
	Dark-sided Flycatcher	*Muscicapa sibirica*	Ter
	Asian Brown Flycatcher	*Muscicapa dauurica*	Ter uk

Table 1 (Contd.)...

...Table 1 (Contd.)

Family	English Name	Scientific Name	Local Name(Mizo)
	Vivid Niltava	*Niltava vivida*	Be-ai-ral
	Blue-throated Blue Flycatcher	*Cyornis rubiculoides*	Vadumdeleng
	Small Niltava	*Niltava macgrigoriae*	Be-ai-ral te zawk
	Grey-headed Canary Flycatcher	*Culicicapa ceylonensis*	Mauhmun vate
Nectarinidae	Crimson Sunbird	*Aethopyga siparaja*	Dawithiama arpa
	Mrs Goulds Sunbird	*Aethopyga gouldiae*	Dawithiama arpa
	Ruby-cheeked Sunbird	*Chalcoparia singalensis*	Dawithiama arpa
	Little Spiderhunter	*Arachnothera longirostra*	Kireuh te/Tumbu ar/Zetzet/ Lawizit
	Streaked Spiderhunter	*Arachnothera magna*	Kireuh
	Plain Flowerpecker	*Dicaeum minullum*	Tiktik
	Yellow-vented Flowerpecker	*Dicaeum chrysorrheum*	Tiktik awmtial
	Scarlet-backed Flowerpecker	*Dicaeum cruentatum*	Tek tek
Chloropseidae	Orange-bellied Leafbird	*Chloropsis hardwickii*	Chhawlhring awm eng
	Golden-fronted Leafbird	*Chloropsis aurifrons*	Chhawlhring lu sen
Fringilidae	Common Rosefinch	*Carpodacus erythrinus*	Vasuih
Estrildidae	Little Bunting	*Emberiza pusilla*	Ram chawngzawng
	Crested Bunting	*Melophus lathami*	Ram chawngzawngpui
Zosteropidae	Oriental White-eye	*Zosterops palpebrosus*	Mitval/Pirh/Uichirh
Sittidae	Chestnut-vented Nuthatch	*Sitta nagaensis*	Suklet
	Velvet-fronted Nuthatch	*Sitta frontalis*	Suklet
Sturnidae	Chestnut-tailed Starling	*Sturnia malabarica*	Vamam/Vapaw
	Common Hill Myna	*Gracula religiosa*	Vaiva
Passeridae	Eurasian Tree Sparrow	*Passer montanus*	Chawngzawng
	Scaly-breasted Munia	*Lonchura punctulata*	Pit awmtial
	White-rumped Munia	*Lonchura striata*	Pit(ngumvar)

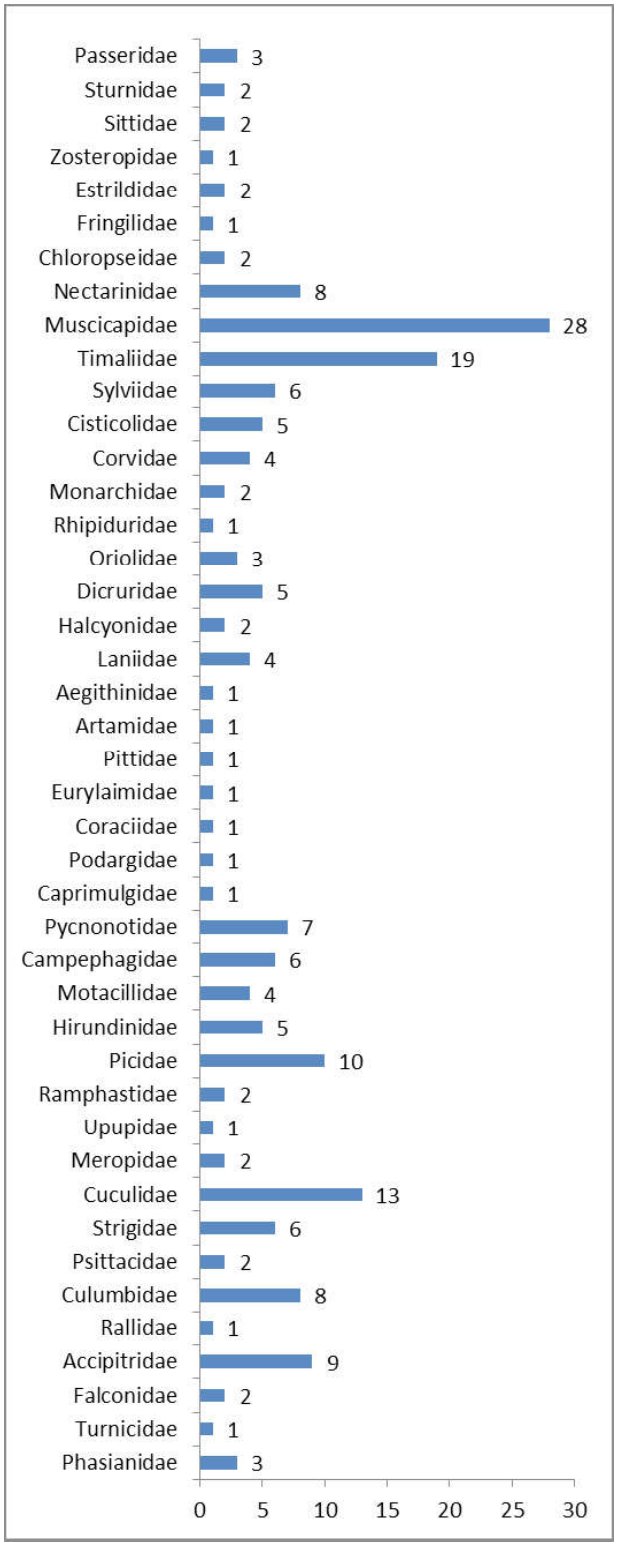

Fig. 1: Summary of Bird Species Recorded

Table 2: Birds Recoded during Winter Season (Winter Visitors)

Family	English Name	Scientific Name	Mizo Name
Falconidae	Amur Falcon	*Falco amurensis*	Sialsir
	Common Kestrel	*Falco tinnunculus*	Mu te
Accipitridae	Oriental Honey Buzzard	*Pernis ptilorynchus*	Khuaimu
	Japanese Sparrowhawk	*Accipiter gularis*	Mute
	Common Buzzard	*Buteo buteo*	Munibuang
Psittasidae	Red-breasted Parakeet	*Psittacula alexandri*	Kiteng
	Vernal Hanging Parrot	*Loriculus vernalis*	Run vaki/Vaki te
Meropidae	Chestnut-headed Bee-eater	*Merops leschenaulti*	Fuanhawr
Upupidae	Common Hoopoe	*Upupa epops*	Chhuangtuar/Vaseek
Picidae	Eurasian Wryneck	*Jynx torquilla*	Valeisei
Hirundinidae	Brown -backed Needletail	*Hirundapus giganteus*	Murpui
	Fork-tailed Swift	*Apus pacificus*	Murpui
Motacilidae	Grey Wagtail	*Motacilla cinerea*	Lailen
	White Wagtail	*Motacilla alba*	Lailen var
Sylviidae	Yellow-browed Leaf Warbler	*Phyloscopus inornatus*	Chivit/Saivate/Chilim/Chhawlchhaih
	Grey-crowned Warbler	*Seicercus burkii*	Chivit/Saivate/Chilim/Chhawlchhaih
	Yellow-vented Warbler	*phylloscopus cantator*	Chivit/Saivate/Chilim/Chhawlchhaih
	Common Stonechat	*Saxicola torquatus*	Tep
Muscicapidae	White-capped Redstart	*Chaimarrornis leucocephalus*	Vachalde
	Verditer Flycatcher	*Eumyias thalassinus*	Vapawl
	Taiga Flycatcher	*ficedula albicilla*	Ter
	Grey-sided Thrush	*Turdus faea*	Tiau
	Long-billed Thrush	*Zoothera monticola*	Ramchippui hmuisei
	Dark-sided Thrush	*Zoothera marginata*	Ramchippui
	Siberian Rubythroat	*Luscinia calliope*	Tawktawk awrsen
	White-tailed Rubythroat	*Luscinia pectoralis*	Tawktawk awrsen(a chang var)
	Himalayan Bluetail	*Tarsiger rufilatus*	
	Blue-fronted Redstart	*Phoenicurus frontalis*	
	Dark-sided Flycatcher	*Muscicapa sibirica*	Ter
	Asian Brown Flycatcher	*Muscicapa dauurica*	Ter uk
Fringilidae	Common Rosefinch	*Carpodacus erythrinus*	Vasuih
Total Number of families: 11 and species : 31 are winter visitors			

Table 3: Birds Recoded during Summer Season (Summer Visitors)

Family	English Name	Scientific Name	Mizo Name
Cuculidae	Large Hawk Cuckoo	*Hierococcyx sparverioides*	Kiltheihrawk
	Common Hawk Cuckoo	*Hierococcyx varius*	Kiltheihrawk
	Asian Koel	*Eudynamys scolopaceus*	Mitthi ar
	Jacobin Cuckoo	*Clamator jacobinus*	
	Chestnut-winged cuckoo	*Clamator coromandus*	
	Banded Bay Cuckoo	*Cacomantis sonneratii*	Thangfenpabawp
	Asian Emerald Cuckoo	*Chrysococcyx maculatus*	
	Lesser Cuckoo	*Cuculus poliocephalus*	Thangfenpabawp te zawk
	Hodgson's Hawk Cuckoo	*Hierococcyx nisicolor*	Kiltheihrawk
	Violet Cuckoo	*Chrysococcyx xanthorynchus*	Mawntaipirtliak
Hirundinidae	Nepal House Martin	*Delichon nipalense*	Vamurte
Muscicapidae	Vivid Niltava	*Niltava vivida*	Be-ai-ral
	Blue-throated Blue Flycatcher	*Cyornis rubiculoides*	Vadumdeleng
	Small Niltava	*Niltava macgrigoriae*	Be-ai-ral te zawk
	Orange-headed Thrush	*Zoothera citrina*	Vakhuang
Total no of families: 3 and species: 15 are summer visitors			

Table 4: Passage Migrant Birds

Family	English Name	Scientific Name	Mizo Name
Pittidae	Hooded Pitta	*Pitta sordida*	Buarchawm lu uk
Motacillidae	Forest Wagtail	*Dendronanthus indicus*	Sehnungzui/Ngawkar Lailen

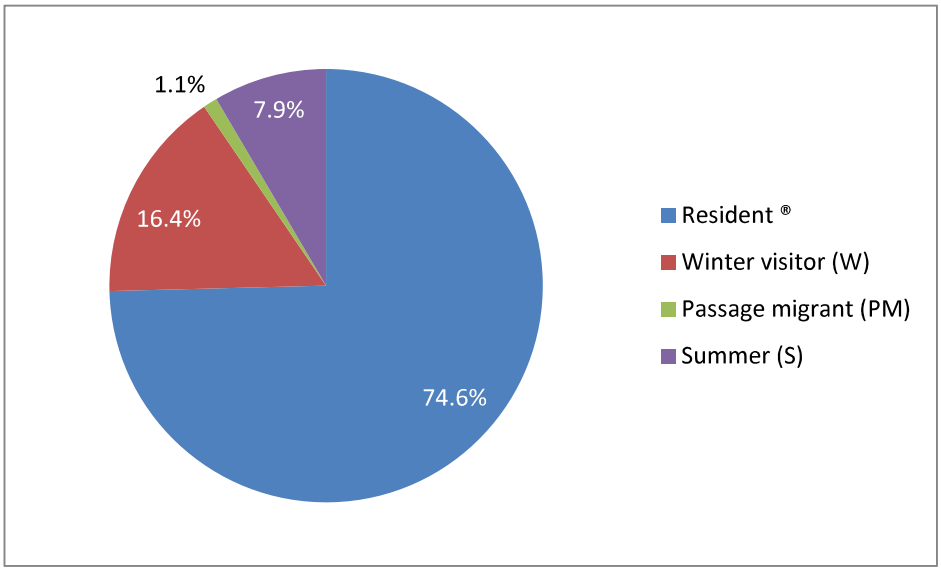

Fig. 2: Patterns of Occurrence of Avian Groups

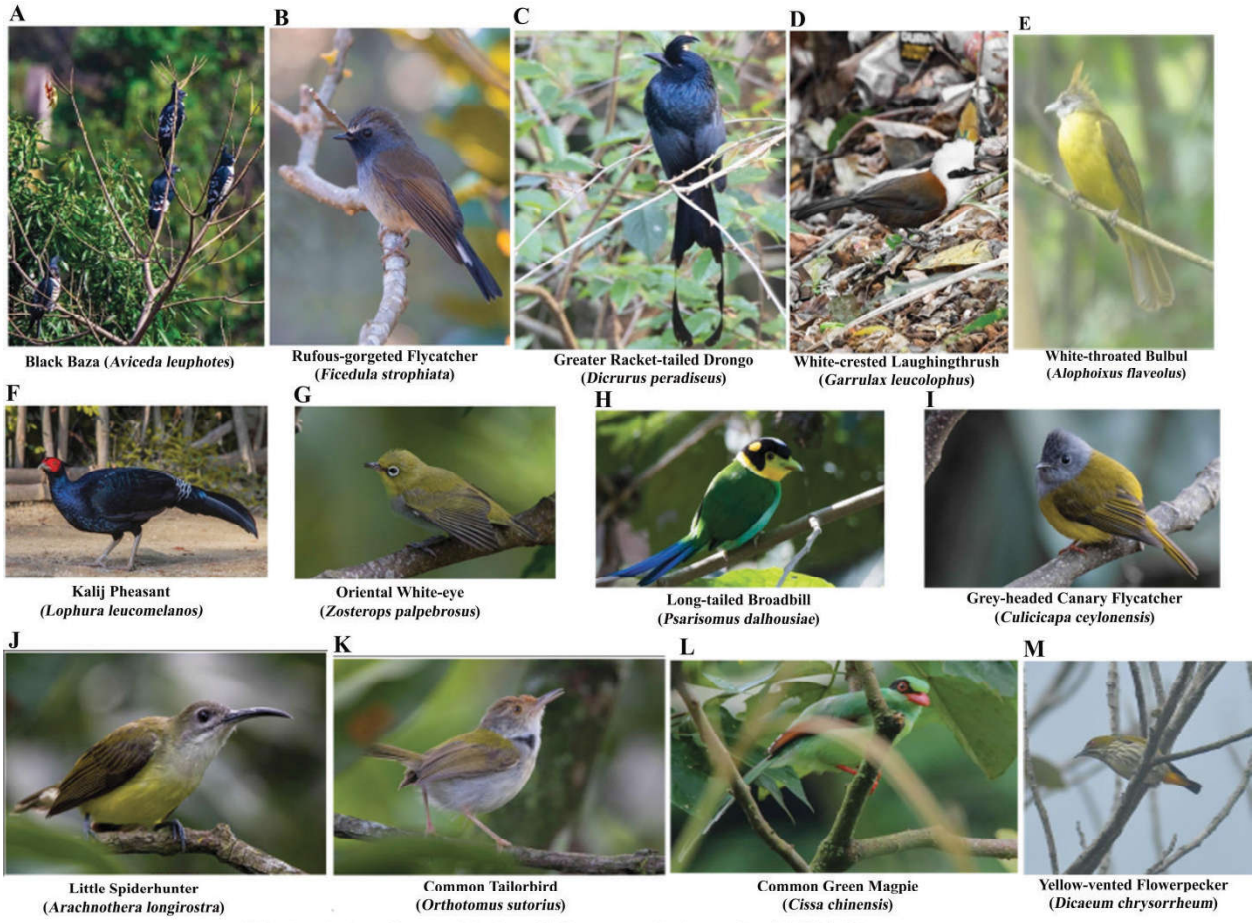

Fig. 3: Photoplate: Some Birds of Mizoram University (MZU) Campus

REFERENCES

Environment and forest. Birds; 2019 [cited on 27.7.19]. Available from: http://envformizo.in/forest/birds.htm

Chakdar, B., Choudhury, P. and Singha, H. 2016. Avifaunal Diversity in Assam University Campus, Silchar, India. J. of Threat. Taxa 8(1):8369-8378.

Chettri, N., Sharma, E. and Deb, D. C. 2001. Bird community structure along a trekking corridor of Sikkim Himalaya:A conservation Perspective. Biological conservation, 12:150-158.

Choudhury, A. 2008. A Pocket Guide to the Birds of Mizoram. Gibbon Books, Guwahati, Assam and The Rhino Foundation for Nature in NE India, Guwahati, Assam, India, pp 1-122.

Dey, A., Deb, D., Chaudhuri, S. D. and Chaudhuri, P. S. 2013. A Preliminary Study on Avifaunal Species Diversity of Maharaja Bir Bikram College Campus, Tripura, North East India. Int. Multidisc. Res. J., 2013, 3(2):36-43

Envis Centre on Avian Ecology. Statewise list of Birds of India. 2019 [cited on 7.8.2019] Available from: http://www.bnhsenvis.nic.in/Database/Statewise%.

Gaston, K. J., Blackburn, T. M. and Goldewijk, K. K. 2003. Habitat conversion and global avian biodiversity loss. Proc. R. Soc. Lond. B (2003) 270, 1923-1300.

Ghose, D. 1999. Birds recorded at Blue Mountain (Phawngpui) National Park, Mizoram Between February - May, 1997. Twilight, 1,16-18.

Grimmett, R., Inskipp, C. and Inskipp, T. 2011. Birds of the Indian Subcontinent (Second Edition). Oxford University Press, India. Pages 528.

Lalchhuanawma. 2008. Ecological studies on plant diversity and productivity of herbaceous species in Mizoram Universityu campus at Tanhril, Aizawl, Mizoram (N.E.India). Ph.D. thesis submitted to Mizoram University.

Lalthanzara, H. 2010. Recent status of threatened birds of Mizoram. Sci Vis, 10 (4), 168-169.

Lalthanzara, H., Kasambe, R. 2015. Popular Birds of Mizoram. Scientific Book Centre, Guwahati.Pages124

Lalthanzara, H., Lalramliana, Vanramliana, Lalnunzira, Vanlalsiama, Liana, J.P. 2011. Blyth's Tragopan (Tragopan blythii) in Lengteng Wildlife Sanctuary, Mizoram, India. Sci. Vis., 11(2), 108-112.

Lalthanzara, H., Ramanujam, S.N., Solanki, G.S. and Sailo, L. 2013. Survey on distribution of pheasants (Galliformes) in Mizoram, India. Sci. Vis., 13(2), 90-95.

Lalthanzara, H., Sailo, L., Solanki, G.S. and Ramanujam, S.N. 2014. Galliformes and Their Conservation Issues in Mizoram, India. Cibtech J Zool, 3(1), 42-48.

Lalthanzara, H., Sailo, L., Solanki, G.S., Ramanujam, S,N,, Lallianthanga, R.K. and Lalbiakmawia. 2014. Grey Peacock Pheasant (Polyplectron bicalcaratum) as probable candidate for Ecological Indicator in Tropical Montane Forest of Mizoram, Northeast India. In Lalnuntluanga *et al.* Eds. Issues and Trends of Wildlife Conservation in Northeast India. pp. 233-239.

Lalthanzara, H., Vanramliana and Lalramliana. 2011. Pheasants of Mizoram (India): Present status of diversity and distribution. Sci. Vis., 11(4), 218-223.

Lepage, D. 2018. Checklists of Birds of Mizoram. Avibase, the world bird database. Retrieved from http://avibase.bsc-eoc.org/checklist.jsp?region=INnemz&list=howardmoore on 08.07.2019.

McArthur, R.H. and McArthur, J.W. 1961. On bird species diversity. Ecology 42:594-599.

Manakadan, R. and Pittie, A. 2001. Standardised common and scientific names of the birds of the Indian subcontinent. Buceros 6(1): 1–37.

Magurran, A. E. 1985. Measuring Biological diversity. Black Well Publishing company, UK.

Schulte, L.A. and Niemi, G. J. 1998.Bird communities of early successional burned and logged forest. J. Wildlife Mgmt.62:1418-1429.

Shankar Raman, T.R., Rawat, G.S. and Johnsingh, A. J. T. 1998. Recovery of tropical rainforest avifauna in relation to vegetation succession following shifting cultivation in Mizoram, north-east India. J. Appl. Ecol., 35, 214-231.

Shankar Raman, T.R. 2001. Effect of slash-and –burn shifting cultivation on rainfgorested birds in Mizoram, Northeast, India. Conser. Biol.,15:685-698.

Steele, B.B., Bayn, R.L.Jr. and Grant, C.V. 1984. Environmental Monitoring using population of birds and small mammals: Analysis of sampling efforts. Biol. Conser., 30:157-172.

US Fish and Wildlife Service. The four essential Elements of Habitat. 2002. [cited on 12.8.2019]. Available from: https://digitalmedia.fws.gov/digital/collection/document/id/1426/

Vanlalsawmi, R., Solanki, G.S. and Zakhuma. 2011. Birds of Dampa Tiger Reserve in Mizoram, India. Proceedings of Advances in Environmental Chemistry, pp. 242-244.

Wiens, J.A. 1989. The ecology of the bird communities Vol.1.Foundation and pattern Cambridge University press.

Zothanpuii, J.H. 2019. Faunal diversity and distribution within Mizoram Univesity campus using camera trap technique. M.Sc. dissertation submitted for part fulfillment of degree of Master of Science in Zoology. Mizoram University, Aizawl. Pages 40.

Zoological Survey of India. 2007. Fauna of Mizoram. State Fauna Series 14, pp 1-691. 6.

Science and Technology Journal, Vol. 7 Issue: I ISSN: 2321-3388

Thermal Diffusion (Soret Effect) on an Unsteady MHD Mixed Convective Heat and Mass Transfer Flow through Vertical Porous Medium with Chemical Reaction

Sujan Sinha[1] and Maushumi Mahanta[2]
[1]Assistant Professor, Department of Mathematics, Assam Down Town University, Guwahati-26, Assam
[2]Assistant Professor, Department of Mathematics, Saraighat College, Changsari-101, Assam
E-mail: [1]mathssujangu@gmail.com, [2]maths.mmahanta@gmail.com

Abstract—A parametric study to investigate the effect of thermal diffusion (Soret effect) on an MHD mixed convective heat and mass transfer flow of an incompressible viscous electrically conducting fluid past a vertical porous plate. The magnetic Reynolds number is assumed to be so small that the induced magnetic field can be neglected as compared with the applied magnetic field. The resultant set of the non-dimensional governing equations are solved analytically by adopting perturbation technique. The profiles of the velocity, temperature, concentration, skin friction, Nusselt number and Sherwood number at the plate are demonstrated graphically for various values of the parameters involved in the problem and the results are physically interpreted. It is found in our discussion that thermal diffusion effect raises the fluid flow.

Keywords: Thermal-Diffusion, MHD, Dimensional, Perturbation Technique, Heat and Mass Transfer

INTRODUCTION

MHD is the science of movement in which all the characteristics of fluid with the magnetic benefits under the conduction of electric current. There are lots of applications of MHD principles in Engineering, Plasma Physics, in area of Biotechnology and Bio medical science. The effects of MHD in various heat and mass transfer problems with mixed convection are applied by several authors such as Elbashbeshy (2003), Singh *et al.* (2000) and Ahmed (2010).

Soret effect which is also known as thermal-diffusion effect concerns with the methods of separating heavier gas molecules from lighter ones by maintaining temperature gradient over a volume of a gas containing particles of different masses. The mass flux created by temperature gradient is termed as Soret or thermal –diffusion effect. In view of the importance of Soret effect, several authors have carried out their research works to investigate the problems related to thermal-diffusion effect. Some of them are Anghel *et al.* (2000), Postenlnicu (2004), Alam *et al.* (2004) and Ahmed (2010).

Several investigators have studied the impact of reaction in several convective heat and mass transfer flows of whom Apelblat (1982) and Anderson *et.al* (1994) are price mentioning. Chambre and Young (1958) have conferred a primary order reaction within the neighbourhood of a horizontal plate. Muthucumaraswamy (2002) conferred heat and mass transfer effects on an endlessly moving isothermal surface with uniform suction by taking in to account the homogenous reaction of 1st order.

The main aim of present study is to investigate the effect of thermal-diffusion (Soret effect) on a mixed convective heat and mass transfer flow through vertical porous plate with MHD. The work is an extension to the work done by Allan and Derbery (2018).

http://doi.org/10.22232/stj.2019.07.01.09

MATHEMATICAL FORMULATION OF THE PROBLEM

In the present study, an MHD conducting heat and mass transfer flow of a viscous incompressible electrically conducting fluid past an infinite vertical porous plate with constant suction is considered as well as a uniform transverse magnetic field. This investigation is considered with the following assumptions:

- The polarization effects are assumed to be negligible and so electric field is also negligible.
- The suction velocity is constant.
- The variations of all fluid properties other than the variation of fluid density are completely ignored.
- When the plates are infinite, all the physical variables are functions of y' and t' only.
- It is assumed that the variation of expansion co-efficient is negligibly small and assumed pressure and influence of the pressure on the density is negligible.
- The free stream oscillates about a steady mean.

Here, it is assumed $U'(t) = U_0(1+\varepsilon e^{i\omega t})$, where U_0 is the mean stream velocity, ε is the amplitude of the free stream variation and U' is velocity along the plate.

We introduce a co-ordinate system, where X-axis vertically upwards along the plate, Y-axis remains perpendicular to the plate and directed to the fluid region and Z-axis remains along the width of the plate as shown in **Figure 1**

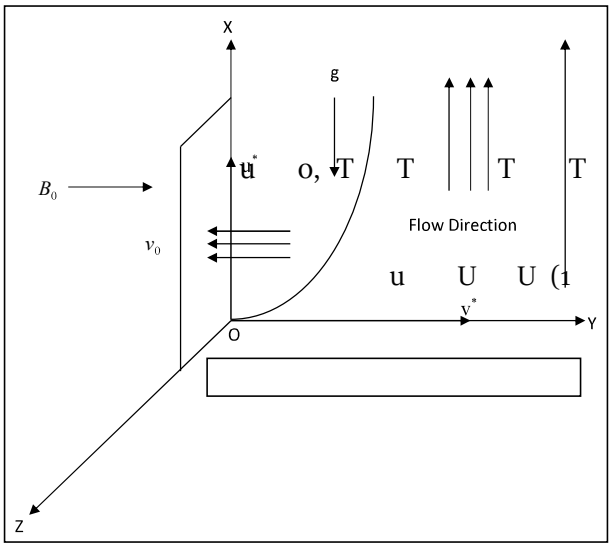

Fig. 1: Physical Model of the Problem

Let the components of velocity along the X-axis be u' and components of velocity along the Y-axis be v'. So u' is chosen in the upward direction along the plate and v' are chosen normal to the plate.

Under the given assumptions, the equations that describe the physical situation are given by:

1. **Equation of Continuity:**

$$\frac{\partial v'}{\partial y'} = 0 \Rightarrow v' = -v_0 \tag{1}$$

2. **Momentum Equation:**

$$\frac{\partial u'}{\partial t'} + v'\frac{\partial u'}{\partial y'} = -\frac{1}{\rho}\frac{\partial p'}{\partial x'} + \upsilon\frac{\partial^2 u}{\partial y'^2} - \frac{\sigma\beta^2{}_o}{\rho}u' \quad g \quad T \quad T \quad g \quad c \quad c$$

$$u + g\beta\left(T^{/} - T_\infty\right) + g\beta_c\left(c' - c'_\infty\right) - \upsilon\frac{u'}{k'} \tag{2}$$

3. **Energy Equation:**

$$\frac{\partial T'}{\partial t'} + v'\frac{\partial T'}{\partial y'} = \frac{k}{\rho c_p}\frac{\partial^2 T'}{\partial y'^2} - \frac{1}{\rho c_p}\frac{\partial q_r}{\partial y'} \tag{3}$$

4. **Concentration Equation:**

$$\frac{\partial c'}{\partial t'} + v'\frac{\partial c'}{\partial y'} = D\frac{\partial^2 c'}{\partial y'^2} - \gamma\left(c' - c'_\infty\right) + D_T\frac{\partial^2 T'}{\partial y'^2} \tag{4}$$

The boundary conditions for the velocity, temperature and concentration fields are:

$$u' = o,\ T' = T'_w + \varepsilon\left(T'_w - T'_\infty\right)e^{i\omega t},\quad c \quad c \quad c \quad c \quad e$$

$$c' = c'_w + \varepsilon\left(c'_w - c'_\infty\right)e^{i\omega t} \quad at \quad y' = o \tag{5}$$

$$u' \to U' = U_o(1+\varepsilon e^{i\omega t}),\quad T \quad T \quad , \quad c \quad c \quad at \quad y$$

$$u \quad U \quad U \ (1 \quad e \ ),\ T' \to T'_\infty,\ c' \to c'_\infty \quad at \quad y' \to \infty \tag{6}$$

Radiative heat flux term is given by

$$\frac{\partial q_r}{\partial y'} = 4\alpha^2\left(T'_\infty - T'\right) \tag{7}$$

Outside the boundary layer we consider

$$-\frac{1}{\rho}\frac{\partial \rho'}{\partial x'} = \frac{dU'}{dt'} + \frac{\nu}{K'}U' + \frac{\sigma}{\rho}B_0^2 U' \tag{8}$$

We now consider the following dimensionless variables as follows:

$$u=\frac{u'}{U_0},\ y=\frac{V_0 y'}{\nu},\ \omega=\frac{\nu\omega'}{v_0^2},\ U=\frac{U'}{U_0}$$

$$t=\frac{t'\,V_0^2}{\nu},\theta=\frac{T'-T'_{\infty'}}{T'_w-T'_\infty},\ \phi=\frac{C'-C'_\infty}{C'_w-C'_\infty}$$

$$N=\frac{4\alpha^2\nu}{\rho c_p v_0^2}K=\frac{K'\,V_0^2}{\nu^2},\ Pr=\frac{\rho\nu c_p}{k}$$

$$M=\frac{\sigma B_0^2\nu}{\rho V_0^2},Sc=\frac{\nu}{D},\ Sr=\frac{D_T(T'_w-T'_\infty)}{\nu(C'_w-C'_\infty)}$$

$$Kr=\frac{\nu\gamma}{v_0^2},\ Gr=\frac{\nu\beta g(T'_\omega-T'_\infty)}{U_0V_0^2},\ Gm=\frac{\nu\beta_c g(C'_w-C'_\infty)}{U_0V_0^2} \tag{9}$$

From the equation (7)–(9), the governing equations (2)–(4) are reduced to the non- dimensional form as follows:

$$\frac{\partial u}{\partial t}-\frac{\partial u}{\partial y}=\frac{\partial U}{\partial t}+\frac{\partial^2 u}{\partial y^2}+Gr\theta+Gm\phi+M_1(U-u) \tag{10}$$

$$\frac{\partial\theta}{\partial t}-\frac{\partial\theta}{\partial y}=\frac{1}{Pr}\frac{\partial^2\theta}{\partial y^2}+N\theta \tag{11}$$

$$\frac{\partial\phi}{\partial t}-\frac{\partial\phi}{\partial y}=\frac{1}{Sc}\frac{\partial^2\phi}{\partial y^2}-Kr\phi+Sr\frac{\partial^2\theta}{\partial y^2} \tag{12}$$

Where

$$M_1=M+\frac{1}{K}$$

Applying non-dimensional variables given in equation (9), the boundary conditions (5) and (6) are reduced to the following dimensionless form as follows:

$$u=0,\quad \theta=1+\varepsilon e^{i\omega t},\quad \phi=1+\varepsilon e^{i\omega t}\quad \text{at } y=0$$
$$u\to 1+\varepsilon e^{i\omega t},\quad \theta\to 0,\quad \phi\to 0\quad \text{as } y\to\infty \tag{13}$$

$$u_0\quad 0,\quad u_1\quad 0,\quad {}_0\quad 1,\quad {}_1\quad 1,$$
$$u_0\quad 1,\quad u_1\quad 1,\quad {}_0\quad 0,\quad {}_1\quad 0,$$

METHOD OF SOLUTION

Now we have needed to reduce the above system of partial differential equations (10)–(12) into a system of ordinary differential equations in dimensionless form, we may consider the velocity, temperature and concentration as follows:

$$u(y,t)=u_0(y)+\varepsilon e^{i\omega t}u_1(y) \tag{14}$$

$$\theta(y,t)=\theta_0(y)+\varepsilon e^{i\omega t}\theta_1(y) \tag{15}$$

$$\phi(y,t)=\phi_0(y)+\varepsilon e^{i\omega t}\phi_1(y) \tag{16}$$

Where u_0 , θ_0 , ϕ_0 are respectively the mean velocity, mean temperature and mean concentration.

Substituting the equations (14), (15) and (16) into the equation (10), (11) and (12), neglecting the higher of ε and equating the harmonic and non-harmonic terms, we get following equations as follows:

$$\left[\frac{d^2}{dy^2}+\frac{d}{dy}-M_1\right]u_0=-Gr\theta_0-Gm\phi_0-M_1 \tag{17}$$

$$\left[\frac{d^2}{dy^2}+\frac{d}{dy}-(M_1+i\omega)\right]u_1\quad {}_1\quad {}_1\quad {}_1$$
$$_1=-Gr\theta_1-Gm\phi_1-(M_1+i\omega) \tag{18}$$

$$\left[\frac{d^2}{dy^2}+Pr\frac{d}{dy}+NP_r\right]\theta_0=0 \tag{19}$$

$$\left[\frac{d^2}{dy^2}+Pr\frac{d}{dy}+P_r(N-i\omega)\right]\theta_1=0 \tag{20}$$

$$\left[\frac{d^2}{dy^2}+Sc\frac{d}{dy}-KrSc\right]\phi_0=-SrSc\theta_0'' \tag{21}$$

$$\left[\frac{d^2}{dy^2}+Sc\frac{d}{dy}-Sc(Kr+i\omega)\right]\phi_1=-SrSc\theta_1'' \tag{22}$$

Applying the equations (14), (15), and (16) the boundary conditions (13) can be written as

$$u_0=0,\quad u_1=0,\quad \theta_0=1,\theta_1=1,\quad {}_0\quad 1,\quad {}_1\quad 1,\quad \text{at } y\quad 0$$
$$\phi_0=1,\ \phi_1=1,\quad \text{at } y=0 \tag{23}$$

$$u_0=1,\quad u_1=1,\quad \theta_0=0,\quad {}_1\quad 0,\quad {}_0\quad 0,\quad {}_1\quad 0,\quad \text{at } y$$
$$\theta_1=0,\ \phi_0=0,\ \phi_1=0,\quad \text{at } y\to\infty \tag{24}$$

Solving the equations from (17) to (22) and applying the boundary conditions (23) and (24), getting following equations:

$$\theta_0(y) = e^{m_1 y} \quad (25)$$

$$\theta_1(y) = e^{m_2 y} \quad (26)$$

$$\phi_0(y) = (1 - A_1)e^{m_3 y} + A_1 e^{m_1 y} \quad (27)$$

$$\phi_1(y) = (1 - A_2)e^{m_4 y} + A_2 e^{m_2 y} \quad (28)$$

$$u_0(y) = (A_3 + A_4 + A_5 - 1)e^{m_5 y} + 1 - A_3 e^{m_1 y} - A_4 e^{m_3 y} - A_5 e^{m_1 y} \quad (29)$$

$$u_1(y) = A_8 e^{m_6 y} + 1 - A_6 e^{m_2 y} - A_7 e^{m_4 y} \quad (30)$$

Where

$$m_1 = \frac{-Pr - \sqrt{Pr^2 - 4N\,Pr}}{2},$$

$$m_2 = \frac{-Pr - \sqrt{Pr^2 - 4\,Pr\,(N - i\omega)}}{2},$$

$$m_3 = \frac{-Sc - \sqrt{Sc^2 + 4KrSc}}{2},$$

$$m_4 = \frac{-Sc - \sqrt{Sc^2 + 4Sc\,(Kr + i\omega)}}{2},$$

$$M_1 = M + \frac{1}{K}, \quad M = \frac{\sigma\beta_o^2 \upsilon}{\rho v_o^2}, \quad K = \frac{K' v_o^2}{\upsilon^2},$$

$$m_5 = \frac{-1 - \sqrt{1 + 4M_1}}{2}$$

$$m_6 = \frac{-1 - \sqrt{1 + 4(M_1 + i\omega)}}{2},$$

$$A_1 = \frac{-m_1^2 ScSr}{m_1^2 + Scm_1 - KrSc},$$

$$A_2 = \frac{-m_2^2 ScSr}{m_2^2 + Scm_2 - Sc(Kr + i\omega)},$$

$$A_3 = \frac{Gr}{m_1^2 + m_1 - M_1},$$

$$A_4 = \frac{Gm(1 - A_1)}{m_3^2 + m_3 - M_1}, \quad A_5 = \frac{GmA_1}{m_1^2 + m_1 - M_1},$$

$$A_6 = \frac{Gr + GmA_2}{m_2^2 + m_2 - (M_1 + i\omega)},$$

$$A_7 = \frac{Gm(1 - A_2)}{m_4^2 + m_4 - (M_1 + i\omega)}, \quad A_8 = A_6 + A_7 - 1, \quad (31)$$

From the equations (14) to (16), we obtain velocity, temperature and concentration as follows:

$$u(y,t) = 1 + A_9 e^{m_5 y} - A_{10} e^{m_1 y} - A_4 e^{m_3 y} + \varepsilon e^{i\omega t}\left[A_8 e^{m_6 y} + 1 - A_6 e^{m_2 y} - A_7 e^{m_4 y}\right] \quad (32)$$

$$\theta(y,t) = e^{m_1 y} + \varepsilon e^{i\omega t} e^{m_2 y} \quad (33)$$

$$\phi(y,t) = (1 - A_1)e^{m_3 y} + A_1 e^{m_1 y} + \varepsilon e^{i\omega t}\left[(1 - A_2)e^{m_4 y} + A_2 e^{m_2 y}\right] \quad (34)$$

Where,

$$A_8 = A_6 + A_7 - 1, \quad A_9 = A_3 + A_4 + A_5 - 1, \quad A_{10} = A_3 + A_5 \quad (35)$$

Now we can calculate co-efficient of skin-friction at the wall of plate is given by

$$\tau_\omega = \left[\frac{\partial u}{\partial y}\right]_{y=0} = A_9 m_5 - m_1 A_{10} - m_3 A_4 + \varepsilon e^{i\omega t}\left[A_8 m_6 - A_6 m_2 - A_7 m_4\right] \quad (36)$$

The rate of heat transfer in terms of Nusselt number (Nu) as follows:

$$Nu = -\left[\frac{\partial \theta}{\partial y}\right]_{y=0} = -m_1 - m_2\,\varepsilon e^{i\omega t} \quad (37)$$

The rate of mass transfer co-efficient in terms of Sherwood number as follows:

$$Sh = -\left[\frac{\partial \phi}{\partial y}\right]_{y=0} = -(1 - A_1)\,m_3 - m_1 A_1 - \varepsilon e^{i\omega t}\left[(1 - A_2)m_4 + A_2 m_2\right] \quad (38)$$

RESULTS AND DISCUSSIONS

In the present discussion, the expressions of fluid velocity, temperature, concentration viscous drag, co-efficient of rate of heat transfer and co-efficient of rate of mass transfer are piled up to get a variety of graphs with their substantial interprtations by taking some random values of different parameters implicated in the problem.

The velocity profile under the influence of Hartmann number M, Chemical reaction parameter Kr, Soret number Sr and Schmdit number Sc against the normal co-ordinate y are exhibited in figures 2-5. It is contingent from figure 2 and 3 that, an increase in magnetic parameter M and chemical reaction parameter Kr has an inhibiting effect on fluid velocity. The fluid velocity is continuously condensed with increasing M and Kr. In other words the obligation of the transverse magnetic field and reaction tends to slow down the fluid flow. In figure 5, we observe the same trend of performance with Schmdit number Sc is concerned. But figure 4 displays the opposite behavior with respect to the above figures. i.e. the fluid motion gets accelerated under the action of mass flux.

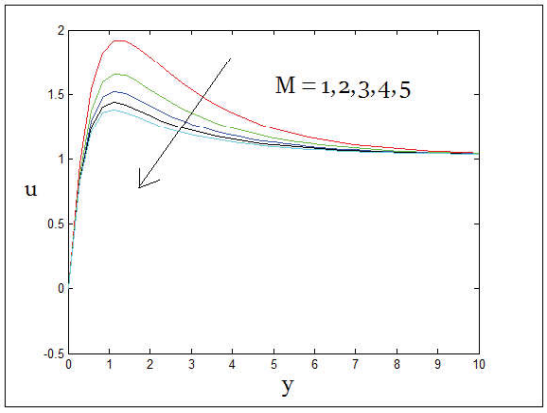

Fig. 2: Velocity Versus y under K=2, N=0.2, Gr=2, Gm=2, Kr=2, Sc=0.22, Pr=0.71, Sr=2, ε=0.5, ω=10, t=0.15

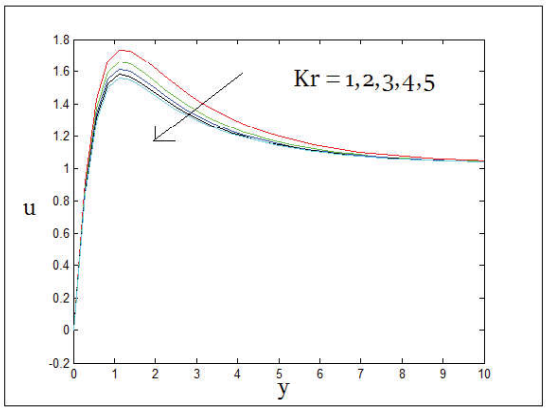

Fig. 3: Velocity Versus y under K=2, N=0.2, Gr=2, Gm=2, M=2, Sc=0.22, Pr=0.71, Sr=2, ε=0.5, ω=10, t=0.15

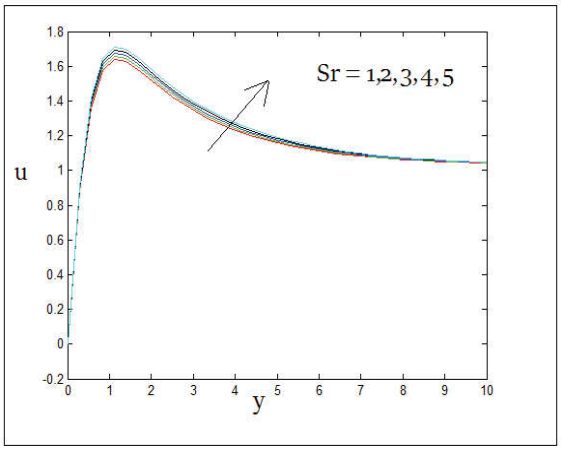

Fig. 4: Velocity Versus y under K=2, N=0.2, Gr=2, Gm=2, Kr=2, Sc=0.22, Pr=0.71, M=2, ε=0.5, ω=10, t=0.15

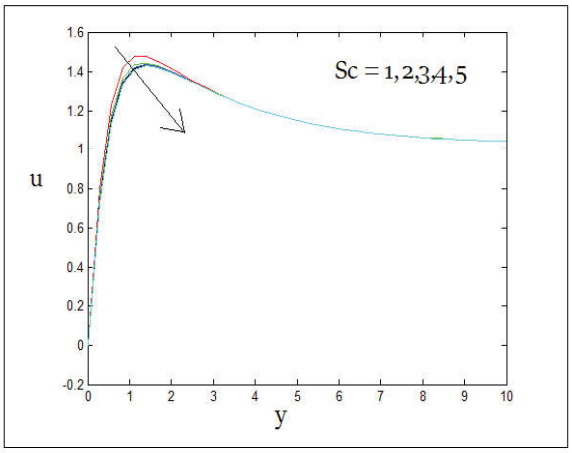

Fig. 5: Velocity Versus y under K=2, N=0.2, Gr=2, Gm=2, Kr=2, M=2, Pr=0.71, Sr=2, ε=0.5, ω=10, t=0.15;

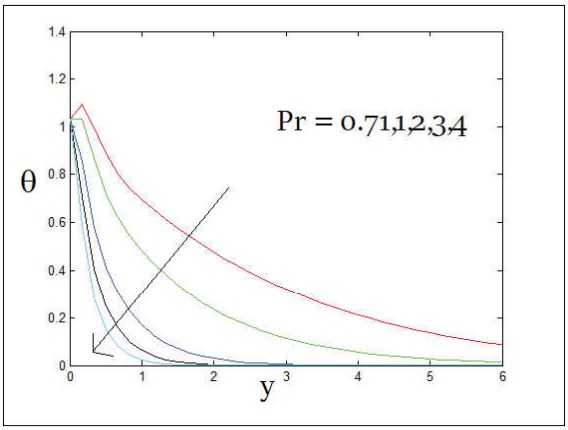

Fig. 6: Temperature Versus y under N=0.2, ε=0.5, ω=10, t=0.1

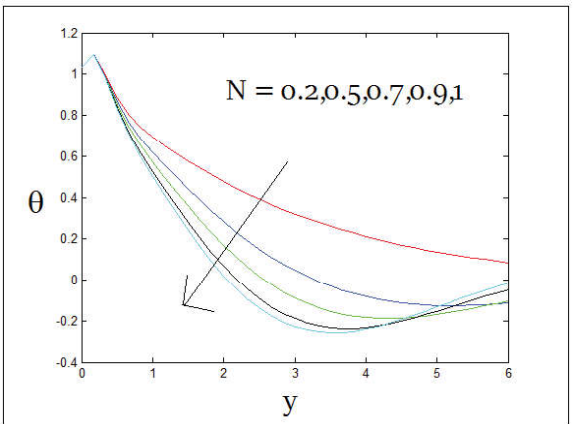

Fig. 7: Temperature Versus y under Pr=0.71, ε=0.5, ω=10, t=0.15

Figures 6 to 7 match up to the temperature distribution θ against y under the effects of the Prandtl number Pr and radiation parameter N. Rising of Pr or N shows a contrasting control on θ which indicates the fact that the fluid temperature falls down gradually for increasing values of Pr and R. It is further noticed from these figures that the fluid temperature as expected asymptotically falls from its maximum value at $y = 0$ to its minimum value at $y \to \infty$.

The effects of Soret number Sr and Schmdit number Sc on species concentration have been displayed in figures 8 and 9. It is contingent from both the figures that concentration level of the fluid quickly rises up for increasing values of Soret number Sr and drops for increasing Schmdit number Sc. It indicates that the concentration level gets enhanced due to mass flux and high mass diffusivity.

The variations of skin friction against ω under the influence of Hartmann number M, Chemical reaction parameter Kr, Soret number Sr and Schmdit number Sc are presented in figures 10-13. It is observed from the figures 10, 11 and 13 that an increase in magnetic intensity, chemical reaction and mass diffusivity tends to minimize the viscous drag. It is seen from figure 12 that the friction is raised by virtue of thermal diffusion effect.

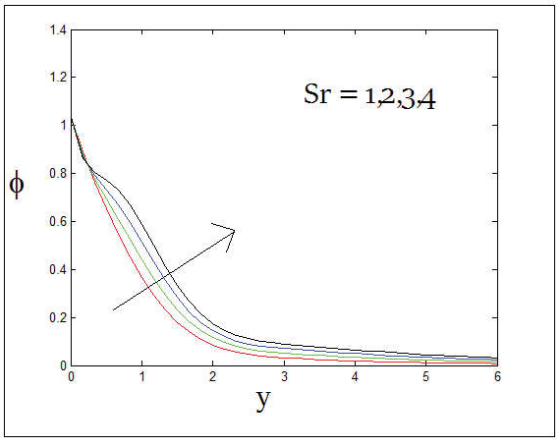

Fig. 8: Concentration Versus y under N=0.2, ε=0.5, ω=10, t=0.15,Pr=0.71, Sc=0.60, Kr=2

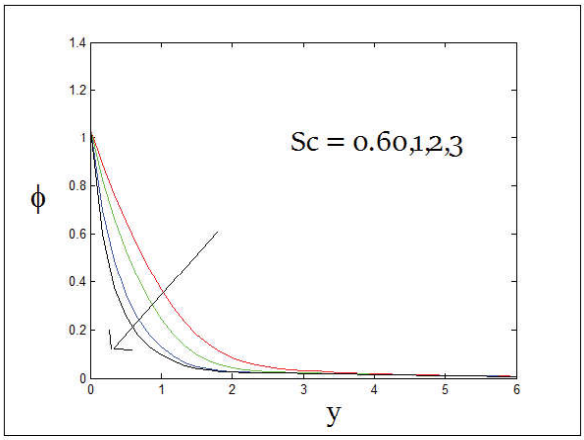

Fig. 9: Concentration Versus y under N=0.2, ε=0.5, ω=10, t=0.15, Pr=0.71, Sr=1, Kr=2

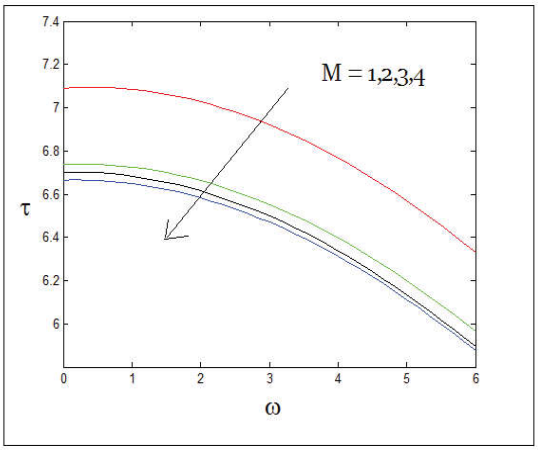

Fig. 10: Skin Friction Versus ω under K=2, N=0.2, Gr=2, Gm=2, Kr=2, Sc=0.22, Pr=0.71,Sr=2, ε=0.5, t=0.15

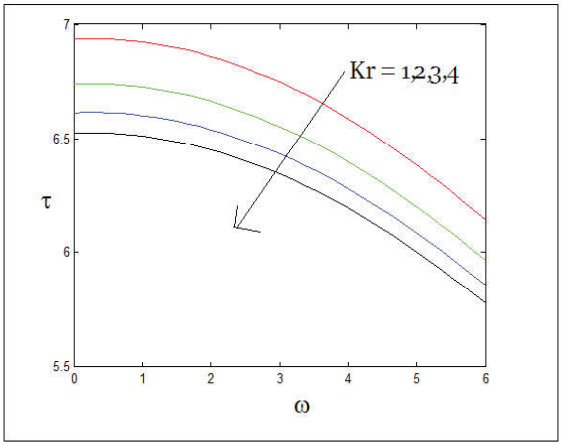

Fig. 11: Skin friction versus ω under K=2, N=0.2, Gr=2, Gm=2, M=2, Sc=0.22, Pr=0.71, Sr=2, ε=0.5, t=0.15

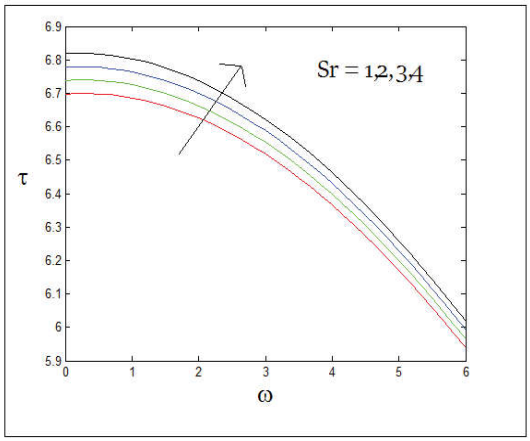

Fig. 12: Skin Friction Versus ω under K=2, N=0.2, Gr=2, Gm=2, Kr=2, Sc=0.22, M=2, t=0.15, Pr=0.71, ε=0.5

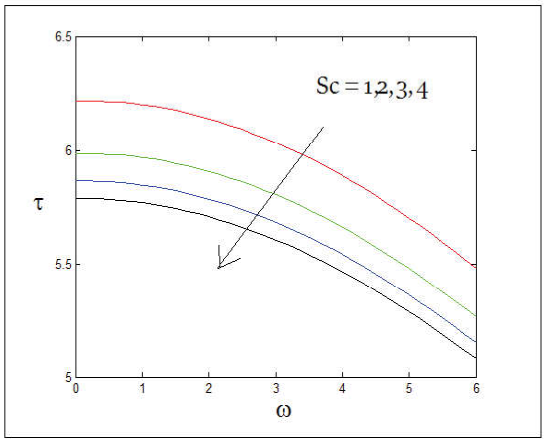

Fig. 13: Skin Friction Versus ω under K=2, N=0.2, Gr=2, Gm=2, M=2, Kr=2, Pr=0.71, Sr=2, ε=0.5, t=0.15

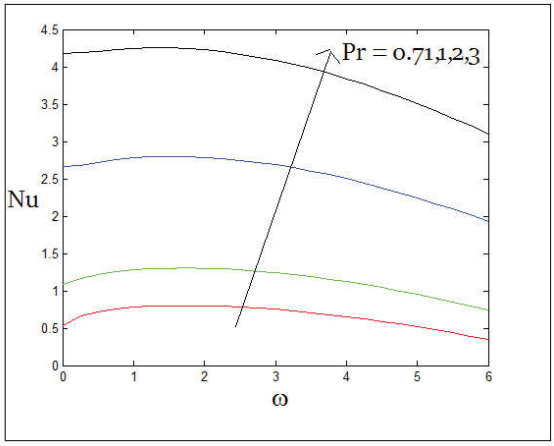

Fig. 14: Nusselt Versus ω under N=0.2, ε=0.5, t=0.15

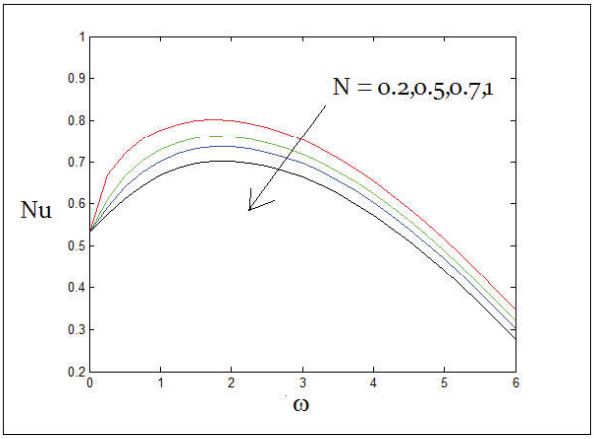

Fig. 15: Nusselt Versus ω under Pr=0.71, ε=0.5,t=0.15

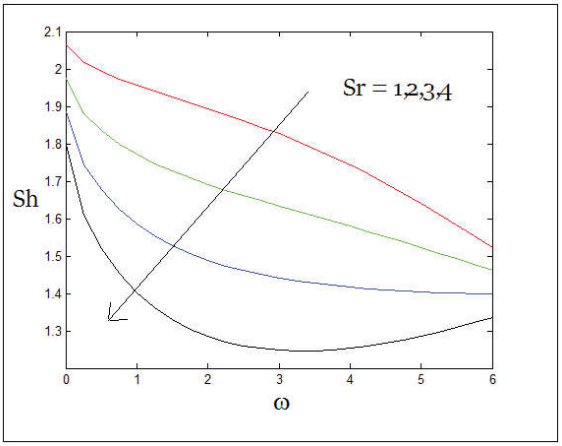

Fig. 16: Sherwood Versus ω under N=0.2 ε=0.5,t=0.15,Pr=0.71,Sc=0.60,Kr=2

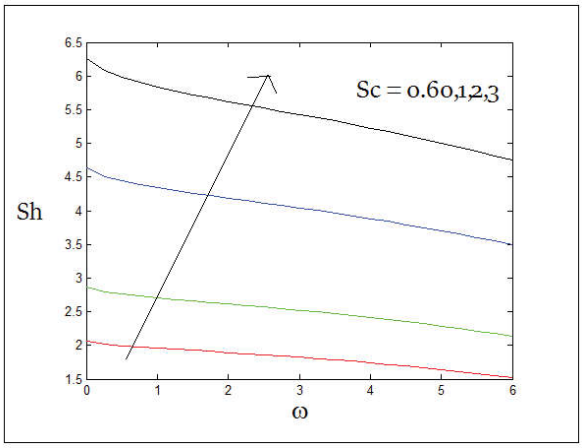

Fig. 17: Sherwood Versus ω under N=0.2, Pr=0.71, Sr=1,Kr=2, ε=0.5, t=0.15

The effects of Prandtl number Pr and radiation parameter N on the co-efficient of rate of heat transfer in terms of Nusselt number have been displayed in figures 14-15. It is found from figure 14 that the magnitude of the rate of heat transfer increases with the increase in Prandtl number Pr. This simulates that low thermal diffusivity leads the substantial rise in the heat transfer rate. Figure 15 demonstrates that the co-efficient of rate of heat transfer is reduced with the increasing values of radiation parameter N. ie the energy flux falls due to low thermal conductivity.

The figures 16 and 17 present the variation of the rate of mass transfer from the plate to the fluid. It is inferred from figure 16 that the Sherwood number falls down under the action of thermal diffusion effect. It is contingent from figure 17 that the co-efficient of rate of mass transfer rises under Schmdit number. i.e. the mass flux from the plate to the fluid get increased under the influence of mass diffusivity.

CONCLUSION

The following conclusions can be drawn from the present investigation of the problem:

1. The primary fluid motion is retarded under the action of transverse magnetic field and accelerated in presence of Soret number.
2. The concentration level of the fluid quickly rises up for increasing values of Soret number Sr and drops for increasing Schmdit number Sc. It indicates that the concentration level gets enhanced due to mass flux and high mass diffusivity.
3. An increase in magnetic intensity and chemical reaction tends to minimize the viscous drag and the friction is raised by virtue of thermal diffusion effect.
4. Sherwood number falls down under the action of thermal diffusion effect and the co-efficient of rate of mass transfer rises under Schmdit number. i.e. the mass flux from the plate to the fluid get increased under the influence of mass diffusivity.

NOMENCLATURE

U	Non dimension velocity along the plate
U_0	Mean stream velocity
U'	Dimensional velocity along the plate
x, y	distances along and perpendicular to the plate, respectively
V_o	Constant suction velocity
x', y'	dimensionless distances along and perpendicular to the plate, respectively
u, v	components of dimensionless velocities along x' and y' directions respectively
u', v'	components of dimensional velocities along x' and y' directions respectively
t	non-dimensional time
t'	dimensional time
D	Diffusion co-efficient

D_T	Thermal Diffusion Ratio
K_r	Non-dimension chemical reaction parameter
K_r'	Dimensional chemical reaction parameter
K	Non-dimension porosity number
K'	Dimensional porosity number
T'	dimensional temperature of the fluid
T_w'	dimensional temperature at the plate
T_∞'	dimensional temperature in the free stream
N	Radiation parameter
K	non-dimension porosity parameter
P_r	Prandtl number
M	Magnetic parameter
Gr	Grashoff number
G_m	Grashoff number for mss transfer
S_c	Schmdit number
Sr	Soret number
C'	dimensional concentration
C_w'	dimensional concentration at the wall
C_∞'	dimensional temperature in the free stream
g	Acceleration due to gravity
p	Non dimension pressure
p'	Dimensional pressure
C_p	Specific heat at constant pressure

GREEK SYMBOLS

ρ	Density of the fluid
ν	fluid kinetic viscosity
α	Radiation absorption co-efficient
β	co-efficient of thermal expansion
β_c	Volumetric expansion co-efficient
θ	non-dimensional temperature
σ	Electrical conductivity
ϕ	non-dimensional concentration
ε	small reference parameter
ω	Frequency parameter

SUBSCRIPTS

w	Wall condition
∞	Free stream condition

SUPERSCRIPTS

/	Dimensional properties
//	Differentiation w. r. to y

REFERENCES

Ahmed N (2010) MHD convection with Soret and Dufour effects in a three dimensional flow past an infinite vertical porous plate. *Can. Jr. Phys.* 88(9): 663-674.

Ahmed N (2010) MHD free and forced convection with mass transfer from an infinite vertical porous plate. *Journal of Energy, Heat and Mass Transfer* 32: 55-70.

Alam S, Rahman M M, Maleque A and Ferdows M (2004) Dufour and Soret effects on steady MHD combined free-forced convective and mass transfer flow past a semi-infinite vertical plate. *Thammasat Int. J. Sc. Tech.* 11(2): 1-12.

Allan M M and Dardery S M (2018) On the effect of convective heat and mass transfer on unsteady mixed convection MHD flow through vertical porous medium. *International Journal of Physical Sciences* 13.5: 66-78.

Anderson H I, Hansen O R and Holmedal B (1994) Diffusion of a chemically reactive species from a stretching sheet. *International Journal of Heat and Mass Transfer* 37: 659-664.

Anghel M, Takhar H S and Pop I (2000) Dufour and Soret effects on free convection boundary layer over a vertical surface embedded in porous medium. *Studiab Universitatis Babes-Bolyai Mathematica* 60(5): 11-21.

Elbashbeshy E M A (2003) The mixed convection along a vertical plate embedded in non- darcian porous medium with suction and injection *Applied Mathematics and Computation* 136(1): 139-149.

Muthukumaraswami R (2002) Effects of a chemical reaction on a moving isothermal surface with suction. *Acta Mechanica 155*: 65-72.

Postelnicu A (2004) Influence of a magnetic field on Heat and Mass Transfer by natural convection from a vertical surface in porous media considering Soret and Dufour effects. *Int. J. of Heat and Mass Transfer* 47: 1467-1472.

Singh N P and Singh Atul K (2000) MHD effects on heat and mass transfer in a flow of viscous fluid with induced magnetic field. *Indian Journal of Pure and Applied Physics* 38: 182-189.

Apelblat A (1982) Mass transfer with a chemical reaction of the first order effect of axial diffusion. *The chemical Engineering Journal* 23: 193-203.

Chambre P L and Young J D (1958) On the diffusion of a chemically reactive species in a laminar boundary layer flow. *Phys. Fluids Flow* 1: 48-54.

Science and Technology Journal, Vol. 7 Issue: 1 ISSN: 2321-3388

Effect of NAVA for Dense Optical Communication System

Ghanendra Kumar[1] and Chakresh Kumar[2]*
[1]Department of Electronics and Communication Engineering
National Institute of Technology, Delhi–110040, India
[2]University School of Information, Communication & Technology,
Guru Gobind Singh Indraprastha University, New Delhi–110078, India
E-mail: *chakreshk@gmail.com

Abstract—Viterbi Algorithm (VA) is basically an algorithm that is implemented for the detection & estimation of a sequence of symbols in digital communication and signal processing. It calculates a survivor path with minimum metric value, but cannot detect any error. The VA is scrutinized to upgrade the transmission process and provide the plate form in terms of the existence, linear phase noise as well as non-linear phase noise. In contradiction to non-adaptive MLSD (Maximum Likelihood Sequence Detection), the Viterbi algorithm renders the exemplary performance.

Keywords: NAVA (Newly Viterbi Algorithm), Optical, EDFA(Erbium-Doped Fiber Amplifier), SOA(Semiconductor Optical Amplifier)

INTRODUCTION

The need and urgency for optimal performance in optical fiber communication systems has stimulated interest in coherent detection**.** Many compatible identification (coherent detection) methods are used to support other advanced modulation techniques, for example, M-ary phase-shift-keying (MPSK). The basic principle of PSK modulation is that, for every bit, the phase of the carry signal is changed. The 'M' in the M-ary PSK stands for the degree of the phase shift in the given Phase Shit Keying (PSK) [1-5]**.** Also, it increases the spectral efficiency by a factor of logbase2 (M). Due to the easy availability of high-level technology & high speed converters in the form of Analog to digital, the data or the statistics can be preserved on the electric field, and linear impairments such as Chromatic dispersion of the polarization mode, etc. is severly reduced. However, the major issue arises regarding mitigation of carrier phase noise during the usage of local-oscillator, in coherent detection. The presence of phase noise can lead to the reduction of the effective signal-to-noise ratio (SNR) calculated at receiver, decrement the bit error rate (BER) and data rate, corruption of the received signal & limitation of transmission distance [6-8]. We observe, therefore, that phase noise causes system performance degradation. Several solutions and algorithms have been put forward to eliminate Linear-Phase-Noise (LPN) and Non-Linear-Phase-Noise (NLPN) by using either DSP techniques, or with the usage of optical components. Linear phase noise is explored as noise resulting from concise term phase fluctuations in the signal**.** Fluctuations reveal themselves as a sideband appearing in the form of a noisy spectrum, which is observed to spread out on either sides of the signal**.** As a result of the reciprocity in the presence of fiber losses in optical medium and the intensified or increased spontaneous-emission (ASE) noise due to wrong setting of higher power amplification**.** We observe amplified noise and degradation levels in the performance behaviour of modulation techniques that encode data information in the optical carrier phase [9-11]. This is known as non-linear phase noise. The Decision Aided Maximum Likelihood scheme and the Viterbi adaptive maximum likelihood sequence detection schemes, both, are symbol-by-symbol (SBS) algorithms. MLSD's goal is to reduce the application complexity in communication over channels where channels behaviour are nonlinear dispersive. MLSD dramatically diminishes the Viterbi decoder (VD) states and provides a resolution between the two characteristics, the complexity and the performance. In this paper, the performance of MLSD, an Adaptive MLSD, in the existence of linear phase noise & non-linear phase noise, is studied.

http://doi.org/10.22232/stj.2019.07.01.10

ADAPTIVE MLSD ALGORITHM

Primarily, the effect of a multitude of noises are proceeded upon based on a presumption of removal of anomalies like Polarization mode dispersion (PMD) with the help of optical methods and Digital Signal Processor (DSP), and no contribution of the MLSD algorithm is considered for their processing.

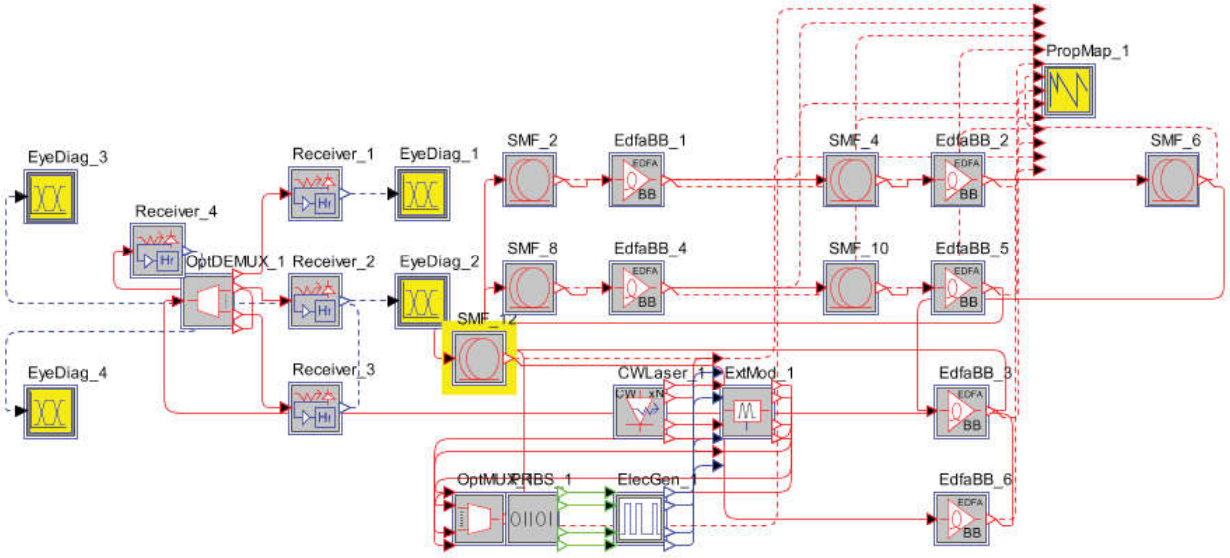

Fig. 1: Proposed Setup for Dense Optical Communication

In the above long haul system given by Fig. 1, optical amplifiers are installed at a range of 100 Kilometers on the fibre span to reduce attenuation in the signal being transmitted. Acquired one made to combine with an LOl signal (2 x 4 90^{o})optical hybrid made up of a ferroelectric material $LiNbO_3$ or Lithium Niobate which has a large acousto–optic and electro–optic coefficients**.** The output signal later on is further finded by the receiving detectors for the signals. The i^{th} symbol quoted as one acquired for the interval (iT,(i+1)T).

$$s(k)=m(i)\exp(j\Theta(i))+n(i)$$

Where n(i) is sent Mean phase shift keyed or Multi-ary quadrature amplitude modulated singal & o(i) is AWGN**.** The wobble of the CPN Θ(i) is derived from two parts, namely LPN & NLPN. Priori LPN which is Wiener process $\Theta_{LPN}(i)=\Sigma^{i}_{h=-\infty}v(h)$ where v(h) is tha free and same distributed gaussian random variable having null mean and $\sigma^2_{LPN}=2\pi\Delta fT$, with T denoting duration and Δf denoting the 3 dB Laser Line width. The later benefactor of PN also known as Non Linear PN which is accumulated by passing it through N_A is given by –

$$\theta_{NL}(i) = \Sigma^{NA}_{i-1}\ \theta_{NL}(a,i) = \Sigma^{NA}_{i-1}\gamma\ \ L_{eff}|E_o(i,k)|^2$$

Where the electric field $Eo(a,i)=Eo(0,i)+N_1(i)+N_2(i)+\ldots+N_i(i)$, $N_i(i)$ being the noise induced by the i^{th} amplifier, γ is the nonlinearity coeff & L_{eff} stands for the effective non linear length per fiber span**.**The viterbi type algorithm is now implemented as the block assessment of the sent signal m=[m(0)+m(1)+.....+m(D-1)] from the acquired signal r=[r(0)+r(1)+.....+r(D-1)] is improbable and won't give us the required output. Therefore, now the sent array is treated as trelli path given in figure 2 and the survivor in each state is the sequence with the max possibility among all the permutations entering that scenario. Hence at an instant T=iT, the reciever works on the possibility fn P(R(i)|n(i)) of every hypothised subsequence in the sent signal n(k)=[n(0)+n(1)+n(2)+.....n(i-1)] as per given the acquired sequence R=[R(0)+R(1)+.....+R(i-1)]. The deciding qty $\mu(i_o,m(i_o))=\mu(i_o\text{-}1,n(i_o\text{-}1))+|r(i_o)\text{-}n(i_o)V_n(i_o|i_o\text{-}1)|^2$ only involves linear calculations and it can be subjected to recursive calculations, having it's complexity fixed notwithstanding of array length. In order to apply MLSD we need to calculate a reference phasor from the sequence of previous L symbols.A block length effect arsies in MLSD due to different memory lengths.Therefor we use a better approach called adaptive MLSD algorithm in which we apply a first-order filter for the calculation of reference phasor and it also minimizes theestimation error. Here, sift requires pre state info other

than L as the length stored is automatically self-adjusted. So the coherent receiver requires very less memory**.** The filter is required to be trained to steadty state. This can be done by transmitting a short prologue in the beginning of the sequence. Each data sequence with a length D is attached with a symbol at the end to cause paths recombination.

DISCUSSION AND RESULTS

First we will do the analysis of how MLSD will perform in presence of LPN and NLPN wihtout using any adaptation mechanism. For doing so the variance in phase error for reference phasor is derived and it is found that it obeys the Gaussian distribution having a zero mean and variance of MLSD is given by

$$E[\Delta\theta(k)|2] = \frac{2L^2+3L+1}{6L}\sigma^2{}_{LPN} + \left(\frac{1}{L}+1\right)\sigma^2{}_{NL} + \left(\frac{1}{2L}\right)\sigma^2{}_{n'}$$

The resolution between balancing the NLPN, LPN and additive noise is explained by Eq.(5).To minimize error of estimation the optimum value of L can be calculated using Eq.(5) given as

$$L_{opt} = \left[\sqrt{\frac{\sigma^2{}_{LPN} + 6\sigma^2{}_{NL} + 3\sigma^2{}_{n'}}{2\sigma^2{}_{LPN}}}\right]$$

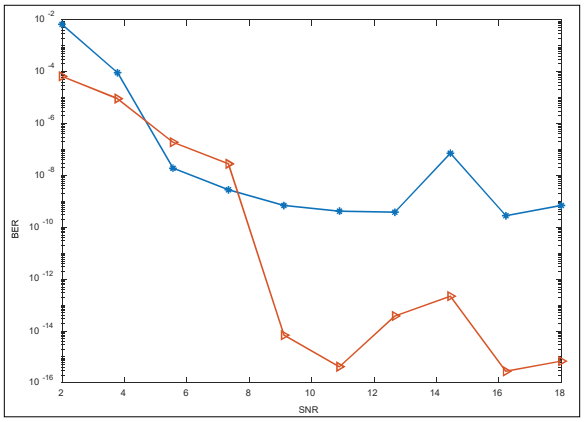

Fig. 2: BER *vs.* SN Simulation at 25 Gbaud/s QPSK Signal Considering Only LPN with LLW = 200k/5M

Fig. 2 shows a comparison of BER *vs.* SNR for Adaptive MLSD and MLSD algorithms. It is observed that when the LLW is large, a shorter L is required by the phase noise for tracking which is varying fast. On the other hand the salient feature of longer L is that additive noise compensated by it. In case of unknown channel statistics and usage of improper receiver and memory value being employed, it will be observed that especially in the low BER region the performance of BER will degrade.

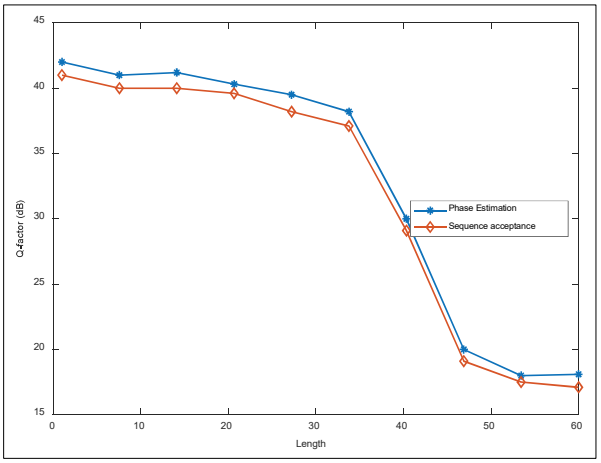

Fig. 3: Curve of Q-factor *vs.* Memory Length for DAML and MLSD at 25 GBaud/s DQPSK Signals having 20 Spans

Fig. 3 shows a comparison of the plot for Q-factor *vs.* memory length between MLSD and DAML with only NLPN for a fibre which has 20 spans transmitting in which is a 25 Gbaud/s DQPSK signal. It can be seen that when Q-factor is low sequence detection algorithm(MLSD) excel SBS algorithm(DAML). Increasing the memory length results in the increase in Q-factor for both the algoritms but after certain poitn the curve saturates which is evident from equation (5)**.** Larger the number of amplifiers higher will be the variance of NLPN. So in order to have a higher Q-factor the error variance must be reduced which is possible only by having a longer memory length L. Consequently,the complexity of the receiver is increased which is undesirable. To avoid receiver complexity, we use the adaptive version of MLSD in order to have an optimal performance. The memory requirement for a first-order filter is same as L=1 in MLSD**.**

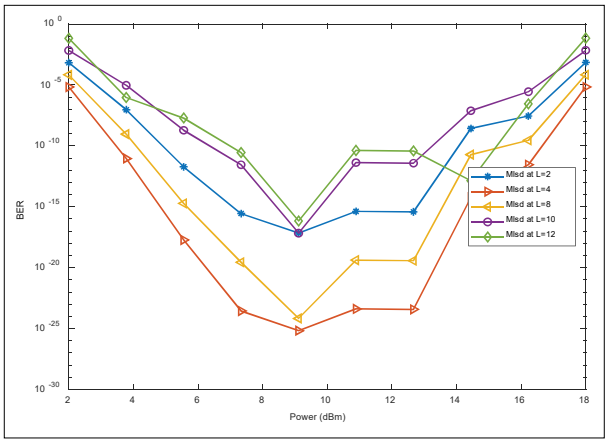

Fig. 4: Curve of BER *vs.* Launched Power for Adaptive MLSD *vs.* Non-adaptive MLSD having 23 Spans for LLW = 10MHz at 25GBaud/s DQPSK

In Fig. 4, we consider both type of noises i.e. LPN and NLPN which is a real situation. It is found that simply increasing memory length due to LPN does not made any improvement in the error-rate performance. In the region where SNR is low,with increasing SNR the BER decreases as the dominant distortion in this region is additive noise. In the region where the launched power is greater than optimum launched power the noise is mainly because of Non-Linear Phase Noise which is due to the fact that power of signal is large. It can be seen from Fig. 5 that at optimum launched power there is a considerable improvement in BER performance of adaptive MLSD over non-adaptive MLSD which can be even more better if receiver knows the statistics of the channel.

CONCLUSION

Adaptive MLSD algorith of the type Viterbi for optical systems which are coherent in nature having NLPN & LPN both was studied and it was concluded that favourable and best performance was delivered with the complexity of the receiver being low.

REFERENCES

Sorokin E, Naumov S, Sorokina I T (2005) Ultra broadband infrared solid-state lasers: IEEE J. Sel. Topics Quantum Electron 11: 690–712.

Lo C Y, Huang K Y, Chen J C, Tu S Y, Huang S L (2004) Glass-clad Cr4þ: YAG crystal fiber for the generation of super wideband amplified spontaneous emission: Opt. Lett. 29: 439–441.

Alcock A J (2005) Ultrashort pulse Cr4þ: YAG laser for high precision infrared frequency interval measurements: Opt. Exp.13: 8837–8844.

Tang P (2013) Topological insulator: Bi2Te3 saturable absorber for the passive Q-switching operation of an in-band pumped 1645-nm Er:YAG ceramic laser: IEEE Photon. J. 5: 1500707.

Zhang X (2014) Widely tunable, narrow bandwidth polycrystalline ceramic Er: YAG laser with a volume Bragg grating: Opt. Exp. 22: 7154–7159.

Liu J (2013) Volume Bragg grating-based tunable Er,Yb fiber lasers covering the whole C- and L- band: IEEE Photon. Technol. Lett. 25: 1488–1491.

Wu B, Liu Y, Dai Z, Liu S (2007) Stable narrow linewidth Er-doped fiber laser at 1550 nm: Microwave: Opt. Technol. Lett. 49: 1453–1456.

Desmoulins S, Teodoro F D (2007) Watt-level, high-repetition-rate, mid-infrared pulses generated by wavelength conversion of an eye-safe fiber source: Opt. Lett. 32: 56–58.

Wang M, Zhu L, Chen W, Fan D (2012) Efficient all-solid-state mid-infrared optical parametric oscillator based on resonantly pumped 1.645 m Er:YAG laser: Opt. Lett. 37: 2682–2684.

Philippov V (2004) High-energy in-fiber pulse amplification for coherent lidar applications: Opt. Lett. 29: 2590–2592.

Ma J (2009) Experimental investigation of radiation effect on erbium–ytterbium co-doped fiber amplifier for space optical communication in low-dose radiation environment: Opt. Exp.17: 15 571–15 577.

Science and Technology Journal, Vol. 7 Issue: I ISSN: 2321-3388

In-vitro Evaluation of Actinobacteria for its Potential in Bio-control of Fungal Plant Pathogens

Zothanpuia*[1], W. Carrie[2], V.V. Leo[3], A.K. Passari[4] R. Lalmuanpuii[5] and B.P. Singh[6]
[1]Department of Biotechnology, Pachhunga University College,
College Veng, Aizawl, Mizoram–796005
[2,3,4,6]Department of Biotechnology, Mizoram University, Tanhril, Mizoram–796004
[5]Department of Botany, Mizoram University, Tanhril, Mizoram–796004
E-mail: *jpahnamte6@gmail.com

Abstract—Infections caused by fungal plant pathogens are recently recognized as a threat to food security worldwide and its control strategies need to be taken care where naturally synthesized fungicides such as those obtained from actinobacteria are becoming an area of great interest. A total of 68 isolates of actinobacteria were evaluated for their antagonistic potential against four fungal plant pathogens viz., *Fusarium oxysporum* CABI-293942, *Fusarium udum* MTCC-2755, *Fusarium proliferatum* MTCC-286 and *Fusarium graminearum* MTCC-1893 by dual culture *in-vitro* assay. It was found that 83.8% of the isolates showed inhibitory activity against at least one of the tested plant pathogens with the percentage of inhibition ranging from 20–87.2. Thirteen *Streptomyces* isolates and one *Nocardiposis* isolate exhibited inhibition activity against all the tested pathogens. Overall, this study gives a basic understanding of the potential aspect of freshwater sediments derived actinobacteria against fungal phytopathogens.

Keywords: Anti-fungal, Phyto-pathogens, *Nocardiopsis*, *Streptomyces*

INTRODUCTION

Fungal diseases are one of the most common problems to certain crops upon which humanity depends (Godfray *et al.* 2016) and compounds derived from actinobacteria represent a promising agent to tackle the problems (Wang *et al.* 2018; Qi *et al.* 2019). Actinobacteria are Gram +ve bacteria, ubiquitous in nature, typically soil dwellers (Goodfellow and Williams 1983), found commonly in freshwater ecosystems (Sibanda *et al.* 2010). Various habitats have been explored in search of actinobacteria and several useful compounds have been expansively reported from different ecosystems (Maldonado *et al.* 2005; Passari *et al.* 2015). However, there has been a significant decline in the rate of discovery of novel actinobacteria in recent years and there has been increasing isolation of known organisms besides re-isolation of known compounds (Zotchev 2012).

Mizoram, Northeast India, is a large bio-prospecting area identified as the Indo-Burma mega-biodiversity hotspot by Conservation International (Myers *et al.* 2000). All the lakes and rivers of Mizoram are freshwater (Zothanpuia *et al.* 2015). Few actinobacteriological research has been reported from Mizoram such as freshwater sediments derived actinobacteria for its potential as antimicrobial agent and secondary metabolites producer (Zothanpuia *et al.* 2018), endophytic actinobacteria as biologically active compounds and phytohormone producers (Passari *et al.* 2015) and plants growth promoters (Passari *et al.* 2016). Investigation on the antifungal potential of actinobacteria from freshwater sediments may give a basic understanding and will provide baseline data for further studies that are significant for biotechnological exploitation especially in the management of food security.

MATERIALS AND METHODS

Isolation and Characterization of Actinobacteria

Serial dilution and spread plate technique were used for the isolation actionobacteria from freshwater sediments of Tlawng river, Tuirial river and Tamdil lake (Yuan *et al.* 2014;

http://doi.org/10.22232/stj.2019.07.01.11

Zothanpuia *et al.* 2018). Seven different nutritional media were used for the isolation such as starch-casein agar (SCA), yeast-extract malt-extract agar (ISP2), Actinomycetes-isolation agar (AIA), Streptomyces agar (SA), glycerol-asparagine agar (ISP5), tyrosine-agar medium (ISP7), and tap-water yeast-extract agar (TW-YE), the isolated organisms were characterized as exactly reported in the previous studies (Zothanpuia *et al.* 2018).

SCREENING FOR ANTIFUNGAL ACTIVITY

The actinobacterial isolates were evaluated for their antagonistic potential against four fungal phytopathogens collected from microbial type culture collection (MTCC), Chandigarh, India *viz.*, *Fusarium oxysporum* CABI-293942, *Fusarium udum* MTCC-2755, *Fusarium proliferatum* MTCC-286 and *Fusarium graminearum* MTCC-1893 by dual culture *in-vitro* assay (Khamna *et al.* 2008). Colony growth inhibition (%) was calculated by using the formula: C - T/C × 100, where C is the colony growth of the fungal pathogen in control, and T is the colony growth of the fungal pathogen in presence of actinobacteria. All isolates were tested in triplicate and mean values were calculated.

RESULTS AND DISCUSSION

Actinobacteria remains an important source of important biologically active compounds effective against certain plant and animal diseases (Goodfellow and Fiedler 2010; Yuan *et al.* 2014). The present investigation isolated 68 actinobacteria from freshwater sediments of Mizoram, Northeast India; 30 isolates from Tamdil Lake, 19 from Tlawng River, 19 from Tuirial River, and were earlier discussed in the previous article (Figure 1) (Zothanpuia *et al.* 2018).

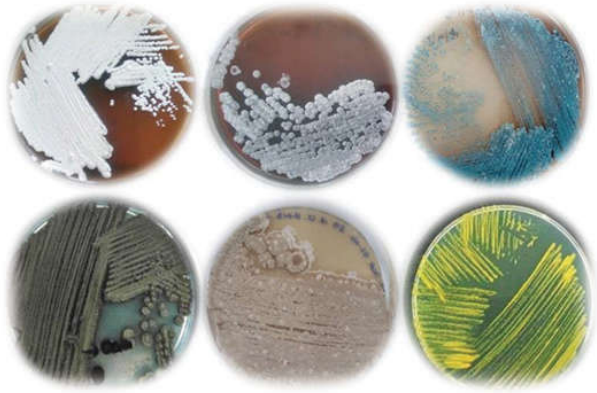

Fig. 1: Morphological Features of Actinobacteria Isolated from Freshwater Sediments

Streptomyces represent the most dominant genus among the isolated organisms (72%), followed by *Nocardiopsis*, *Saccharopolyspora, Rhodococcus, Prauserella, Amycolatopsis, Promicromonospora, Kocuria* and *Micrococcus,* the 16S rRNA gene sequences of all the isolates were deposited in NCBI GenBank database and accession numbers were given as cited (Zothanpuia *et al.* 2018). This study revealed that Lakes and rivers are important reservoirs of actinobacteria (Leiva *et al.*, 2004).

Aactinobacteria represents one of the most potential candidates to tackle the problems associated with the fungal plant pathogens that were largely reported as a potent biocontrol agent (Nafis *et al.* 2018; Qi *et al.* 2019). Diseases and the problems caused especially by the genus *Fusarium* were reported worldwide (Lamprecht *et al.* 2011) which include wilting, chlorosis, necrosis, premature leaf fall, stunting, etc. The antifungal activity was checked to understand the inhibition ability of the isolated actinobacteria against four fungal pathogens by dual culture *in-vitro* assay, which is a method widely used for preliminary screening (Zothanpuia *et al.* 2018a). The phytopathogens include *F. udum, F. oxysporum, F. graminearum* and *F. proliferatum* which were reported as pathogens maintained in the microbial type culture collection. From a total of 68 actinobacterial isolates tested, 83.8 % (n=57) of the isolates showed inhibition activity against at least one of the tested pathogens (Table 1). This justified the antifungal potential of actinobacteria from freshwater sediments supported by the findings of Rifaat (2003) that demonstrated the anti-mycotic activity of 114 freshwater actinobacteria from Nile River. 14 isolates *viz.* ***Streptomyces cyaneofuscatus*** DST15, ***Streptomyces*** sp. DST16, ***Streptomyces*** sp. DST25, *Saccharopolyspora* sp. DST31, *Streptomyces* ***griseoplanus*** DST53, ***Streptomyces*** sp. DST54, *Streptomyces* ***cyaneofuscatus*** DST64, *Streptomyces albidoflavus* DST71, ***Streptomyces*** sp. DST86, *Streptomyces albidoflavus* DST102, ***Streptomyces*** sp. DST104, *Nocardiopsis* sp. DST105, ***Streptomyces*** sp. DST116 and *Streptomyces* sp. DST119 showed activity against all the tested four *Fusarium* pathogens. Maximum inhibitory activity of the actinobacterial isolates was found against *F. graminearum* (46.4%) [Figure 2 (I)], followed by *F. proliferatum* (30.4%) [Figure 2 (II)], *F. oxysporum* (29.5%) [(Figure 2 (III)] and *Fusarium udum* (26.9%) [(Figure 2 (IV)] with percentage of inhibition ranging from 20-87.2. It was earlier reported the antifungal potential of two actinobacterial isolates ***Streptomyces*** sp. DST23 and ***Streptomyces parvus*** DST24 against *F. oxysporum, F. proliferatum*, and *F. oxy. ciceri* from freshwater Tuichang river (Zothanpuia *et al.* 2015)

which was in accordance with the reports of *Streptomyces* from Krishna river showing antibacterial and antifungal activity (Ellaiah *et al.* 2002). A similar investigation was also executed in Lake Baikal, the largest freshwater lake worldwide that described more than 70% of the isolates having an antifungal activity (Protasov *et al.* 2017). Among all the isolated organisms, *Streptomyces* sp. DST25 showed the maximum percentage of inhibition against *Fusarium Udum* (87.20%) which justified the potential of Actinobacteria especially *Streptomyces* in fighting the diseases caused by fungal pathogens supported by the findings of Nafis *et al.* (2018) and Qi *et al.* (2019). *Streptomyces* are among the largest contributors of antibiotics in the microbial world, widely distributed in soil and also colonize water and other natural environments (Goodfellow and Fiedler 2010). Most research including the present study is an early experimental stage but revealed the ability of *Streptomyces* in the control of fungal plant pathogens which was also supported by the review of Bubici (2018). Upon further investigations on the lead compounds, isolation, identification, and bio-formulation of freshwater sediments derived actinobacteria may help in the development of control strategies of fungal plant diseases which remains a great concern worldwide.

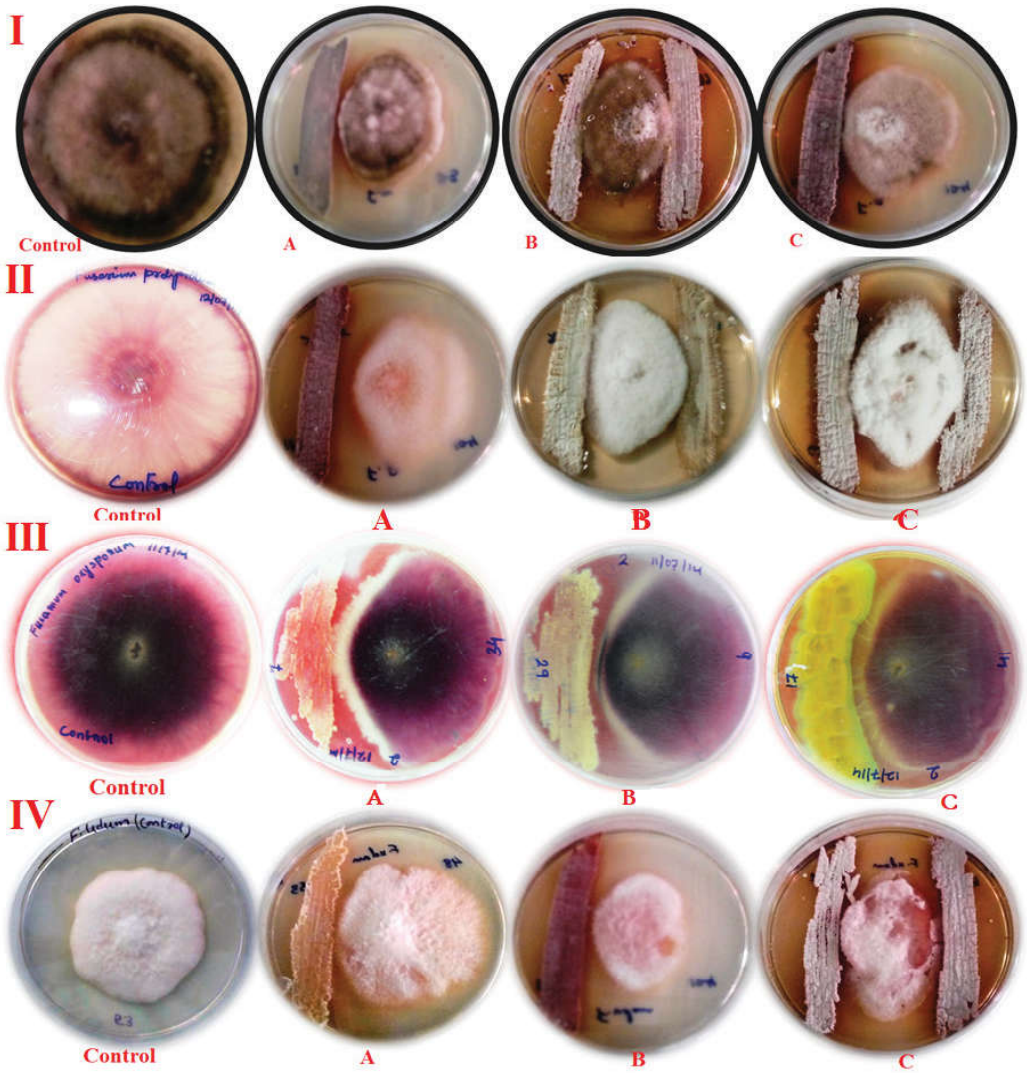

Fig. 2: (I) Antifungal Activity of Actinobacterial Isolates Against *F. graminearum* (II) *F. proliferatum* (III) *F. oxysporum* and (IV) *F. udum.* Control-Fungal Pathogens without Actinobacteria and A, B and C Denotes the Dual Culture; Growth of Pathogens Inhibited by Actinobacteria

Table 1: *In-vitro* Antagonistic Activity of Actinobacterial Isolates Against Four Fungal Phytopathogens

Sl. No.	Isolate Name	Isolate No.	Antifungal Properties C-T/CX100			
			F. udum	*F. oxysporum*	*F. graminearum*	*F. proliferatum*
1	*Streptomyces* sp.	DST13	-	48.50±0.29	20.40±0.65	46.00±0.30
2	***Streptomyces cyaneofuscatus***	**DST 15**	**74.40±0.16**	**54.60±0.42**	**42.00±0.25**	**55.00±0.63**
3	***Streptomyces* sp.**	DST 16	61.00±0.69	**45.50±0.44**	**52.00±0.69**	**62.20±0.33**
4	*Streptomyces* sp.	DST 17	59.00±0.03	-	61.29±0.98	-
5	*Streptomyces* sp.	DST 18	-	-	-	46.50±0.93
6	*Streptomyces* sp.	DST19	61.54±0.49	39.40±0.13	-	47.00±0.38
7	*Prauserella* sp.	DST22	48.71±0.14	-	35.50±0.41	37.84±0.29
8	*Streptomyces* sp.	DST23	-	73.68±0.01	-	57.89±0.36
9	Streptomyces parvus	DST24	-	50.68±0.00	-	67.12±0.18
10	***Streptomyces* sp.**	**DST25**	**87.20±0.37**	**69.69±0.41**	**54.84±0.84**	**72.97±0.075**
11	*Kocuria* sp.	DST27	73.68±0.01	45.20±0.09	-	48.65±0.53
12	Streptomyces cellulosae	DST28	43.59±0.46	-	32.25±0.69	-
13	Streptomyces intermedius	DST29	57.89±0.36	35.48±0.28	-	52.63±0.00
14	Streptomyces flavogriseus	DST30	-	48.49±0.24	-	-
15	***Saccharopolyspora* sp.**	**DST31**	**58.97±0.33**	**51.52±0.68**	**48.39±0.24**	**56.76±0.35**
16	*Streptomyces* sp.	DST35	-	-	23.60±0.29	-
17	*Rhodococus* sp.	DST38	-	54.55±0.5	-	45.95±0.25
18	Streptomyces pactum	DST44	-	-	22.58±0.64	-
19	Streptomyces koyangenesis	DST48	-	-	-	45.94±0.21
20	*Streptomyces* sp.	DST50	-	-	35.48±0.41	-
21	*Rhodococcus* sp.	DST51	54.00±0.85	45.45±0.49	41.94±0.38	-
22	Streptomyces flavogriseus	DST52	48.72±0.49	-	19.35±0.79	32.43±0.59
23	***Streptomyces griseoplanus***	**DST53**	**58.97±0.63**	**58.00±0.33**	**48.50±0.39**	**56.76±0.44**
24	***Streptomyces* sp.**	**DST54**	**58.97±0.98**	**57.58±0.62**	**48.40±1.39**	**56.76±0.44**
25	*Streptomyces* sp.	DST56	-	-	41.94±0.71	-
26	Streptomyces somaliensis	DST58	43.59±0.14	-	-	-
27	Streptomyces cyaneofuscatus	DST59	-	39.39±0.36	22.58±0.39	45.95±0.38
28	*Streptomyces* sp.	DST60	-	39.39±0.61	29.03±0.5	40.54±0.96

Table 1 (Contd.)...

...Table 1 (Contd.)

Sl. No.	Isolate Name	Isolate No.	Antifungal Properties C-T/CX100			
			F. udum	*F. oxysporum*	*F. graminearum*	*F. proliferatum*
29	*Streptomyces* sp.	DST63	59.00±0.12	-	48.39±0.56	59.46±0.99
30	***Streptomyces cyaneofuscatus***	**DST64**	**58.97±0.02**	**39.39±0.35**	**35.48±0.52**	**59.46±0.76**
31	Streptomyces lavendulae	DST65	-	-	54.84±0.28	-
32	Streptomyces olivaceus	DST66	-	-	35.48±0.16	-
33	Streptomyces griseoplanus	DST67	-	-	41.94±0.73	-
34	*Streptomyces* sp.	DST69	-	-	35.50±0.34	43.24±0.73
35	***Streptomyces albidoflavus***	**DST71**	**53.8±0.76**	**45.45±0.44**	**35.48±1.29**	**51.35±0.57**
36	Streptomyces rubiginosohelvolus	DST72	38.46±0.44	-	-	-
37	Streptomyces atratus	DST73	-	40.35±0.81	9.68±0.45	43.24±0.73
38	Streptomyces atroolivaceus	DST74	53.85±0.16	39.40±1.39	41.94±0.06	-
39	Streptomyces koyangenesis	DST75	61.53±0.53	42.50±0.43	51.61±0.56	-
40	***Streptomyces* sp.**	**DST86**	**66.67±0.37**	**39.39±0.61**	**41.93±0.38**	**37.84±0.48**
41	*Saccharopolyspora* sp.	DST89	53.85±0.09	45.45±0.55	35.48±0.62	-
42	Nocardiopsis	DST95	-	-	-	35.14±0.64
43	Streptomyces albidoflavus	DST96	-	37.88±0.25	-	-
44	*Saccharopolyspora* sp.	DST97	-	-	22.60±0.27	-
45	Streptomyces cyaneofuscatus	DST99	-	51.52±0.32	35.48±0.71	-
46	Streptomyces albidoflavus	DST100	-	-	41.94±0.37	-
47	***Streptomyces albidoflavus***	**DST102**	**49.52±0.39**	**51.52±0.25**	**48.45±0.17**	**40.54±0.71**
48	Streptomyces cyaneofuscatus	DST103	48.72±0.19	54.55±0.25	-	45.95±0.95
49	***Streptomyces* sp.**	**DST104**	**66.67±0.84**	**51.52±0.38**	**48.40±0.54**	**64.86±0.44**
50	***Nocardiopsis***	**DST105**	**60.26±0.26**	**51.52±0.29**	**49.50±0.77**	**45.95±0.42**
51	Streptomyces atroolivaceus	DST106	-	-	23.00±0.52	45.95±0.56
52	***Streptomyces* sp.**	**DST116**	**48.71±0.48**	**51.52±0.21**	**29.03±1.06**	**45.95±0.63**
53	Streptomyces griseus	DST118	-	39.39±0.69	-	43.24±0.42
54	***Streptomyces* sp.**	**DST119**	**49.00±0.39**	**45.45±0.52**	**51.61±0.39**	**56.76±0.55**
55	Streptomyces fulvissimus	DST120	50.50±0.48	39.39±0.43	-	51.35±0.57
56	*Streptomyces* sp.	DST142	42.50±0.19	-	-	-
57	*Nocardiopsis* sp.	DST145	28.00±0.08	-	-	-

CONCLUSION

In this study, sixty-eight actinobacteria were isolated from the sediments of three freshwater systems using serial dilution and spread plate technique, where the genus *Streptomyces* was found to be dominant. They were evaluated for their anti-fungal activity against four *Fusarium* plant pathogens collected from microbial type culture collection and found that 83.8% of the isolated organisms showed inhibitory activity against at least one of the tested plant pathogenic fungi and 13 *Streptomyces* isolates were found to inhibit all the tested pathogens which undoubtedly presented the anti-fungal potential of actinobacteria and might be a good candidate as biocontrol agent especially disease caused by *Fusarium* pathogens.

REFERENCES

Bubici G (2018) *Streptomyces* spp. as biocontrol agents against Fusarium species. CAB Reviews 13, No. 050 doi: 10.1079/PAVSNNR201813050

Ellaiah P, Adhinarayana K, Adhinarayana K, Saisha V, Madhavi S, Premkumar J (2002) Bioactive actinomycete from Krishna River sediments of Andhra Pradesh. Hindustan Antibiot Bull 44:8-16

Godfray HC, Mason-D'Croz D, & Robinson S (2016) Food system consequences of a fungal disease epidemic in a major crop. Philosophical transactions of the Royal Society of London. Series B, Biological sciences *371* (1709) 20150467. doi:10.1098/rstb.2015.0467

Goodfellow M, Fiedler HP (2010) A guide to successful bioprospecting: informed by actinobacterial systematics. Anton Van Leeuwen 98:119-142 doi: 10.1007/s10482-010-9460-2

Goodfellow M, Williams ST (1983) Ecology of actinomycetes. Annu Rev Microbiol 37:189-216

Khamna S, Yokota A, Lumyong S (2008) Actinomycetes isolated from medicinal plant rhizosphere soils: diversity and screening of antifungal compounds, indole-3-acetic acid and siderophore production. World J Microbiol Biotechnol 25:649

Lamprecht SC, Tewoldemedhin YT, Botha WJ, Calitz FJ (2011) *Fusarium graminearum* species complex associated with maize crowns and roots in the KwaZulu-Natal Province of South Africa. Plant Disease 95:1153-1158. DOI: 10.1094/PDIS-02-11-0083

Leiva S, Yanez M, Zaror L, Rodrıguez H, Garcıa-Quintana H (2004) Antimicrobial activity of actinomycetes isolated from aquatic environments in Southern Chile. Rev Med Chile 132:151-159

Maldonado LA, Stach JE, Pathom-aree W, Ward AC, Bull AT, Goodfellow M (2005) Diversity of cultivable Actinobacteria in geographically widespread marine sediments. Anton Van Leeuwen 87(1): 8-11

Myers N, Mittermeier RA, Mittermeier CG, da Fonseca GAB, Kent J (2000) Biodiversity hotspots for conservation priorities. Nature 403:853-858

Nafis A, Elhidar N., Oubaha B, Samri SE, Niedermeyer T, Ouhdouch Y,... Barakate M (2018) Screening for Non-polyenic Antifungal Produced by Actinobacteria from Moroccan Habitats: Assessment of Antimycin A19 Production by *Streptomyces albidoflavus* AS25. International J Mol Cell Med *7*(2): 133–145 doi:10.22088/IJMCM.BUMS.7.2.133

Passari AK, Chandra P, Zothanpuia, Mishra VK, Leo VV, Gupta VK, Kumar B, Singh BP (2016) Detection of biosynthetic gene and phytohormone production by endophytic actinobacteria associated with *Solanum lycopersicum* and their plant-growth promoting effect. Res Microbiol 167:692-705

Passari AK, Mishra VK, Gupta VK, Yadav MK, Saikia R, Singh BP (2015) *In-vitro* and *in-vivo* plant growth promoting activities and DNA fingerprinting of antagonistic endophytic actinobacteria associates with medicinal plants. Plos One doi:10.1371/journal.pone.0139468

Protasov ES, Axenov-Gribanov DV, Rebets YV, Voytsekhovskaya IV, Tokovenko BT, Shatilina ZM, Luzhetskyy AN, Timofeyev MA (2017) The diversity and antibiotic properties of actinobacteria associated with endemic deepwater amphipods of Lake Baikal. Anton van Leeuwen 110:1593

Qi D, Zou L, Zhou D, Chen Y, Gao Z, Feng R, Zhang M, Li K, Xie J and Wang W (2019) Taxonomy and Broad-Spectrum Antifungal Activity of *Streptomyces* sp. SCA3-4 Isolated From Rhizosphere Soil of *Opuntia stricta*. *Front Microbiol* 10:1390. doi: 10.3389/fmicb.2019.01390

Qi D, Zou L, Zhou D, Chen Y, Gao Z, Feng R, Zhang M, Li K, Xie J, Wang W (2019) Taxonomy and Broad-Spectrum Antifungal Activity of *Streptomyces* sp. SCA3-4 Isolated From Rhizosphere Soil of *Opuntia stricta*. *Front Microbiol.* 10:1390. doi: 10.3389/fmicb.2019.01390

Rifaat HM (2003) The biodiversity of actinomycetes in the river Nile exhibiting antifungal activity J Mediterr Ecol 4:5-7

Sibanda T, Mabinya LV, Mazomba N, Akinpelu DA, Bernard K, Olaniran AO, Okoh AH (2010) Antibiotic producing potentials of three freshwater actinomycetes isolated from the Eastern Cape Province of South Africa. J Mol Sci 11:2612-2323

Wang X, Zhang M, Gao J, Pu T, Bilal M, Wang Y, Zhang X (2018) Antifungal activity screening of soil actinobacteria isolated from Inner Mongolia, China. Biol Control 127:78–84 https://doi.org/10.1016/j.biocontrol.2018.07.007

Yuan M, Yu Y, Li HR, Dong N, Zhang XH (2014) Phylogenetic diversity and biological activity of actinobacteria isolated from the Chukchi Shelf marine sediments in the Arctic Ocean. Mar Drugs 12:1281-97

Zotchev SB (2012) Marine actinomycetes as an emerging resource for the drug development pipelines. J Biotechnol 158:168-175

Zothanpuia P, Passari A, Singh BP (2015) Molecular characterization of actinomycetes isolated from Tuichang river and their biosynthetic potential. Sci Vis 15:136

Zothanpuia, Passari AK, Chandra P, Leo VV, Mishra VK, Kumar B & Singh BP (2018) Bioprospection of actinobacteria derived from freshwater sediments for their potential to produce antimicrobial compounds. *Microb Cell Fact* 17:68 https://doi.org/10.1186/s12934-018-0912-0

Zothanpuia, Passari AK, Yadav MK, Singh BP (2018a) *In vitro* evaluation of antimicrobial activities and antibiotic susceptibility profiling of culturable actinobacteria from freshwater streams. Indian J Exp Biol 56:665-673

Science and Technology Journal, Vol. 7 Issue: I ISSN: 2321-3388

Calorimetric Computation of Enthalpy of Formation of Trisacetylacetonato Chromium(III) [$Cr(C_5H_7O_2)_3$(c)]

Madhvendu Pathak[1] and Raghvendu Pathak[2]*
[1]Department of Chemistry, Lunglei Government College, Lunglei–796701, Mizoram, India
[2]Department of Chemistry, Pachhunga University College, Aizawl–796001, Mizoram, India
E-mail: *rppuc41@yahoo.com

Abstract—From thermochemical studies of organometallic compounds, a host of thermodynamic parameters viz., heat capacity, entropy, Gibbs energy etc., can be evaluated. The present communication deals with the evaluation of enthalpy of combustion and thereby estimation of enthalpy of formation of crystalline trisacetylacetonato chromium(III) [Cr $(C_5H_7O_2)_3$ (c)] or [Cr $(acac)_3$ (c)] bomb-calorimetrically. The enthalpy of combustion (Δ_cH) and enthalpy of formation (Δ_fH°) values have been evaluated to be –7997·16 ± 10 k J mol^{-1} and –1470·315 ± 15 kJ mol^{-1} respectively. Experimental data obtained are in good agreement with one another.

Keywords: Calorimetric Computation, Organometallic Compounds, Combustion Enthalpy, Trisacetylacetonato Chromium (III)

INTRODUCTION

Thermochemical studies of organometallic compounds of s, p, d and f block elements have evoked a lot of interest among the researchers of various fields since long as they provide a lot of physico-chemical data for scientists to deal with (Cavell *et al.,* 1977, Lalancette *et al.,* 2018, Ismail 1991, Semyannikov *et al.,* 2005, Pathak 2016, da Silva *et al.,* 2011, Thakur *et al.,* 1995, da Silva *et al.,* 1988, Thakur *et al.,* 1992, Melia *et al.,* 1968) which can be applied in various fields ranging from material chemistry to energetic and from environmental chemistry to biochemistry. Available literature also buttresses such facts. Quantitative measurements of enthalpy changes involving various physico-chemical and biological processes are tedious tasks and usually done through the help of various types of calorimeters (Ribeiro da Silva 2010) or otherwise. The data so obtained as a consequence of such thermochemical investigations by several investigators are, therefore, of much empirical importance. The present paper deals with the bomb- calorimetric evaluation of enthalpy of combustion and thereby estimation of enthalpy of formation of trisacety lacetonatochromium(III) [Cr $(C_5H_7O_2)_3$ (c)].

EXPERIMENTAL

Preparation of trisacetylacetonato chromium(III) [Cr $(C_5H_7O_2)_3$ (c)]:

Trisacetylacetonato chromium(III) was prepared by adding 5g of chromium(III) oxide [CrO_3 (s), Merck grade] gradually in very small amounts to about 25g of acetyacetone (b.p. 137–140°C) with constant stirring until the exothermicity of the reaction subsided and the solution turned violet. Stirring continued for another 10 minutes when 5 ml of C_2H_5OH was added. The solution was heated over a steam bath for about 4 hours and then allowed to cool in a freezer for about an hour when dark pink solids separated out. After aqueous-washing of the precipitate (ppt) several times, it was recrystallised in minimum volume of benzene with the addition of small amount of light petroleum (b.p. 40 –60°C). It was then cooled in a freezer for an hour whereby shining pink crystals of the compound separated out. It was then filtered and dried in vacuum (m.p. 215°C). The said compound was analysed for chromium. (Found: Cr = 15%; calculated for Cr $(C_5H_7O_2)_3$; 14·9%. It may be sublimed without any residue. However, preparation of the said compound as reported by few other

http://doi.org/10.22232/stj.2019.07.01.12

investigators is also given here (Fernelius *et al.,* 1957, Chaudhuri, *et al.,* 1982). The compound is usually prepared by the action of acetylacetone (Hacac) on Chromium (III) oxide (Fernelius *et al.,* 1957)

$$Cr_2O_3 + 6\ Hacac \rightarrow 2\ Cr(acac)_3 + 3\ H_2O$$

Derived from gum benzoin and used as food preservatives, benzoic acid is a colourless crystalline solid occurring naturally in many plants (Qualley *et al.,* 2012) and fruits including berries (~0.05%) and serves as an intermediate in the biosynthesis of many secondary metabolites. Benzoic acid usually contains phthalic acid and benzylbenzoate as impurities, hence for calibration of the bomb calorimeter extra pure benzoic acid usually called certified grade pure benzoic acid is utilized**.** It is usually a stable compound and relatively non-toxic.

'Toshniwal' static oxygen bomb calorimeter having capacity of 303 ml and which can withstand a pressure of 200 atm. was used in the present work. The mean heat capacity of the bomb calorimeter was determined by burning a certified grade pure benzoic acid and it was found to be 10550 ± 10 $J°C^{-1}g^{-1}$.

The problems of not using differential scanning calorimetry (DSC) in the present work were manifold. First of all the reference sample should have a well**-**defined heat capacity over the range of temperatures to be scanned and secondly either the power supply remains constant throughout or the heat flux remains constant throughout during scanning of the sample, which are difficult to control**.** Moreover, due to a combination of relatively poor sensitivity, slower than normal scan rates (typically 2–3°C/min, due to much heavier crucible) and unknown activation energy, it makes imperative to deduct about 75–100°C from the initial start of the observed exotherm to suggest a maximal temperature for the material (Wikipedia). Moreover, DSC curves reveal considerably less energy release than the true reaction-heats of the oxidation of organic materials which may be due to the low oxidation rate of some primary volatile products, especially carbon monoxide, inevitably forming during the oxidation of organic and carbonaceous materials at the temperatures of DSC experiments (Várhegyi *et al.,* 1986).

RESULTS AND DISCUSSION

Recording temperature rise by burning a weighed amount of the sample in a specified amount of water in presence of excess of O_2 (g) under pressure, the enthalpy of combustion (Δ_cH) of the compound was evaluated using the relation

$$\Delta_cH = M\ W\ \Delta t \qquad [1]$$

where, M is the formula weight of the crystalline complex, W the water equivalent of the bomb calorimeter and Δt, the temperature rise per gram of the sample due to calorimetric combustion. Mean water equivalent of the bomb calorimeter was obtained experimentally by burning certified grade benzoic acid and was found to be 10550 ± 10 $J°C^{-1}g^{-1}$. The molar enthalpy of combustion of the sample was given in table 1.

By substituting the supplementary thermochemical data from the standard reference sources (Wagman *et al.,* 1965, Weast 1986), the standard enthalpies of formation of [Cr $(C_5H_7O_2)_3$ (c)] was computed using the relation $\Delta_cH = \Sigma\ \Delta_fH°$ (products) $- \Sigma\ \Delta_fH°$ (reactants). The auxiliary enthalpy of formation data for products like metal oxides, CO_2 (g) and H_2O (l) have also been taken from standard reference sources (Codata 1978, Weast 1978 Lange's Handbook of Chemistry. (1973).

Table 1: Molar Enthalpy of Combustion (Δ_cH) of [Cr $(C_5H_7O_2)_3$ (c)]

(Molar mass = 349·32 g mol^{-1})

Experiment No.	1	2	3
Wt. of the sample (g)	0·3385	0·5435	0·6324
Temperature rise (°C)	0·737	1·179	1·368
Temp. rise per g of the sample Δt (°C)	2·180	2·169	2·163

Mean temperature rise per gm of the sample, Δt = 2·170

Now, $-\Delta_cH = M \times W \times \Delta t$

$= 349{\cdot}32 \times 10550 \times 2{\cdot}170$

$= 7997157{\cdot}42\ J\ mol^{-1}$

$= 7997.16\ kJ\ mol^{-1}$

Therefore, $\Delta_cH = -7997{\cdot}16 \pm 10\ k\ J\ mol^{-1}$

where, M = molar mass of the sample, W = water equivalent of the bomb calorimeter = 10550 $J°C^{-1}g^{-1}$, and Δt = mean temperature rise per gm combustion of the sample = 2.170 °C.

Computation of standard enthalpy of formation ($\Delta_fH°$) of [$Cr(C_5H_7O_2)_3$(c)]:

By substituting supplementary data from literatures [17–18], standard enthalpy of formation of trisacetylaceton atochromium(III) [Cr $(C_5H_7O_2)_3$ (c)] was computed.

$Cr(C_5H_7O_2)_3(c) + O_2$ (g) (excess) = ½ Cr_2O_3 (c) + 15CO_2 (g) + 10·5 H_2O (l) $\Delta H = \Delta_c H$

$\Delta_c H = \Sigma\, \Delta_f H°$ (products) – $\Sigma\, \Delta_f H°$ (reactants)

$\Delta_c H$ = ½ $\Delta_f H° Cr_2O_3$ (c) + 15 $\Delta_f H° CO_2$ (g) + 10·5 $\Delta_f H° 10H_2O$ (l) – $\Delta_f H° Cr(C_5H_7O_2)_3$(c)

Therefore,

$\Delta_f H° Cr(C_5H_7O_2)_3(c)$ = ½ $\Delta_f H° Cr_2O_3$ (c) + 15 $\Delta_f H° CO_2$ (g) + 10·5 $\Delta_f H° 10H_2O$ (l) – $\Delta_c H$

= ½ × (–1128·15 + 15 × (–393·5) + 10.5 × (–285·8)

– (–7997·16)

= –564·075 –5902·5 –3000·9 + 7997·16

= –9467·475 + 7997·16

= –1470·315 ± 15 kJmol^{-1}.

The present value of –1470·315 ± 15 kJmol^{-1} was compared with those obtained by Hill and Irving {$\Delta H°_f$ = –366·48 ± 0·67 kcal/mole} (Hill *et al.,*1967) and Silva and Ferrao, {–1564·8 ± 8·9 kJmol^{-1}} (da Silva *at el.,* 1988). However, Melia and Merrifield (Melia *at el.,* 1968) have calculated the standard heat of formation and entropy of gaseous tris (acetylacetonato) chromium (III) at 298·16°K and 1 atmosphere pressure to be $\Delta H_f°$ = –344·7 ± 1·0 k cal mole^{-1} and $S°_{298·16} – S_0°$ = 142·4 ± 1·0 cal deg $^{-1}$ mole^{-1} respectively.

CONCLUSION

Oxygen consumption calorimetry is used to measure the heat of combustion of the pyrolysis products and the maximum amount of heat released per unit mass per degree of temperature (Jg^{-1}K^{-1}) is a material property that appears to be a good indicator of flammability or efficiency of the process (Lyon *et al.,* 2004). As we all know, chemical, physical and biological changes are often accompanied by energy transfer. The high negative value of $\Delta_f H°$ of [$Cr(C_5H_7O_2)_3$(c)] indicates the exothermicity of the reaction and stability of the compound. The enthalpy of formation a compound can be correlated to the efficiency of a heat engine. The higher the negative value of standard enthalpy of formation of a compound, the more heat will be given off, and therefore the more fuel-efficient the compound would be.

REFERENCES

Cavell KJ, Pilcher G (1977) Enthalpies of combustion of tris-(acetylacetonato) derivatives of aluminium(III), gallium(III) and indium(III). J. Chem. Soc., Faraday Trans. 1. 73: 1590–1594.

Chaudhuri MK, Roy N, Khathing DT (1982) Synthesis of Tris (Acetylacetonato) Cheomium (III), $Cr(C_5H_7O_2)_3$. J. Synth. React. Inorg. Metal-Org. Chem., 12: 715–720.

Codata (1978) The International Council of Scientific Union (ICSU) Committee on Data for Science and Technology. 10: 903–1010.

Fernelius WC, Blanch JE, Bryant, BE, Terada K, Drago RS, Stille JK (1957) Chromium(III) Acetylacetonate. In: Inorganic Syntheses (ed) Therald Moeller, McGraw-Hill Book Company, Inc. NY, 5: 130-131.

Hill JO, Irving RJ (1967) Standard heat of formation of tris (acetylacetonato) chromium(III) at 25° and the metal-oxygen bond energy. J. Chem. Soc. A. 1413-1416.

Ismail HM (1991) A thermoanalytic study of metal acetylacetonates. J. Analy. Appl. Pyrol. 21: 315-326.

Lalancette R, Syzdek D, Grebowicz J, Arslan E (2018) The thermal decomposition and analyses of metal tris-acetylacetonates: Free radical formation from Al, Cr, Mn, Fe and Co complexes. J. Therm. Analy. Calorim. 135 3463-3470.

Lange's Handbook of Chemistry (1973) Dean, JA, (ed), 11th Edition, McGraw Hill Book, NY., 1600.

Lyon RE, Walters RN (2004) Pyrolysis combustion flow calorimetry. J. Analy. Appl. Pyrol. 71: 27-46.

Melia TP, Merrifield R (1968) Thermal properties of transition-metal compounds. Part I. Heat capacity, entropy, and standard heat of formation of tris(acetylacetonato)chromium(III). J. Chem. Soc. A. 2819-2820.

Pathak R (2016) Thermochemical studies of thorium(IV) and zirconium(IV) tetrabenzoates. Sci. Vis. 16: 10-15.

Qualley AV, Widhalm JR, Adebesin F, Kish CM Dudareva N (2012) Completion of the core β-oxidative pathway of benzoic acid biosynthesis in plants, Proceedings of the National Academy of Sciences, 109: 16383-16388.

Retrieved January 3, 2020, from https:// en. wikipedia. org/ wiki/ Differential scanning calorimetry

Ribeiro da Silva MAV, Ferrao MLCCH (2011) Standard enthalpies of formation of tris(β-diketonate) manganese(III) complexes: the mean (Mn-O) bond-dissociation enthalpies. Canad. J. Chem. 66: 651-654.

Ribeiro da Silva MAV, Ferrao MLCCH (1988) Energetics of metal-oxygen bonds in metal complexes of β-diketones. Pure & Appl. Chem. 60: 1225-1234.

Ribeiro da Silva MAV (2010) The development of calorimetry and thermochemistry in Portugal. J. Therm. Anal. Calorim. 100: 373-374.

Semyannikov PP, Igumenov IK, Trubin SV, Chusova TP, Semenova ZI (2005) Thermodynamics of chromium acetylacetonate sublimation. Thermochim. Acta 432: 91-98.

Thakur S, Kumar A, Pathak R. (1995) Standard Heats of Formation of Uranyl (II) and Thorium (IV) Oxinates. J. Indian Chem. Soc. 72: 823-24.

Thakur L, Thakur S, Pathak M, Jha RN (1992) Thermochemical Studies of diaquodipropionatodioxouranium (VI). J. Indian Council of Chemists. VIII: 25-26.

Várhegyi G, Szabó P, Till F (1986) Problems in the DSC and DTA study of the burning properties of fuels and other organic materials, Thermochim. Acta, 106:191-199.

Wagman DD, Evans WH, Halow I, Parker VB, Baitey SM, Schumm RH, Churney KL (1965).'Selected Values of Chemical Thermodynamic Properties', NBS, Technical Notes, Washington D.C., 1-132.

Weast RC (1986) Handbook of Chemistry and Physics, 61st Edition, CRC Press, Florida

Weast RC (1978) Handbook of Chemistry and Physics, 59th Edition, CRC Press, Florida, 1- 2488.

Science and Technology Journal, Vol. 7 Issue: I ISSN: 2321-3388

Common Fixed Point Theorems on Multi-Valued Mappings in 2-Metric Space using T-Hardy Rogers Contraction Condition and F-Contraction

Dinanath Barman[1], Krishnadhan Sarkar[2]* and Kalishankar Tiwary[3]
[1,3]Department of Mathematics, Raiganj University, Raiganj, West Bengal, India–733134
[2]Department of Mathematics, Raniganj Girls College, Raniganj, Paschim Bardhaman, West Bengal, India–733158
E-mail: [1]dinanathbarman85@gmail.com, [2]*sarkarkrishnadhan@gmail.com, [3]tiwarykalishankar@yahoo.com

Abstract—In this paper we have introduced multi-valued 2-metrices on 2-metric space and have proved some fixed point theorems for multi-valued mappings on 2-metric space using T-Hardy and Rogers type contraction condition. We have also used F-contraction conditions, occasionally weakly compatible to prove the theorems.

Keywords: Weakly Compatible, CLRf-property, OWC-property, D-mapping

Mathematics Subject Classification: 47H10, 54H25

INTODUCTION

IIn 1922, Banach proved a fixed point theorem which is also known as Banach contraction theorem.This theorem has been generalized by various research workers in different spaces for point valued as well as multi valued mappings. It is Nadler (1969) who introduced the notion of multi-valued contraction mapping on metric spaces. Thereafter Joseph and Ramganesh(2013), Abdou(2016) have also worked on multi-valued mappings on metric spaces. Also Cho(2016), Jinakul et al. (2017) have worked on multi-valued mappings in b-metric spaces. Abdou (2016) introduced the notion CLRf –property and OWC-property. Djoudi and Khemis(2005) have introduced D -mappings in metric spaces. Gahler(1963) introduced the concept of 2-metric spaces. Abd El-Monsef et al. (2007) have worked on 2-metric spaces using multi-valued mappings and have defined δ. Various authors have used the notion of D, H, δ to obtain their results in metric spaces. In the present role we have used these symbols with their usual meanings to obtain our results in 2-metric space.

DEFINITIONS

Definition 2.1 [9]: Let X be a non-empty set and d: X × X × X ⟶ [0, ∞) be a real valued function which satisfy the following conditions:

1. For every distinct points x, y there is a point z in X such that d(x, y, z) ≠ 0;
2. d(x, y, z) = 0 if any two of three of x, y, z is equal;
3. d(x, y, z) = d(p(x, y, z)) for all x, y, z∈X and for all permutations p(x, y, z) of x, y, z;
4. d(x, y, z) ≤ d(x, y,w) + d(x,w, z) + d(w, y, z) for all x, y, z, w ∈ X.

Then d is called a 2-metric and (X, d) is called a 2-metric space.

We write X a 2-metric space unless otherwise stated. Here by CB(X) we mean the class of all nonempty closed and bounded subsets of X, by 2^X we mean the class of all non-empty compact subsets of X and by B(X) we mean the class of all bounded subsets of X.

http://doi.org/10.22232/stj.2019.07.01.13

For all A, B, C in B(X) we define the following definitions:

Definition 2.2 [2]**.** Let $\delta : X\times X \times X \longrightarrow [0,\infty)$ be defined as $\delta(A, B, C) = \sup\{ d(a, b, c) : a \in A, b \in B, c \in C\}$.

If $A = \{a\}$ we write $\delta(A, B,C) = \delta(a, B,C)$.

If $A = \{a\}$, $B = \{b\}$ then we write $\delta(A, B, C) = \delta(a, b, C)$.

If $A = \{a\}$, $B = \{b\}$, $C = \{c\}$ then we write $\delta(A, B, C) = \delta(a, b, c) = d(a, b, c)$.

From the definition of δ it follows that for A, B, C, E ∈ B(X):

1. $\delta(A, B, C) \geq 0$;
2. $\delta(A, B, C) = 0$ if at least two of A, B, C consist of equal single point;
3. $\delta(A, B, C) = \delta(p(A, B, C))$ where p(A, B, C) is the permutation of A, B, C;
4. $\delta(A, B, C) \leq \delta(A, B, E) + \delta(A, E, C) + \delta(E, B, C)$.

With this definition we say that δ is a multi-valued 2- metric on B(X).

Clearly, $d \leq \delta$.

We now introduce the following definition.

Definition 2.3: For all A, B, C ∈ CB(X), let us consider a function $D: X \times X \times X \longrightarrow [0, \infty)$ defined by

$D(A, B, C) = \inf \{d(a, b, c) : a \in A, b \in B, c \in C\}$.

If $A = \{a\}$, we write $D(A, B, C) = D(a, B, C) = \inf\{d(a, b, c) : b \in B, c \in C\}$.

If $A = \{a\}$, $B = \{b\}$ then we write $D(A, B, C) = D(a, b, C) = \inf\{d(a, b, c) : c \in C\}$.

If $A = \{a\}$, $B = \{b\}$, $C = \{c\}$ then we write $D(A, B, C) = D(a, b, c) = d(a, b, c)$.

From the definition of D it follows that for A, B, C, E ∈ CB(X):

1. $D(A, B, C) \geq 0$;
2. $D(A, B, C) = 0$ if at least two of A, B, C consist of equal single point;
3. $D(A, B, C) = D(p(A, B, C))$ where p(A, B, C) is the permutation of A, B, C;
4. $D(A, B, C) \leq D(A,B,E) + D(A,E,C) + D(E,B,C)$.

With this definition we say that D is another multi-valued 2-metric on CB(X).

From the definition it is clear that $D \leq d$.

NOTE 2.1: In case of A, B, C ∈ B(X) then the condition i) would be D(A, B, C) = 0 if at least two of A, B, C consist of equal single point or they have a non-empty intersection.

NOTE 2.2: From the definitions of δ, D and d, it is clear that $D \leq d \leq \delta$.

Again we are going to introduce another function H(A, B, C).

Definition 2.4: Let A, B, C in CB(X) and be pairwise disjoint. We define a function H(A, B, C) where $H(A, B, C) : X \times X \times X \longrightarrow [0,\infty)$ defined by

$H(A, B, C) = \max\{\sup_{a\in A} D(a, B, C), \{\sup_{b\in B} D(b, C, A), \sup_{c\in C} D(c, A, B)\}$.

Now,

1. Clearly $H(A, B, C) \geq 0$ and $H(A, B, C) = 0$ i.e., $\max\{\sup_{a\in A} D(a, B, C), \{\sup_{b\in B} D(b, C, A), \sup_{c\in C} D(c, A, B)\} = 0$ implies, $\sup_{a\in A} D(a, B, C) = 0$, $\sup_{b\in B} D(b, C, A) = 0$, $\sup_{c\in C} D(c, A, B) = 0$.

   Again, $\sup_{a\in A} D(a, B, C) = 0$ implies, $\sup_{a\in A} \{\inf\{d(a, b,c): b \in B, c \in C\}\} = 0$ i.e., $\inf d(a, b, c) = 0$, for all $a \in A$ i.e., $d(a, b, c) = 0$, for all $a \in A$ i.e., $b = c$ i.e., $B = C$. Similarly, we can show that $\sup_{b\in B} D(b, C, A) = 0$ implies, $A = C$, and $\sup_{c\in C} D(c, A, B) = 0$ implies, $A = B$. Thus $H(A, B, C) = 0$ if two of A, B, C are equal.
2. From definition it is clear that $H(A, B, C) = H(p(A, B, C))$ where p(A, B, C) is the permutation of A, B, C;
3. Since d is a 2-metric on X we have for all $a \in A, b \in B, c \in C, e \in E$ $d(a, b, c) \leq d(a, b, e) + d(a, e, c) + d(e, b, c)$

Taking infimum on the both sides we have

$\inf d(a, b, c) \leq \inf d(a, b, e) + \inf d(a, e, c) + \inf d(e, b, c)$ for all $a \in A, b \in B, c \in C, e \in E$, which implies, $\sup_{a\in A} \{\inf\{d(a, b, c): b \in B, c \in C\}\} \leq \sup_{a\in A} \{\inf\{d(a, b, e) : b \in B, e \in E\}\} + \sup_{a\in A} \{\inf\{d(a, e, c) : e \in E, c \in C\}\} + \sup_{e\in E} \{\inf\{d(e, b, c) : b \in B, c \in C\}\}$ implies, $\sup_{a\in A} D(a, B, C) \leq \sup_{a\in A} D(a, B, E) + \sup_{a\in A} D(a, E, C) + \sup_{e\in E} D(e, B, C)$ Similarly, we can show that $\sup_{b\in B} D(b , C, A) \leq \sup_{b\in B} D(b, C, E) + \sup_{b\in B} D(b, E, A) + \sup_{e\in E} D(e, C, A)$ and $\sup_{c\in C} D(c, A, B) \leq \sup_{c\in C} D(c, A, E) + \sup_{c\in C} D(c, E, B) + \sup_{e\in E} D(e, A, B)$.

Therefore, $\max\{\sup_{a\in A} D(A, B, C); \sup_{b\in B} D(B, C, A); \sup_{c\in c} D(C, A, B)\} \leq \max\{\sup_{a\in A} D(a, B, E); \sup_{b\in B} D(b, E, A); \sup_{e\in E} D(e, A, B)\} + \max\{ \sup_{a\in A} D(a, E, C); \sup_{e\in E} D(e, C, A); \sup_{c\in c} D(c, A, E)\} + \max\{\sup_{e\in E} D(e, B, C); \sup_{b\in B} D(b, C, E); \sup_{c\in c} D(c, E, B)\}$ implies, $H(A, B, C) \leq H(A, B, E) + H(A, E, C) + H(E, B, C)$.

Therefore H is a 2-metric called 2-Hausdorff metric and (CB(X), H) is called 2-Hausdoff metric space. From the definition we have D ≤ H.

Lemma 21: If A, B, C ∈ CB(X), then H ≤ δ.

Proof. We know D(A, B, C) = inf{d(a, b, c) : a ∈ A, b ∈ B, ∈ ∈ C} and H(A, B, C) = max{$\sup_{a\in A}$ D(a, B, C); $\sup_{b\in B}$ D(b, C, A); $\sup_{c\in C}$ D(c, A, B)}.

CASE I: If A = {a}, B = {b}, C = {c} then D(a, b, c) = D(b, c, a) = D(c, a, b) = d(a, b, c) = δ(A, B, C) and so H(A, B, C) = δ (A, B, C).

CASE II: If A = {a}, B = {b} then D(a, b, C) = inf{d(a, b, c): c ∈ C} ≤ inf d(a, b, c) ≤ $\sup_{c\in C}$ d(a, b, c) = δ (A, B, C) implies, $\sup_{c\in C}$ D(A, B, C) = $\sup_{c\in C}$ D(a, b, C) ≤ δ(A, B, C) So H(A, B, C) ≤ δ(A, B, C).

CASE III: If A = {a}, then D(a, B, C) = inf{d(a, b, c) : b ∈ B, c ∈ C} and suppose H(A, B, C) = $\sup_{a\in A}$ D(a, B, C).

Since, inf{d(a, b, c) : b ∈ B, c ∈ C}≤ {d(a, b, c) : b ∈ B, c ∈ C} ≤ sup{d(a, b, c) : b ∈ B, c ∈ C} implies, D(a, B, C) ≤ δ (a, B,C) implies, $\sup_{a\in A}$ D(a, B,C) ≤ δ(a, B, C) i.e., H(A, B, C) ≤ δ(A, B, C).

CASE IV: If A, B, C are not single point sets, then inf{$d_{a\in A}$ (a, B, C) : b∈B, c ∈ C} ≤ inf{d(a, B, C) : b ∈ B, c ∈ C} i.e., D(A, B, C) = $D_{a\in A}$ (a, B, C) ≤ δ (A, B, C) implies, {$\sup_{a\in A}$ D(,B,C) ≤ δ(A, B, C). Similarly $\sup_{b\in B}$ D(b, C, A) ≤ δ (B, C, A) and $\sup_{c\in C}$ D(c, A, B) ≤ δ (C, A, B).

Thus H(A, B, C) ≤ δ (A, B, C).

Nadler(1969) has defined multi-valued contraction mapping on metric space. We are to define it in 2-metric spaces.

Definition 2.5. A sequence $\{x_n\}$ is said to converge to x in (X, D) if $\lim_{n\to\infty} x_n = x$ i.e., $\lim_{n\to\infty} D(x_n, x, a) = 0$.

Definition 2.6. Let (X, d) be a complete 2-metric space and F: X→CB(X). Then F is said to be a multi-valued contraction mapping on 2-metric space if there exists a constant α where 0 < α < 1 such that H(F(x), F(y), a) ≤ α d(x, y, a).

Definition 2.7. [Jungck(1986)]. Let (X, d) be a 2-metric space. A single valued mapping f : X → X and a multi-valued mapping S : X → CB(X) are said to be weakly compatible if they commute at their coincidence points, i.e., if fSx = Sfx whenever fx ∈ Sx.

Definition 2.8. [Sintunavarat and Kumar (2011)]. Let (X, d) be a 2-metric space. Two mappings f, g: X → X are said to satisfy the common limit in the range of f with respect to g (shortly, the $(CLR)_f$ – property with respect to g) if there exists a sequence $\{x_n\}$ in X such that

$\lim_{n\to\infty} fx_n = \lim_{n\to\infty} gx_n = fu$, for some u in X.

We shall exhibit in the following example the existence of two mappings which satisfy CLR_f – property.

Example 2.1: Let X = R+ and d : X × X ×X → R_+ defined by d(x, y, a) = min{ |x-y|, |y-z|, |z-x| }. Then clearly (X, d) is 2-metric space. Let f; g : X → X be given by $fx = \frac{x}{k}$ and $gx = \frac{x}{m}$ where k ≠ m ∈ N for all x ∈ X. Consider the sequence $\{x_n\} = \left\{\frac{1}{n}\right\}$ for each n ∈ N. Clearly $\lim_{n\to\infty} fx_n = \lim_{n\to\infty} gx_n = f(0)$. Therefore f, g satisfies the $(CLR)_f$ – property with respect to g.

Definition 2.9. [1]: Let (X, d) be a 2-metric space. Two mappings f : X → X and S : X → CB(X) are said to be occasionally weakly compatible(shortly, (OWC)-property) if fSx ⊂ Sfx for some x ∈ X with fx ∈ Sx.

Definition 2.10. [8]: Let (X, d) be a 2-metric space. Then two mappings f : X → X and S : X → CB(X) are said to satisfy D-mapping if there exists a sequence $\{x_n\}$ in X such that $\lim_{n\to\infty} fx_n = z$ and $\lim_{n\to\infty} Sx_n = \{z\}$.

Example 2.2: Let X = [0, ∞) and F : X → B(X), f : X → X defined by Fx = [0, x^2] and $fx = \frac{x}{k}$; k ∈ N for all x ∈ X. Consider the sequence $\{x_n\} = \left\{\frac{1}{n}\right\}$ for all n ∈ N. Then clearly, $\lim_{n\to\infty} fx_n = 0$ and $\lim_{n\to\infty} fx_n = f\{0\}$.

Definition 2.11. Let (X, d) be a 2-metric space. A mapping T : X → X is said to be an F – contraction if there exists τ ∈ $\mathbf{R}_+$ and a function F ∈ **F** such that for all x, y ∈ X, d(Tx, Ty, a) > 0 implies, τ + F (d(Tx, Ty, a)) ≤ F (d(x, y, a)).

Definition 2.12. [Ahmad *et al.*, 2015] A function F: $\mathbf{R}_+ \to \mathbf{R}_+$ be such that for h > 1, F(hH(Tx, Ty, a)) ≤ F(H(Tx, Ty, a)). Then F is called a function continuous from right.

MAIN RESULTS

Nadler(1969) proved the following theorem:

Theorem: Let (X, d) be a complete metric space. If F: X → CB(X) is a multi-valued contraction mapping, then F has a fixed point.

We have generalized it to 2-metric space as below:

Theorem 3.1. If X is a complete 2-metric space and F: X → CB(X) is a multi-valued contraction mapping, then F has a fixed point in X.

Proof. Let x_0 be arbitrary. Since F is a multi-valued contraction mapping, there is a positive constant ε < 1 such that H(F(x), F(y), a) ≤ εd(x, y, a).

Now choose a point $x_1 \in F(x_0)$. Since $F(x_0)$ and $F(x_1)$ are in CB(X), for $x_1 \in F(x_0)$ there is a point $x_2 \in F(x_1)$ such that $d(x_1, x_2, a) \le H(F(x_0), F(x_1), a) + \varepsilon$ ...(2.1)

Again since $F(x_1)$, $F(x_2) \in CB(X)$ and $x_2 \in F(x_1)$ there is a point $x_3 \in F(x_2)$ such that $d(x_2, x_3, a) \le H(f(x_1), F(x_2), a) + \varepsilon^2$

Considering that way we can get a sequence $\{x_n\}$ in X such that $d(x_n, x_{n+1}, a) \le H(F(x_{n-1}), F(x_n), a) + \varepsilon^n$

Now

$$\begin{aligned} d(x_n, x_{n+1}, a) &\le H(F(x_{n-1}), F(x_n), a) + \varepsilon^n \\ &\le \varepsilon d(x_{n-1}, x_n, a) + \varepsilon^n \\ &\le \varepsilon(H(F(x_{n-2}), F(x_{n-1}), a) + \varepsilon^{n-1}) + \varepsilon^n \\ &= \varepsilon(H(F(x_{n-2}), F(x_{n-1}), a) + 2\,\varepsilon^n \\ &\le \varepsilon^2 d(x_{n-2}, x_{n-1}, a) + 2\,\varepsilon^n \\ &\;\;\vdots \\ &\le \varepsilon^n\, d(x_0, x_1, a) + n\,\varepsilon^n. \end{aligned}$$

Taking limit as n → ∞ on the both side of the above inequality we get $\lim_{n\to\infty} d(x_n, x_n + 1, a) = 0$ [as ε < 1]

So $\lim_{n\to\infty} d(x_n, x_m, x_{n-1}) = 0$.

Thus for $n \ge m \in \mathbf{N}$; $\lim_{n,m\to\infty} d(x_n, x_m, a) \le \lim_{n,m\to\infty} (d(x_n, x_m, x_{n-1}) + d(x_n, x_{n-1}, a) + d(x_{n-1}, x_m, a)) = \lim_{n,m\to\infty} d(x_{n-1}, x_m, a) \le \dots \le \lim_{n,m\to\infty} d(x_m, x_m, a) = 0$.

Therefore $\{x_n\}$ is a Cauchy sequence in X. Since X is complete, there exists an $x \in X$ such that $x_n \to x$ as $n \to \infty$. So $\{F(x_n)\}$ converges to F(x) and hence $x \in F(x)$. Therefore x is a fixed point of F in X.

Note 3.1: If A, B ∈ CB(X) and a ∈ A then from (3.1) of the above theorem we get b ∈ B such that d(a, b, x) ≤ H(A, B, x) + α, 0 < α < 1. ...(2.2)

Theorem 3.2. Let (X, d) be a 2-metric space. f, g : X → X and S, T : X → CB(X) satisfying the relation,

Hp(Sx, Ty, a)

$\le \alpha_1 d^p(fx, gy, a) + \alpha_2 \delta^p(fx, Ty, a) + \alpha_3 \delta^p(gy, Sx, a) + \alpha_4 \delta^p(gy, Ty, a) + \alpha_5 \delta^p(fx, Sx, a)$, where $p \ge 1$, $\alpha_i \ge 0$, i = 1, 2, 3, 4, 5 and $\sum_{i=1}^{5} \alpha_i < \frac{1}{n^p}$, n ∈ N. The pairs (S, f) and (T, g) satisfy OWC-property; f(X) and g(X) are closed. Then f, g, S and T have unique common fixed point in X.

Proof. Since the pair (S, f) and (T, g) satisfy OWC-property, there exist u, v ∈ X such that fu ∈ Su, fSu ⊂ Sfu, gv ∈ Tv, gTv ⊂ Tgv which implies, ffu ∈ Sfu and ggv ∈ Tgv.

Now we show that fu = gv. Let us suppose that fu ≠ gv. Then, $D^p(fu, gv, a) \le H^p(Su, Tv, a) \le \alpha_1 d^p(fu, gv, a) + \alpha_2 \delta^p(fu, Tv, a) + \alpha_3 \delta^p(gv, Su, a) + \alpha_4 \delta^p(gv, Tv, a) + \alpha_5 \delta^p(fu, Su, a) \le \alpha_1 dp(fu, gv, a) + \alpha_2 \delta^p(Su, Tv, a) + \alpha_3 \delta^p(Tv, Su, a) + \alpha_4 \delta^p(Tv, Tv, a) + \alpha_5 \delta^p(Su, Su, a) \le (\alpha_1 + \alpha_2 + \alpha_3)\, \delta^p(Su, Tv, a)$ ...(2.3)

Since D ≤ δ; D, δ ∈ R_+ = [0, ∞) there exists n ∈ N such that δ ≤ nD [by Archimedean Property], i.e., $\delta^p(Su, Tv, a) \le n^p D^p(fu, gv, a)$ i.e., $(\alpha_1 + \alpha_2 + \alpha_3)\, \delta p(Su, Tv, a) \le (\alpha_1 + \alpha_2 + \alpha_3)\, n^p D^p(fu, gv, a)$.

From (2.3) we get $D^p(fu, gv, a) \le (\alpha_1 + \alpha_2 + \alpha_3) n^p D^p(fu, gv, a)$ implies, $D^p(fu, gv, a) = 0$ [since $(\alpha_1 + \alpha_2 + \alpha_3) n^p < 1$] i.e., fu = gv.

Now we are to show that fu is fixed point of f. So, $D^p(ffu, fu, a) = D^p(ffu, gv, a) \le H^p(Sfu, Tv, a) \le \alpha_1 d\,(ffu, gv, a) + \alpha_2 \delta\,(ffu, Tv, a) + \alpha_3 \delta\,(gv, Sfu, a) + \alpha_4 \delta^p(gv, Tv, a) + \alpha_5 \delta^p(ffu, Sfu, a) = \alpha_1 d^p(ffu, gv, a) + \alpha_2 \delta^p(ffu, Tv, a) + \alpha_3 \delta^p(Sfu, gv, a) = \alpha_1 d^p(ffu, gv, a) + \alpha_2 \delta^p(ffu, Tv, a) + \alpha_3 \delta^p(Sfu, fu, a)$

$= (\alpha_1 + \alpha_2 + \alpha_3) \delta^p(Su, Tv. a)$. ...(2.4)

Again we know that D(ffu, gv, a) ≤ δ(Sfu, Tv, a) and D(ffu, gv, a), δ(Sfu, Tv, a) ∈ R + by Archimedean Property, there exists a $n_0 \in N$ such that $\delta(Sfu, Tv, a) \le n_0 D(ffu, gv, a)$ implies, $\delta^p(Sfu, Tv, a) \le n_0^p D^p(ffu, gv, a)$.

From (2.4) $D^p(ffu, fu, a) \le (\alpha_2 + \alpha_2 + \alpha_3)\, n_0^p D^p(ffu, gv, a) = (\alpha_1 + \alpha_2 + \alpha_3) n_0^p D^p(ffu, fu, a)$ [since fu = gv] implies, $D^p(ffu, fu, a) \le 0$ i.e., $D^p(ffu; fu; a) = 0$ i.e., ffu = fu i.e., fu is a fixed point of f.

Now we are to show that fu is also a fixed point of g. Since D(fu, Tgv, a) ≤ d(fu, ggv, a), by Archimedean property there exist an n* ∈ N such that $d(fu, gfu, a) \le n^* D(fu, Tfu, a)$ i.e., $d^p(fu, gfu, a) \le n^{*p} D^p(fu, Tfu, a)$.

So, $D^p(fu, gfu, a) = d^p(fu, ggv, a) \le n^{*p}\, D^p(fu, Tgv, a) \le n^{*p}\, H^p(Sfu, Tgv, a) \le n^{*p}[\alpha_1 d^p(ffu, ggv, a) + \alpha_2\delta^p(ffu, Tgv, a) + \alpha_3\delta^p(ggv, Sfu, a) + \alpha_4\delta^p(ggv, Tgv, a) + \alpha_5\delta^p(ffu, Sfu, a)] \le (\alpha_1 + \alpha_2 + \alpha_3)\, n^{*p}\delta^p(Sfu, Tgv, a) \le (\alpha_1 + \alpha_2 + \alpha_3)\, n^{*p}\, n_{00}{}^p D^p(fu, ggv, a)$ [similarly using Archimedean Property for $n_{00} \in N$] $= (\alpha_1 + \alpha_2 + \alpha_3)k^p$[putting $n^{*p}\, n_{00}{}^p D^p = k^p$] i.e., $(1 - (\alpha_1 + \alpha_2 + \alpha_3)k^p)D^p(fu, gfu, a) \le 0$ [since fu = gv] implies, $D^p(fu, gfu, a) = 0$ i.e., fu = gfu.

Therefore, fu = ffu = gfu = ggv ∈ Tgv = Tfu and fu = ffu ∈ Sfu. Thus fu = z (say) is a common fixed point of f, g, S and T.

Now $H^p(Sz, Tz, a) = H^p(Sfu, Tfu, a) = H^p(Sfu, Tgv, a) \le \alpha_1 d^p(ffu, ggv, a) + \alpha_2\delta^p(ffu, Tgv, a) + \alpha_3\delta^p(ggv, Sfu, a) + \alpha_4\delta^p(ggv, Tgv, a) + \alpha_5\delta^p(ffu, Sfu, a) = \alpha_1.0 + \alpha_2.0 + \alpha_3.0 + \alpha_4.0 + \alpha_5.0 = 0$,i.e., Sz = Tz.

Let w be another common fixed point of f, g, S and T. Then we have $D^p(z, w, a) \le H^p(Sz, Tw, a) \le \alpha_1 d^p(fz, gw, a) + \alpha_2\delta^p(fz, Tw, a) + \alpha_3\delta^p(gw, Sz, a) + \alpha_4\delta^p(gw, Tw, a) + \alpha_5\delta^p(fz, Sz, a) = \alpha_1 d^p(z, w, a) + \alpha_2\delta^p(z, Tw, a) + \alpha_3\delta^p(w, Sz, a) \le (\alpha_1 + \alpha_2 + \alpha_3)\, \delta^p(Sz, Tw, a) \le (\alpha_1 + \alpha_2 + \alpha_3)\, n_{000}{}^p D^p(z, w, a)$ [using Archimedean Property similarly for $n_{000} \in \mathbf{N}$] implies, $D^p(z, w, a) = 0$ i.e., z = w. Thus Sz = Tz = {z}. Hence the theorem.

Corollary 3.1. Let (X, d) be a 2-metric space. F, g : X → X and S, T : X → CB(X) satisfying the relation, $H^p(Sx, Ty, a) \le \alpha_1 d^p(fx, gy, a) + \alpha_2 D^p(fx, Ty, a) + \alpha_3 D^p(gy, Sx, a) + \alpha_4 D^p(gy, Ty, a) + \alpha_5 D^p(fx, Sx, a)$, $p \ge 1$, $\alpha_i \ge 0$, i = 1, 2, 3, 4, 5 and $\sum_{i=1}^{5}\alpha_i < 1$. The pairs (S, f) and (T, g) satisfy OWC-property. f(X) and g(X) are closed. Then f, g, S and T have unique common fixed point in X.

Proof. Since, $H^p(Sx, Ty, a) \le \alpha_1 d^p(fx, gy, a) + \alpha_2 D^p(fx, Ty\ a) + \alpha_3 D^p(gy, Sx, a) + \alpha_4 D^p(gy, Ty, a) + \alpha_5 D^p(fx, Sx, a) \le \alpha_1 d^p(fx, gy, a) + \alpha_2\delta^p(fx, Ty, a) + \alpha_3\delta^p(gy, Sx, a) + \alpha_4\delta^p(gy, Ty, a) + \alpha_5\delta^p(fx, Sx, a)$, the result follows from **Theorem 3.2**.

Corollary 3.2. Let (X, d) be a 2-metric space. f, g : X → X and S, T : X → CB(X) satisfying the relation, $H^p(Sx, Ty, a) \le \alpha_1 d^p(x, y, a) + \alpha_2 D^p(x, Ty, a) + \alpha_3 D^p(y, Sx, a) + \alpha_4 D^p(y, Ty, a) + \alpha_5 D^p(x, Sx, a)$; where $p \ge 1$, $\alpha_i \ge 0$, i= 1, 2, 3, 4, 5 and $\sum_{i=1}^{5}\alpha_i < 1$. The pairs (S, f) and (T, g) satisfy OWC-property. f(X) and g(X) are closed. Then f, g, S and T have a unique common fixed point in X.

Proof. Since $D^p(Sx, Ty, a) \le D^p(x, Ty, a)$ and $D^p(Sx, Ty, a) \le D^p(Sx, y, a)$, the result follows from **Corollary 3.1.**

Corollary 3.3. Let (X, d) be a 2-metric space. F, g : X → X and S, T : X → CB(X) satisfying the relation, $D^p(Sx, Ty, a) \le \alpha_1 d^p(fx, gy, a) + \alpha_2 D^p(fx, Ty, a) + \alpha_3 D^p(gy, Sx, a) + \alpha_4 D^p(gy, Ty, a) + \alpha_5 D^p(fx, Sx, a)$; $p \ge 1$, $\alpha_i \ge 0$, i = 1, 2, 3, 4, 5 and $\sum_{i=1}^{5}\alpha_i < 1$. The pairs (S, f) and (T, g) satisfy OWC-property. f(X) and g(X) are closed. Then f, g, S and T have a unique common fixed point in X.

Proof. As we know that D ≤ H then we get, $D^p(Sx, Ty, a) \le H^p(Sx, TY, a) \le \alpha_1 d^p(fx, gy, a) + \alpha_2 D^p(fx, Ty, a) + \alpha_3 D^p(gy, Sx, a) + \alpha_4 D^p(gy, Ty, a) + \alpha_5 D^p(fx, Sx, a)$ and the result follows from **Theorem 3.2**.

Corollary 3.4. Let (X, d) be a 2-metric space. f, g : X → X and S, T : X → CB(X) satisfying the relation, $D^p(Sx, Ty, a) \le \alpha_1 d^p(x, y, a) + \alpha_2 D^p(x, Ty, a) + \alpha_3 D^p(y, Sx, a) + \alpha_4 D^p(y, Ty, a) + \alpha_5 D^p(x, Sx, a)$; where $p \ge 1$, $\alpha_i \ge 0$, i = 1, 2, 3, 4, 5 and $\sum_{i=1}^{5}\alpha_i < 1$. The pairs (S, f) and (T, g) satisfy OWC-property. f(X) and g(X) are closed. Then f, g, S and T have a unique common fixed point in X.

Proof. Since $D^p(Sx, Ty, a) \le H^p(Sx, Ty, a) \le \alpha_1 d^p(x, y, a) + \alpha_2 D^p(x, Ty, a) + \alpha_3 D^p(y, Sx, a) + \alpha_4 D^p(y, Ty, a) + \alpha_5 D^p(x, Sx, a)$, the result follows from **Cololary 3.2.**

Theorem 3.3. Let (X,d) be a 2-metric space. f, g : X→ X and S, T : X → CB(X) satisfying the relation, $H^p(Sx, Ty, a) \le \alpha_1 d^p(fx, gy, a) + \alpha_2 D^p(fx, Ty, a) + \alpha_3 D^p(gy, Sx, a) + \alpha_4 D^p(gy, Ty, a) + \alpha_5 D^p(fx, Sx, a)$, $p \ge 1$, $\alpha_i \ge 0$, i = 1, 2, 3, 4, 5 and $\sum_{i=1}^{5}\alpha_i < 1$. The pairs (S, f) and (T, g) satisfy CLRf -property. Also (S, f) are weakly compatible, f is continuous, g is one-one and f(X), g(X) are closed. Then f, g, S and T have a unique common fixed point in X.

Proof. As the pairs (S, f) and (T, g) satisfy CLRf -property, then there exists two sequences $\{x_n\}$, $\{y_n\}$ in X and A, B ∈ CB(X) such that $\lim_{n\to\infty} Sx_n = A$; $\lim_{n\to\infty} Ty_n = B$ and $\lim_{n\to\infty} fx_n = \lim_{n\to\infty} gy_n = fu \in A \cap B$ for some u ∈ X. Since f(X), g(X) are closed subsets of X, there exist v, w ∈ X such that fu = fv and fu = gw.

We show that gw ∈ Tw. If possible let gw ∉ Tw. Then by the given condition,

$D^p(fx_n, Tw, a) \le H^p(Sx_n, Tw, a) \le \alpha_1 d^p(fx_n, gw, a) + \alpha_2 D^p(fx_n, Tw, a) + \alpha_3 D^p(gw, Sx_n, a) + \alpha_4 D^p(gw, Tw, a) + \alpha_5 D^p(fx_n, Sx_n, a)$.

Taking $\lim_{n\to\infty}$ in the above inequality we have $D^p(fu, Tw, a) \le \alpha_1 d^p(fu, gw, a) + \alpha_2 D^p(fu, Tw, a) + \alpha_3 D^p(gw, A, a) + \alpha_4 D^p(gw, Tw, a) + \alpha_5 D^p(fu, A, a) \le \alpha_1.0 + \alpha_2 D^p(fu, Tw, a) + \alpha_3 D^p(fu, A, a) + \alpha_4 D^p(gw, Tw, a) + \alpha_5.0$

Or,

$D^p(gw, Tw, a) \le \alpha_2 D^p(gw, Tw, a) + \alpha_4 D^p(gw, Tw, a)$ [since fu = gw]

Or,

$(1 - \alpha_2 - \alpha_4)D^p(gw, Tw, a) \le 0$, implies, $1 - \alpha_2 - \alpha_4 \le 0$, which is a contradiction.

Therefore $D^p(gw, Tw, a) = 0$, i.e., $gw \in Tw$ as $n \to \infty$.

Now, we show that $fv \in Sv$. Consider $fv \notin Sv$.

Since, $D^p(Sv, gy_n, a) \le H^p(Sv, Ty_n, a) \le \alpha_1 d^p(fv, gy_n, a) + \alpha_2 D^p(fv, Ty_n, a) + \alpha_3 D^p(gy_n, Sv, a) + \alpha_4 D^p(gy_n, Ty_n, a) + \alpha_5 D^p(fv, Sv, a)$.

Taking limit as $n \to \infty$ both sides in the above inequality we have $D^p(Sv, fu, a) \le \alpha_1 d^p(fv, fu, a) + \alpha_2 D^p(f, B, a) + \alpha_3 D^p(fu, Sv, a) + \alpha_4 D^p(fu, B, a) + \alpha_5 D^p(fv, Sv, a)$ Or, $D^p(Sv, fu, a) \le \alpha_1.0 + \alpha_2.0 + \alpha_3 D^p(fu, Sv, a) + \alpha_4.0 + \alpha_5 d^p(fv, Sv, a)$

implies, $(1 - \alpha_3 - \alpha_5) D^p(Sv, fv, a) \le 0$ i.e., $D^p(Sv, fv, a) = 0$ i.e., $fv \in Sv$.

Now let $v \ne fv$. Since (S, f) is weakly compatible, we have $fv \in Sv$ implies, $ffv \in fSv = Sfv$.

Therefore $d^p(ffv, fv, a) = D^p(ffv, gw, a) \le H^p(Sfv, Tw, a) \le \alpha_1 d^p(ffv, gw, a) + \alpha_2 D^p(ffv, Tw, a) + \alpha_3 D^p(gw, Sfv, a) + \alpha_4 D^p(gw, Tw, a) + \alpha_5 D^p(ffv, Sfv, a) \le \alpha_1 d^p(ffv, gw, a) + \alpha_2 d^p(ffv, gw, a) + \alpha_3 d^p(fv, ffv, a) + \alpha_4.0 + \alpha_5.0 = \alpha_1 d^p(ffv, fv, a) + \alpha_2 d^p(ffv, fv, a) + \alpha_3 d^p(ffv, fv, a)$

implies, $(1 - \alpha_1 - \alpha_2 - \alpha_3) d^p(ffv, fv, a) \le 0$ i.e., $d^p(ffv, fv, a) = 0$ i.e., $ffv = fv$. i.e., $fv = v$ [since f is continuous].

Again, $d^p(v, gv, a) = D^p(fv, gv, a) \le H^p(Sv, Tv, a) \le \alpha_1 d^p(fv, gv, a) + \alpha_2 D^p(fv, Tv, a) + \alpha_3 D^p(gv, Sv, a) + \alpha_4 D^p(gv, Tv, a) + \alpha_5 D^p(fv, Sv, a) \le \alpha_1 d^p(v, gv, a) + \alpha_2 d^p(v, Tv, a) + \alpha_3 D^p(v, gv, a) + \alpha_4.0 + \alpha_5.0$ implies, $(1 - \alpha_1 - \alpha_2 - \alpha_3) d^p(v, gv, a) \le 0$ i.e., $d^p(v, gv, a) = 0$ i.e., $v = gv$.

Therefore, $v = fv = gv$ and $fv \in Sv$; $gv = fv = fu = gw \in Tw$ implies, $gv = gw$ i.e., $v = w$ [since g is one one]. Thus $v = fv = gv$, $fv \in Sv$, $gv \in Tv$.

Thus v is a common fixed point of f, g, S and T. Let x be another common fixed point of f, g, S and T. Then $d^p(v, x, a) = D^p(fv, gx, a) \le H^p(Sv, Tx, a) \le \alpha_1 d^p(fv, gx, a) + \alpha_2 D^p(fv, Tx, a) + \alpha_3 D^p(gx, Sv, a) + \alpha_4 D^p(gx, Tx, a) + \alpha_5 D^p(fv, Sv, a) \le \alpha_1 d^p(v, x, a) + \alpha_2 d^p(fv, gx, a) + \alpha_3 d^p(gx, fv, a) + \alpha_4.0 + \alpha_5.0 = \alpha_1 d^p(v, x, a) + \alpha_2 d^p(v, x, a) + \alpha_3 d^p(x, v, a)$

implies, $(1 - \alpha_1 - \alpha_2 - \alpha_3) d^p(x, v, a) \le 0$ i.e., $d^p(x, v, a) = 0$ i.e., $x = v$. Hence f, g, S and T has unique common fixed point in X.

Theorem 3.4. Let (X, d) be a 2-metric space. $f, g : X \to X$ and $S, T : X \to CB(X)$ satisfying the relation, $H^p(Sx, Ty, a) \le \alpha_1 d^p(fx, gy, a) + \alpha_2 D^p(fx, Ty, a) + \alpha_3 D^p(gy, Sx, a) + \alpha_4 D^p(gy, Ty, a) + \alpha_5 D^p(fx, Sx, a)$, $p \ge 1$, $\alpha_i \ge 0$, $i = 1, 2, 3, 4, 5$ and $\sum_{i=1}^{5} \alpha_i < 1$.

The pairs (S, f) and (T, g) satisfy D–mapping and f(X), g(X) are closed. Then f, g, S and T has unique common fixed point in X.

Proof. Let $x_0 \in X$ be arbitrary. We construct two sequences $\{x_n\}$ and $\{y_n\}$ such that $y_{n-1} = fx_n \in Sx_{n-1}$; $y_n = gx_{n+1} \in Tx_n$ for all $n \in N$.

Now since (S, f) and (T, f) satisfy D-mapping, then for the sequences $\{x_n\}$ and $\{y_n\}$ we have $\lim_{n\to\infty} fx_n = x$ and $\lim_{n\to\infty} Sx_n = \{x\}$ and $\lim_{n\to\infty} gy_n = y$ and $\lim_{n\to\infty} Ty_n = \{y\}$ for some $x, y \in X$.

Since $D^p(fx, Ty_n, a) \le D^p(fx, gy_n, a) \le H^p(Sx, Ty_n, a) \le \alpha_1 d^p(fx, gy_n, a) + \alpha_2 D^p(fx, Ty_n, a) + \alpha_3 D^p(gy_n, Sx, a) + \alpha_4 D^p(gy_n, Ty_n, a) + \alpha_5 D^p(fx, Sx, a) \le \alpha_1 d^p(fx, gy_n, a) + \alpha_2 D^p(fx, Ty_n, a) + \alpha_3 [D^p(gy_n, Sx, fx) + D^p(gy_n, fx, a) + D^p(fx, Sx, a)] + \alpha_4.0 + \alpha_5.0 = \alpha_1 d^p(fx, gy_n, a) + \alpha_2 D_p(fx, Ty_n, a) + \alpha_3 D^p(fx, gy_n, a)$

Or, $(1 - \alpha_2 - \alpha_3) D^p(fx, gy_n, a) \le \alpha_1 d^p(fx, gy_n, a)$ Or, $(1 - \alpha_2 - \alpha_3) d^p(fx, gy_n, a) \le \alpha_1 d^p(fx; gy_n, a)$ Or, $(1 - \alpha_1 - \alpha_2 - \alpha_3) D^p(fx, gy_n, a) \le 0$ implies, $D^p(fx, gy_n, a) = 0$ i.e., $fx = gy_n$.

i.e., $\lim_{n\to\infty} fx = \lim_{n\to\infty} gy_n = y$ i.e., $fx = y$.

Again, $D^p(Sx, y, a) \le d^p(fx, y, a) = 0$ implies, $y \in Sx$. Therefore, $y = fx \in Sx$. Also $y \in Ty_n$.

Now we show that $y = gy \in Ty$.

Since $D^p(y, Ty, a) = D^p(fx, Ty, a) \le H^p(Sx, Ty, a) \le \alpha_1 d^p(fx, gy, a) + \alpha_2 D^p(fx, Ty, a) + \alpha_3 D^p(gy, Sx, a) + \alpha_4 D^p(gy, Ty, a) + \alpha_5 D^p(fx, Sx, a) \le \alpha_1 d^p(fx, gy, a) + \alpha_2 D^p(y, Ty, a) + \alpha_3 D^p(gy, fx, a) + \alpha_4.0 + \alpha_5.0$ implies, $(1 - \alpha_2) D^p(y, Ty, a) \le \alpha_1 d^p(y, gy, a) + \alpha_3 D^p(gy, y, a)$ i.e., $(1 - \alpha_2) D^p(y, Ty, a) \le (\alpha_1 + \alpha_3) D^p(y, gy, a)$.

Let $D^p(y, Ty, a) \ne D^p(y, gy, a)$. Then from the above inequality we get

$$\left(\frac{1-\alpha_2}{\alpha_1+\alpha_3}\right) D^p(y, Ty, a) \le D^p(y, gy, a) \qquad \ldots(2.5)$$

Since $D^p(y, Ty, a) \le D^p(y, gy, a)$ using (2.5), we have

$\frac{1-\alpha_2}{\alpha_1+\alpha_3} \le 1$ implies, $1 - \alpha_2 \le \alpha_1 + \alpha_3$

i.e., $1 \le \alpha_1 + \alpha_2 + \alpha_3$, which is a contradiction.

Therefore $D^p(y, Ty, a) = D^p(y, gy, a) = d^p(y, gy, a)$. From (2.5) we have

$\left(\frac{1-\alpha_2}{\alpha_1+\alpha_3}\right) d^p(y, gy, a) \le d^p(y, gy, a)$ implies, $\left(\frac{1-\alpha_2-\alpha_1-\alpha_3}{\alpha_1+\alpha_3}\right)$ $d^p(y, gy, a) \le 0$ i.e., $d^p(y, gy, a) = 0$ i.e., $y = gy \in Ty$.

Next we show that $x = y$.

So, $\lim_{n\to\infty} D^p(x, y, a) \le \lim_{n\to\infty} H^p(Sx_n, Ty_n, a) \le \lim_{n\to\infty} [\alpha_1 d^p(fx_n, gy_n, a) + \alpha_2 D^p(fx_n, Ty_n, a) + \alpha_3 D^p(gy_n, Sx_n, a) + \alpha_4 D^p(gy_n, Ty_n, a) + \alpha_5 D^p(fx_n, Sx_n, a)]$

$= \alpha_1 d^p(x, y, a) + \alpha_2 D^p(x, \{y\}, a) + \alpha_3 D^p(y, \{x\}, a) + \alpha_4.0 + \alpha_5.0$

implies, $d^p(x, y, a) \le (\alpha_1 + \alpha_2 + \alpha_3)d^p(x, y, a)$ i.e., $d^p(x, y, a) = 0$ i.e., x =y.

Therefore, x = y = fx ∈ Sx; x = y = gx ∈ Tx.

Also, $\lim_{n\to\infty} Sx_n = \{x\} = \{y\} = \lim_{n\to\infty} Ty_n$.

Again, $D^p(Sx,Ty, a) \le H^p(Sx, Ty, a) \le \alpha_1 d^p(fx, gy, a) + \alpha_2 D^p(fx, Tx, a) + \alpha_3 D^p(gx, Sx, a) + \alpha_4 D^p(gy, Tx, a) + \alpha_5 D^p(fx, Sx, a)]$

$= \alpha_1.0 + \alpha_2.0 + \alpha_3.0 + \alpha_4.0 + \alpha_5.0 = 0$ implies, Sx = Ty = {x}.

Thus x is common fixed point of f, g, S and T. To show the uniqueness of x, let z be another fixed point.

Then $D^p(x, z, a) \le H^p(Sx, Tz, a) \le \alpha_1 d^p(fx, gz, a) + \alpha_2 D^p(fx, Tz, a) + \alpha_3 D^p(gz, Sx, a) + \alpha_4 D^p(gz, Tz, a) + \alpha_5 D^p(fx, Sx, a)$

$= \alpha_1 d^p(x, z, a) + \alpha_2 D^p(x, Tz, a) + \alpha_3 D^p(z, Sx, a) + \alpha_4.0 + \alpha_5.0$

$\le (\alpha_1 + \alpha_2 + \alpha_3) D^p(x, z, a)$ ...(2.6)

If $D^p(x, z, a) \ne d^p(x, z a)$, then since $D^p(x, z, a) \le d^p(x, z a)$, we have from (2.6), $1 \le \alpha_1 + \alpha_2 + \alpha_3$, which is a contradiction by the given condition. Therefore $D^p(x, z, a) = d^p(x, z a)$

implies, x = z. Hence f, g, S and T have unique common fixed point in X.

Wardowski (2012) has defined the set **F** of all functions F : **R**+ → **R** satisfying the conditions:

I): F is strictly increasing;

II): for all sequence $\{\alpha_n\}$ in R +, $\lim_{n\to\infty} \alpha_n = 0$ if and only if $\lim_{n\to\infty} F(\alpha_n) = -\infty$;

III): there exists 0 < k < 1 such that $lim_{\alpha\to 0+} \alpha^k F(\alpha) = 0$.

Theorem 3.5. Let (X, d) be a complete 2-metric space and let T : X → CB(X) be a multivalued mapping. Also let F ∈ F is a function continuous from right and for τ ∈ R+ such that $2\tau + F(H(Tx, Ty, a)) \le F(\alpha_1 d(x, y, a) + \alpha_2 D(x, Tx, a) + \alpha_3 D(y, Ty, a) + \alpha_4 D(x, Ty, a) + \alpha_5 D(y, Tx, a))$ for all x, y ∈ X where $\alpha_i \ge 0$; i = 1, 2, 3, 4, 5 and $\alpha_1 + \alpha_2 + \alpha_3 + 3\alpha_4 + \alpha_5 < 1$.

Then T has a unique fixed point in X.

Proof. Let for arbitrary $x_0 \in X$ we choose a point $x_1 \in X$ such that $x_1 \in Tx_0$. If $x_1 \in Tx_1$ then x_1 is a fixed point of T and the proof completed. Clearly $D(x_0, Tx_0, a) \le d(x_0, x_1, a)$.

Therefore, $2\tau + F(H(Tx_0, Tx_1, a)) \le F(\alpha_1 d(x_0, x_1, a) + \alpha_2 D(x_0, Tx_0, a) + \alpha_3 D(x_1, Tx_1, a) + \alpha_4 D(x_0, Tx_1, a) + \alpha_5 D(x_1, Tx_0, a)) \le F(\alpha_1 d(x_0, x_1, a) + \alpha_2 d(x_0, x_1, a) + \alpha_3 D(x_1, Tx_1, a) + \alpha_4 D(x_0, Tx_1, a) + \alpha_5.0)$ ...(2.7)

Since (X, d) is a complete 2-metric space, we have for 0 < α < 1, $H(Tx_0, Tx_1, a) \le \alpha d(x_0, x_1, a)$.

Let us choose h > 1 such that $d(p, q, a) \le H(T_p, T_q, a)$ where p ∈ Tp, q ∈ Tq. Thus there exists $x_2 \in Tx_1$ such that $D(x_1, Tx_1, a) \le d(x_1, x_2, a) \le h\, H(Tx_0, Tx_1, a)$. ...(2.8)

Thus in general $d(x_n, x_m, a) \le hH(Tx_{n-1}, Tx_{m-1}, a)$; ...(2.9)

where $x_n \in Tx_{n-1}$ for all n ∈ N.

Since F is continuous from right, for h > 1 we have from (2.7) and (2.8)

$F(d(x_1, x_2, a)) \le F(hH(Tx_0, Tx_1, a)) \le H(Tx_0, Tx_1, a) + \tau$

implies, $2\tau + F(d(x_1, x_2, a)) \le 2\tau + F(H(Tx_0, Tx_1, a)) + \tau \le F(\alpha_1 d(x_0, x_1, a) + \alpha_2 D(x_0, Tx_0, a) + \alpha_3 D(x_1, Tx_1, a) + \alpha_4 D(x_0, Tx_1, a)) + \tau$

implies, $\tau + F(d(x_1, x_2, a)) \le F((\alpha_1 + \alpha_2) d(x_0, x_1, a) + \alpha_3 d(x_1, x_2, a) + \alpha_4(d(x_0, x_2, x_1) + d(x_0, x_1, a) + d(x_1, x_2, a)))$

i.e., $d(x_1, x_2, a) \le (\alpha_1 + \alpha_2 + 2\alpha_4)d(x_0, x_1, a) + (\alpha_3 + \alpha_4)d(x_1, x_2, a)$

i.e., $(1 - \alpha_3 - \alpha_4)d(x_1, x_2, a) \le (\alpha_1 + \alpha_2 + 2\alpha 4)d(x_0, x_1, a)$

i.e., $d(x_1, x_2, a) \le \left(\frac{\alpha_1+\alpha_2+2\alpha_4}{1-\alpha_3-\alpha_4}\right) d(x_0, x_1, a) < d(x_0, x_1, a)$

[since $\frac{\alpha_1+\alpha_2+2\alpha_4}{1-\alpha_3-\alpha_4} < 1$].

Therefore, $\tau + F(d(x_1, x_2, a)) \le F(d(x_0, x_1, a))$.

Continuing this process we can get a sequence $\{x_n\} \in X$ such that $x_n \notin Tx_n$, $x_{n+1} \in Tx_n$ and $\tau + F(d(x_{n-1}, x_n, a)) \le F(d(x_{n-2}, x_{n-1}, a)) \forall \in \mathbf{N}$.

Therefore, $F(d(x_n, x_{n+1}, a)) \le F(d(x_{n-1}, x_n, a)) - \tau \le F(d(x_{n-2}, x_{n-1}, a)) - 2\tau \le \ldots \le F(d(x_0, x_1, a)) - n\tau$.

Since F ∈ **F**, taking limit as n → ∞,

we have $\lim_{n\to\infty} F(d(x_n, x_{n+1}, a)) = -\infty$ if f $\lim_{n\to\infty} d(x_n, x_{n+1}, a) = 0$ and so $\lim_{n\to\infty} d(x_n, x_{n+1,} a) = 0$.

Let n > m > $n_1 \in$ N. Then $\lim_{n,m\to\infty} d(x_n, x_m, a) \le \lim_{n,m\to\infty} d(x_n, x_m, x_{n-1}) + d(x_n, x_{n-1}, a) + d(x_{n-1}, x_m, a)] = \lim_{n,m\to\infty} d(x_n, x_m, x_{n-1}) + \lim_{n,m\to\infty} d(x_n, x_{n-1}, a) + \lim_{n,m\to\infty} d(x_{n-1}, x_m, a) = \lim_{n,m\to\infty} d(x_{n-1}, x_m, a) \le d(x_m, x_m, a) = 0$.

Thus $\{x_n\}$ is a Cauchy sequence. Since X is complete, there exists x ∈ X such that $x_n \to x$, as n → ∞. Thus there exists a subsequence $\{x_{n_k}\}$ such that $x_{n_k} \in Tx$ for all $n_k \in \mathbf{N}$. As T is closed and $x_{n_k} \to x$. So we get x ∈ Tx and the proof is completed. So we assume that there exists $n_0 \in$ N such that $x \notin Tx$ for all $n \ge n_0 \in \mathbf{N}$.

Now $D(x_n, Tx, a) \le d(x_n, x_{nk}, a) \le hH(Tx_{n-1}, Tx, a)$ [using (2.9)]

implies, $F(D(x_n, Tx, a)) \le F(hH(Tx_{n-1}, Tx, a)) \le F(H(Tx_{n-1}, Tx, a)) + \tau$ i.e., $2\tau + F(D(x_n, Tx, a)) \le 2\tau + F(H(Tx_{n-1}, Tx, a)) + \tau$

$\le F(\alpha_1 d(x_{n-1}, x, a) + \alpha_2 D(x_{n-1}, Tx_{n-1}, a) + \alpha_3 D(x, Tx, a) + \alpha_4 D(x_{n-1}, Tx, a) + \alpha_5 D(x, Tx_{n-1}, a)) + \tau$

implies, $\tau + F(D(x_n, Tx, a)) \le F(\alpha_1 d(x_{n-1}, x, a) + \alpha_2 D(x_{n-1}, Tx_{n-1}, a) + \alpha_3 D(x, Tx, a) + \alpha_4 D(x_{n-1}, Tx, a)$ i.e., $F(D(x_n, Tx, a)) \le \tau + F(D(x_n, Tx, a))$

$\le F(\alpha_1 d(x_{n-1}, x, a) + \alpha_2 D(x_{n-1}, Tx_{n-1}, a) + \alpha_3 D(x, Tx, a) + \alpha_4 D(x_{n-1}, Tx, a))$

implies, $D(x_n, Tx, a) \le \alpha_1 d(x_{n-1}, x, a) + \alpha_2 D(x_{n-1}, Tx_{n-1}, a) + \alpha_3 D(x, Tx, a) + \alpha_4 D(x_{n-1}, Tx, a)$.

Taking limit as $n \to \infty$ we get, $D(x, Tx, a) \le \alpha_1.0 + \alpha_2 D(x, Tx, a) + \alpha_3 D(x, Tx, a) + \alpha_4 D(x, Tx, a)$ implies, $(1 - \alpha_2 - \alpha_3 - \alpha_4) D(x, Tx, a) \le 0$ implies, $D(x, Tx, a) = 0$ implies, $x \in Tx$.

Therefore, T has a fixed point. To show the uniqueness, let y be another fixed point of T. Then $d(x, y, a) \le hH(Tx, Ty, a)$ implies, $F(d(x, y, a)) \le F(hH(Tx, Ty, a)) \le F(H(Tx, Ty, a))$.

Therefore, $2\tau + F(d(x, y, a)) \le 2\tau + F(H(Tx, Ty, a)) + \tau \le F(\alpha_1 d(x, y, a) + \alpha_2 D(x, Tx, a) + \alpha_3 D(y, Ty, a) + \alpha_4 D(x, Ty, a) + \alpha_5 D(y, Tx, a))$

implies, $\tau + F(d(x, y, a)) \le F(\alpha_1 d(x, y, a) + \alpha_2 D(x, Tx, a) + \alpha_3 D(y, Ty, a) + \alpha_4 D(x, Ty, a) + \alpha_5 D(y, Tx, a))$.

So, $F(d(x, y, a)) \le \tau + F(d(x, y, a)) \le F(\alpha_1 d(x,y,a) + \alpha_2 D(x, Tx, a) + \alpha_3 D(y, Ty, a) + \alpha_4 D(x, Ty, a) + \alpha_5 D(y, Tx, a))$.

Therefore, $d(x, y, a) \le \alpha_1 d(x, y, a) + \alpha_2.0 + \alpha_3.0 + \alpha_4 D(x, Ty, a) + \alpha_5 D(y,Tx, a)$

implies, $d(x, y, a) \le \alpha_1 d(x, y, a) + \alpha_4 d(x, y, a) + \alpha_5 D(y, x, a) \le \alpha_1 d(x, y, a) + \alpha_4 d(x, y, a) + \alpha_5 d(y, x, a)$.

If $d(x, y, a) \ne 0$ then we have $(1 - \alpha_1 - \alpha_4 - \alpha_5) \le 0$ which contradicts the given condition.

Therefore $d(x, y, a) = 0$ i.e., $x = y$.

CONCLUSION

We have reformulated the theorem of Nadler (1969) in 2-metric space for set valued mappings and we have also established some theorems which will give scope for the further works in this area.

ACKNOWLEDGEMENT

The authors are thankful to the referee for the suggestions towards the improvement of the paper.

REFERENCES

Abbas M, Rhoades BE(2009) Common fixed point theorems for hybrid pairs of occasionally weakly compatible mappings and applications. Navi Sad J. Math., 39: 89 - 109.

Abd El-Monsef ME, Abu-Donia HM, Abd-Rabou K(2007) Common Fixed Point Theorems of Single and Set-Valued Mappings on 2-Metric Spaces. Applied Mathematics & Information Science An International Journal,Vol.1(2):185-194.

Abdou AAN(2016) Common fixed point result for multi-valued mappings with, some examples. J. Nonlinear Sci. Appl. 9: 787-798.

Ahmad J, Al-Rawashdeh A, Azam A(2015) New fixed point theorems for generalized F-contractions in complete metric spaces. Fixed Point Theory and Application:2015:80.

Banach S(1922) Sur les operations dans les ensembles abstrits et leur applications aux equations integrals. Fund. Math., 3: 133-181.

Bouhadjera H, Djoudi A(2008) Common fixed point theorems for single and set-valued maps without continuity. An. St. Univ. Ovidius Constanta. Vol. 16(1): 49-58.

Cho SH(2016) Fixed Point for Multivalued Mappings in b-Metris Spaces, Applied Mathematical Sciences. Vol.10: no.59: 2927-2944.

Djoudi A, Khemis R(2005), Fixed points for set and single valued maps without continuity. Demonstratio Mathematica, 38(3): 739-751.

Gahler S(1963) 2-metricsche Raume und ihre topologische structure. Math. Nachr. 26: 115-148.

Iseki K(1975) Fixed point theorems in 2-metric Spaces. Math. Sem. Notes. Kobe. Univ., 3: 133-136.

Jinakul C, Wiwatwanich A, Kaewkhao A(2017) Common Fixed Point Theorem For Multi-Valued Mappings ON BMETRIC SPACES. Int. J. of Pure and Appl.Math., Vol.113: No.1: 167 - 179.

Joseph JM, Ramganesh E(2013) Fixed Point Theorem on Multi-Valued Mappings. Int. J.of Ana.b and App. Vol.1:no 2: 123-127.

Jungck G(1986) Compatible mappings and common fixed points. Internat. J. Math. Math. Sci., 9: 771 - 779.

Nadler SB Jr(1969) Multi-Valued Contraction Mappings, Pacific Journal of Mathematics. Vol. 30: No. 2: 475-488.

Sintunavarat W, Kumar P(2011) Common fixed point theorems for a pair of weakly compatible mappings in fuzzy metric spaces. Hindawi Publishing Corporation Journal of Applied Mathematics, Volume 2011, Article ID 637958: 1-14.

Wardowski D(2012) Fixed points of a new type of contractive mappings in complete metric spaces. Fixed Point Theory and Applications, 2012:94: 1-6